The Cellular Immune Response to Murine Lyme borreliosis

A Dissertation
Presented to
The Faculty of the Graduate School
at the University of Missouri

In Partial Fulfillment
of the Requirements for the Degree

Doctor of Philosophy

by

CARRIE ELIZABETH LASKY

Dr. Charles R. Brown, Dissertation Advisor

May 2015

The undersigned, appointed by the dean of the Graduate School, have examined the dissertation entitled

THE CELLULAR IMMUNE RESPONSE TO MURINE LYME BORRELIOSIS

presented by Carrie E. Lasky,

a candidate for the degree of doctor of philosophy,

and hereby certify that, in their opinion, it is worthy of acceptance.

Professor Charles R. Brown

Professor Guoquan Zhang

Professor Bumsuk Hahm

Professor Deborah Anderson

Professor Mark Daniels

DEDICATION

For mom and dad, because you encouraged my crazy addiction to school. It looks like the money held out! I love you both, and appreciate the sacrifices you made to make my dream possible.

Also, for my future husband. For supporting me and consoling me through the many days and nights of frustration. I love you and can't wait to spend my life with you.

Carrie

ACKNOWLEDGEMENTS

I would like to thank my thesis advisor, Dr. Charles Brown, for his guidance and tough-love. He gave me a lab home to stay in for five years while I slowly learned how to think like a scientist. Thank you for the many hours spent mentoring me, revising my papers, and re-submitting publications. I'd also like to thank Dr. Dan Hassett for the time he spent troubleshooting and training me to use flow cytometry. Without him, I may have remained a "flow-tard" for the rest of my life. I would additionally like to thank Dr. Jerod Skyberg for donating the Cytokine Mouse 20-Plex Panel and helping with the Luminex Assay. I would also like to acknowledge the members of my thesis committee, Mark Daniels, Deborah Anderson, Bumsuk Hahm, and Guoquan Zhang. Each has been very supportive and was an integral part of my education.

TABLE OF CONTENTS

TABLE OF FIGURES

CHAPTER 1

INTRODUCTION

A. *The History of Lyme disease*

Although numerous publications on experimental and human Lyme disease have emerged over the past few decades, the discovery of *Borrelia burgdorferi* is still relatively recent. In 1981, Willy Burgdorfer, a medical entomologist, along with Alan Barbour and Jorge Benach made a discovery while working with *Ixodes* ticks from Shelter Island, New York. They identified *Borrelia* species within the midguts of the ticks (1). This discovery led to the identification and appropriate treatment of the infectious organism that caused the outbreak of unusual rheumatoid arthritis-like symptoms in children in Lyme, Connecticut which had begun in 1976. In honor of Dr. Burgdorfer's discovery, the spirochete was named *Borrelia burgdorferi* by the medical community (1). Over the next few decades, Lyme disease would emerge as the most common vector-borne disease in the United States (2). The importance of understanding the immunological mechanisms behind infection continue to increase in order to provide more effective care.

B. *Lyme Disease in Humans*

There are an estimated 300,000 new cases of Lyme disease each year, primarily affecting individuals from the New England and upper Midwestern United States (2). After the bite of an infected tick, an overwhelming majority (80-90%) of individuals develop erythema migrans, a circular bull's eye rash (3). Doxycycline or amoxicillin are prescribed to prevent bacterial growth and further symptoms from occurring (4).

The timing of treatment is of utmost importance, because bacterial dissemination occurs quickly (5). Upon transmission from the tick to the mammalian host, spirochetes multiply locally in the skin for approximately 48 hours, after which they disseminate to more distant tissues by permeating capillary beds and entering the matrix between cells (5). In some individuals, erythema migrans does not develop, and they do not recognize they are infected. If treatment is not sought, approximately 60% of individuals develop intermittent, yet chronic arthritis of the large joints (2). In fewer cases (2-8%), carditis develops which can be life threatening (6) (7). Although generally self-limiting, Lyme disease in humans can be chronic, and patients may battle debilitating joint pain for a lifetime (8). Despite an increased understanding of *B. burgdorferi* pathogenesis, there is no treatment for chronic Lyme disease. For this reason, using an experimental model of Lyme disease is critical to better understand the mechanisms of the inflammatory response.

C. *Experimental Lyme Disease*

Experimental Lyme disease, which closely recapitulates human disease, has been developed in a murine model (9). Arthritis-susceptible mouse strains (C3H/He or BALB/c) inoculated intradermally with a relatively low dose of *B. burgdorferi* ($2x10^4$), develop an inflammatory arthritis and carditis approximately two weeks after infection (10, 11). Studies have shown that the level of spirochete burden in the tissues does not determine disease severity, but clearance is required for resolution (12). Intradermal inoculation is the most commonly used route of infection because it is thought to more closely recapitulate a natural infection (11). However, our lab

utilizes a foot-pad inoculation, because it causes a more reliable, robust, and repeatable arthritis (12). The kinetics of disease development are slightly altered, but severity and pathology are unchanged (13).

Regardless of route of inoculation, the development of disease in susceptible mouse strains is very similar. Lyme carditis develops as early as 10 days, but spirochetes can be seen in heart tissue as early as 7 days post-infection (10). In the hearts, spirochetes normally localize to the aortic valve and base of the heart and are cleared, inducing resolution. Arthritis of the ankle joints is evident at 14 days post-infection and becomes progressively more severe from days 21-30 (10). Similar to the heart, spirochetes can be detected in joint tissue as early as day 7 post-infection, occurring focally around vessel walls, ligaments and tendons, and periosteum (10). In disease-susceptible mice, both arthritis and carditis resolve in about 4-5 weeks post-infection in an antibody-dependent mechanism (10, 14-16). During resolution, swelling and edema decrease within the joints and leukocyte infiltrate in both joints and hearts dissipates (17). While cellular infiltrate into the tissues is critical in clearance of bacteria, it is also important for returning tissues to homeostasis.

Although infection with *B. burgdorferi* causes inflammation in both joint and heart tissue, it is important to remember that the type of cellular response is highly tissue specific. For this reason, it is critical to study the immune response in both tissues to form a more complete picture. In both joint and heart tissues, the immune response to *B. burgdorferi* is driven by the innate immune system. Both the pathogenesis and

clearance of spirochetes during Lyme arthritis are highly dependent upon neutrophil recruitment to the site of infection (18). A previous study from our lab showed that, in infected joint tissue, expression of KC and monocyte chemoattractant protein (MCP)-1 are upregulated. This upregulation directly correlated with the development of arthritis (18). CXCR2-deficient mice, the receptor for the neutrophil chemoattractant KC, were unable to recruit neutrophils and displayed attenuated disease. CCR2-deficient mice, the receptor for the monocyte chemoattractant MCP-1, showed no attenuation of arthritis. This study demonstrated the importance of chemokine secretion in recruitment of neutrophils in the development of arthritis (18). In a subsequent study, the importance of early neutrophil recruitment for clearance of *B. burgdorferi* was noted. Infection of *B. burgdorferi* that over-expressed KC had significantly elevated numbers of neutrophils recruited to tissue. This increased recruitment of neutrophils dramatically attenuated infectivity of the bacteria (19).

Within Lyme carditis, a large number of macrophages and other mononuclear leukocytes localize to the hearts. It has been shown that during Lyme carditis, macrophages predominantly drive the inflammatory response (7, 17, 20-22). Mice lacking B and T lymphocytes or major histocompatibility complex (MHC) class II determinants infected with *B. burgdorferi* still developed carditis (7, 20, 21). Similar to the 2003 chemokine study done in experimental Lyme arthritis, mice deficient in the macrophage chemokine receptor, CCR2 were unable to recruit macrophages to the tissue (22). While this had no impact on arthritis susceptibility, it greatly affected

the development of Lyme carditis (18, 22). Possibly compensating for a lack of macrophages, neutrophils were recruited to the heart in large numbers altering the delicate balance of inflammation and bacterial clearance. This resulted in more effective clearance of spirochetes but had a detrimental effect on inflammation (22). These studies indicated that the type of cellular infiltration during Lyme borreliosis is tissue specific and care should be taken when manipulating this model system.

The role of T cells during Lyme borreliosis has been debated in the field. T cells isolated from patients with chronic Lyme Disease recognized *B. burgdorferi* antigen and produced pro-inflammatory cytokines, including TNF-α and IFN-γ, suggesting a role for T cells in Lyme pathogenesis (23, 24). Further analysis found that these T cells were Th1 $CD4^{+}$T-bet^{+} T cells that recognized *B. burgdorferi* lipoproteins (25). Using an inbred LSH hamster, the authors found that transfer of T cells from infected hamsters to naïve hamsters induced severe and destructive arthritis after bacterial challenge (26). Furthermore, B6 RAG-1 mice reconstituted with T cells and infected with *B. burgdorferi* displayed severe destructive arthritis (27, 28). This implies that T cells may play a role in the pathogenesis of disease. Later, it was hypothesized that a Th1-specific response elicited a pathogenic response to Lyme borreliosis, and a Th2 response suppressed it. Using the arthritis-susceptible C3H/He mouse strain and the resistant BALB/c strain, the T helper response was assessed after *B. burgdorferi* infection. It was found that a Th2 response preceded the Th1 response in the BALB/c mouse (29). In addition, due to the timing of IL-4 secretion it was predicted that Th2 cells do not play a role in preventing disease onset but hastened its resolution (29). In

support of a pro-resolution Th2 response, it was found that IL-6-deficient mice had a decrease in Th2 cells, more destructive arthritis, and a poor production of *B. burgdorferi*-specific IgG2b antibodies. Antibody class switching or production may be, in part, helped by T cells (30). In the synovial fluid of Lyme patients, a higher ratio of Th1 to Th2 cells correlated with arthritis severity (31). Surprisingly, it was found that IFN-γ secreting $CD4^+$ T cells actually promoted resolution of experimental Lyme carditis, once again showing tissue specific nature of the disease (32). This was the first study showing that T cells may play an active role in resolution of disease (32). In a later study, STAT-1-deficient mice which lack the receptor for IFN-γ, displayed no defect in arthritis development but had more severe carditis. This further promoted the idea of a strong $CD4^+$ T cell response during carditis resolution (33). To flush out the intricacies of the Th1 (IFN-γ) and Th2 (IL-4) balance in Lyme arthritis, IL-4 and IFN-γ deficient mice on either the arthritis susceptible C3H/He or resistant DBA strain were infected with *B. burgdorferi*. DBA mice failed to develop arthritis and C3H/He mice developed arthritis normally (34). The only difference reported was that IL-4-deficient mice failed to make an appropriate *B. burgdorferi*-specific antibody response (34). It appears that the Th1/Th2 dichotomy may not play a role in experimental Lyme arthritis, but $CD4^+$ T cells may aid in the development of the humoral response to *B. burgdorferi* infection (34).

The humoral immune response is primarily controlled by B cells, and these cells are important during experimental Lyme disease. They are critical in resolution of disease because an appropriate antibody response mediates bacterial clearance (14-

16). RAG mice, void of B and T cells, infected with *B. burgdorferi* failed to resolve Lyme arthritis and carditis. This indicated that the adaptive immune system was not necessarily responsible for the pathogenesis of Lyme disease but was perhaps important for its resolution. Following passive transfer of immune serum or the transfer of naïve B and T cells (but not T cells alone), *B. burgdorferi*-infected mice were able to resolve inflammation (15, 35). This data suggested that *B. burgdorferi*-specific antibody production was critical in bacterial clearance and resolution of disease.

D. Recognition of the Bacteria

B. burgdorferi are extracellular bacteria that possess peptidoglycan, a modified but functional lipopolysaccharide (LPS), and numerous lipoprotein outer surface proteins (OSPs) (36-38). Pattern recognition receptors (PRRs) including NOD-like receptors (NLR) and toll-like receptors (TLR) have been implicated in the recognition of *B. burgdorferi*. LPS is normally recognized by the mammalian host through its binding to TLR-4, but LPS from *B. burgdorferi* is atypical and does not signal through this receptor. Therefore, the immune system relies on other mechanisms to recognize the bacteria (39). It is primarily NOD-2 and TLR-1/2 heterodimers responsible for the induction of the inflammatory reaction (39, 40). *B. burgdorferi* express OspA, OspB, and OspD within the tick which promote persistence of spirochetes within the vector (41, 42). Upon feeding, OspA is downregulated and OspC is upregulated which promotes movement of the bacteria from tick salivary glands into the mammalian host (43). Within the host, TLR-1/2 heterodimers are capable of recognizing the

lipoproteins on *B. burgdorferi* which leads to bacterial clearance (44-46). As expected, TLR-2-deficient mice infected with *B. burgdorferi* carried significantly higher bacterial titers in the joint and ear tissues and developed a more severe arthritis compared to WT controls (47). NOD-2 is an intracellular receptor capable of recognizing peptidoglycan. In both human and mouse cells lacking functional NOD-2, *B. burgdorferi* stimulation resulted in defective inflammatory cytokine production, indicating an important role in bacterial recognition (39). More recently, it has been suggested that phagosomal TLRs recognize breakdown products of phagocytosed and degraded *B. burgdorferi* (48). In human monocytes co-cultured with *B. burgdorferi*, signaling through TLR-2 led to uptake of *B. burgdorferi* and formation of the phagosomal vacuole. This was followed by recruitment of TLR-2 and TLR-8, which resulted in degradation of the spirochete (48). TLR-8 signaling, specifically, led to IRF-7-mediated induction of IFN-β (48). Overall, recognition of *B. burgdorferi* is critical in its clearance, and depletion of these receptors in experimental Lyme disease alters normal disease pathogenesis (39, 49).

E. *Macrophage Polarization*

Macrophage polarization has been suggested to drive inflammation, the clearance of bacteria, and tissue repair and resolution in a variety of infectious models. Classically activated M1 macrophages are pro-inflammatory cells capable of destroying pathogens, tumor cells, and various foreign compounds (50). Stimulation of bone marrow derived macrophages (BMDM) with LPS and IFNγ or TNFα induced polarization to the M1 phenotype (51, 52). M1 macrophages can be recognized both

in vitro and *in vivo* by the production of nitric oxide (NO), as well as other pro-inflammatory molecules including TNFα, IL-1, IL-6, and CCL2 (53). These pro-inflammatory macrophages are routinely identified by flow cytometry using antibodies against F4/80, NOS2, Marco, and IL-12b (54). In contrast, alternatively activated M2 macrophages are considered to be responsible for promoting wound healing, tissue regeneration and antagonizing M1 macrophage responses (54). Polarization of BMDM into the M2 subset occurs by stimulation with IL-4, with or without IL-13 (55). M2 macrophages displayed elevated arginase activity and released IL-10, TGF-β, and PDGF (50). Identification of M2 macrophages using flow cytometry relies on expression of F4/80, CD206, and CD163 (56, 57). Transcriptionally, IRF5 promoted M1 differentiation and actively inhibited M2 differentiation (58). M2 polarization was regulated by both IRF3 and IRF4 (59, 60). Subclasses of the M2 phenotype have been described *in vitro*, including M2a, M2b, and M2c (50). The existence or relevance of these subtypes in infectious or autoimmune disease has yet to be explored *in vivo*.

Macrophage phenotype has been shown to play an important role in models of infection. In acute infection, M1 macrophages are often the main form of protection and survival (61). In 1993, it was reported that mice deficient in IFN-γ or TNF would inevitably succumb to infection with *Listeria monocytogenes*. It was later determined that these mice were incapable of inducing an M1 phenotype which was critical for the engulfment and destruction of the bacteria prior to phagosomal escape (61, 62). Similar phenomenon have been reported in *Salmonella* and *Chlamydial* infections

(63, 64). M1 macrophages, while critical, cannot persist in the environment due to the increased potential for tissue damage and chronic inflammation (65). To circumvent this, macrophage phenotype is flexible. Once the infection is cleared and a more anti-inflammatory environment is created, these once highly inflammatory cells may switch to a pro-resolution M2 program or be cleared from the site of infection (66). Manipulation of macrophage polarization to the M2 phenotype can aid in tissue remodeling in a murine model of hindlimb ischaemia (67). A failure to make the switch, as in patients with chronic venous ulcers and severe burns, prolonged inflammation (68, 69).

Despite early hypotheses that M1 macrophages would be present in greater numbers during initiation of inflammation and that M2 macrophages would be recruited or converted from M1 macrophages to aid in resolution, it appears that this may be an extreme oversimplification of what actually occurs during infection. In reality, macrophage polarization represents a spectrum of phenotypes and not that of two extremes (70). The timing at which these cells are recruited or converted during infection is also not as immediate as once predicted. Recently, the existence of a subset of macrophages possessing phenotypic similarities of both M1 and M2 macrophages was discovered (71). They have been classified as a resolution-phase macrophage (rM) (71). As the name implies, these cells may be important in resolution and tissue homeostasis after insult or injury (71). Resolution-phase macrophages generally appeared to be M2 because they expressed mannose receptor (CD206) and produced IL-10 and arginase, but also produced nitric oxide much like

an M1 macrophage (71, 72). Because they possess a phenotype resembling both M1 and M2 cells, rMs exist somewhere on the varied macrophage polarization spectrum. Genetic control of rM's was unique from both M1 and M2 macrophages (72). *In vitro*, increasing the levels of cAMP in M1-polarized macrophages pushed them into an rM phenotype, indicating cAMP acts as an immunomodulator of macrophages (71). A role for rMs during infectious disease has not yet been elucidated.

CHAPTER II

MATERIALS AND METHODS

A. Materials

1. Animals

Female C3H/HeJ (C3H) mice, age 4-6 weeks, were purchased from The Jackson Laboratory (Bar Harbor, ME).). C3H TLR2$^{-/-}$ N6 mice were generously provided by the Bockenstedt lab as breeders. B6 IL17RA$^{-/-}$ mice were donated by Dr. G. Zhang.

2. Bacteria and Infections

Stocks of virulent *B. burgdorferi*, N40 Passage 8 or GFP *B. burgdorferi* were provided by J. Weis, University of Utah. Barbour, Stoenner, Kelly (BSK) II medium with 6% rabbit serum was purchased from Sigma-Aldrich, St. Louis, MO. A Petroff-Hausser counting chamber was purchased from Hausser Scientific in Horsham, PA. Isoflurane (Terrell) was purchased through the University of Missouri Veterinary Medicine Teaching Hospital pharmacy.

3. RNA and DNA isolation and quantitative real-time (qRT) PCR

The Bead Beater homogenizer and 2.0mm Zirconia Beads were purchased from BioSpec Products, Inc., Bartlesville, OK. 2.0 mL siliconized screw-cap microcentrifuge tubes were from Bio Plas, Inc., San Rafael, CA. TRIzol reagent was obtained from Life Technologies, Carlsbad, CA. 100% ethanol was from AAPER Alcohol and Chemical Co, Shelbyville, KY while the choloroform and isopropanol were from Fisher Sceintific, Fair Lawn, NJ. TaqMan Universal PCR Master Mix and the ABI Prism 770 Sequence Detection System came from Applied Biosystems, Branchburg, NJ. Custom Taqman TAMARA labeled Nidogen and Flagellin probes

were obtained from Life Technologies, Carlsbad, CA. Custom Nidogen (F:5'AGGGCAGAATGCCTGAACC3' R:5'AGGATACTGGAGCCCTTCGAG) and Flagellin (F:5'TCTTTTCTCTGGTGAGGGAGC 3' R:TCCTTCCTGTTGAACACCCTCT3')-specific primers were from Integrated DNA Technologies, Coralville, IA.

4. *Determination of antibody levels*

Immulon 2B ELISA plates were purchased from Nalgene, Rochester, NY. The rat anti-mouse IgG was from AnaSpec, San Jose, CA and the goat anti-mouse IgM was from Southern Biotech, Birmingham, AL. Purified mouse IgG or IgM were both from Bethyl Laboratories, Inc., Montgomery, TX.

5. *ELISA and Luminex*

Protein was quantified using a Pierce BCA Protein Assay Kit from Thermo Scientific, Rockford, IL. The ELISA MAX Mouse IL-17A was purchased from BioLegend, San Diego, CA. Measurements were made using a SpectraMax Plus from Molecular Devices, Sunnyvale, CA. The Cytokine Mouse 20-Plex Panel from Life Technologies, Carlsbad, CA, was generously donated by Dr. J. Skyberg. It was run using the BioPlex 200 system from Bio-Rad Laboratories, Hercules, CA.

6. Flow Cytometry Cell Isolation and Cell Permeabilization

10x Phosphate Buffered Saline was obtained from Fisher Scientific, Fair Lawn, NJ and was diluted in water to a 1x concentration. Collagenase/dispase, Version 17 was obtained from Roche Diagnostics, Indianapolis, IN. DNaseI DN-25 was stored in 2mg/mL 50% glycerol, 75mM NaCl, all purchased from Sigma Aldrich, St. Louis, MO. RPMI Medium 1640 was from Life Technologies, Grand Island, NY. Fetal

Bovine Serum (FBS) was purchased from Sigma Aldrich, St. Louis, MO through the University of Missouri Cell and Immunobiology Core. The Foxp3 Intra-nuclear Staining Buffer kit was obtained from eBioscience, San Diego, CA. The Cytofix/Cytoperm Kit for use in intracellular staining for macrophages was obtained from BD in San Diego, CA.

7. *Depleting Antibodies*

Anti-mouse CD4 (GK1.5) and Anti-mouse CD8 (YTS-169) depleting antibodies were purchased from Leinco, Technologies, St. Louis, MO. Anti-mouse CD8 (YTS-156) depleting antibody was donated by Dr. H. Mullen from the University of Missouri.

8. Flow Cytometry Antibodies

Flow cytometry antibodies were obtained from eBioscience (San Diego, CA), Leinco (St. Louis, MO) and BioLegend (San Diego, CA).

Cell Marker	Fluorochrome	Company	Lot Number
CD45.2	PerCP-Cy5.5	eBioscience	E08342-1632
	APC	eBioscience	E07155-1631
F4/80	APC	eBioscience	E07285-1634
	APC-eFluor 780	eBioscience	E10234-1639
Ly6g	APC	Leinco	0114R230
B220	PeCy7	eBioscience	E07658-1633
	PE	eBioscience	E01247-1632
IgM	FITC		
CD19	PerCP-Cy5.5	eBioscience	E08314-1635
CD3e	PE-eFluor 610	eBioscience	E19379-101
	PE	eBioscience	E00992-1632
CD4	APC-eFluor 780	eBioscience	E16066-107
CD8	FITC	Leinco	0813L235
CCR6 (CD196)	eFluor 660	eBioscience	E16509-103
FOXp3	PerCP-Cy5.5	eBioscience	E08397-1633
NKp46 (CD335)	APC-eFluor 780	eBioscience	E20212-101
CD122	Pe-Cy7	eBioscience	E20270-101
CD11b	APC-eFluor 780	eBioscience	E10339-1635
CD5	Pe-Cy7	eBioscience	E07506-1634
NOS2	PE	eBioscience	E17913-104
CD206	APC	BioLegend	B179163
IFN-γ	PerCP-Cy5.5	eBioscience	E08425-1632
IgG	APC	BioLegend	B175712
CD16/CD32 (Fc Block)		eBioscience	E03559-1635
ICAM-1 (CD54)	DyLight 650	Leinco	0315R200
VCAM-1 (CD106)	FITC	eBioscience	E00458-1631

B. METHODS

1. *Animals*

C3H TLR-2 N6 heterozygous mice were donated and fully backcrossed to the 10^{th} generation onto the C3H/HeJ background. B6 IL-17RA$^{-/-}$ mice were donated as breeders and also backcrossed 10 generations onto the C3H/HeJ background. Animals were given sterile food and water ad libitum and housed in a specific pathogen free facility. All work was done in accordance with the Animal Care and Use Committee of the University of Missouri.

2. *Bacteria and Infections*

Stocks of virulent *B. burgdorferi*, N40 Passage 8 or GFP-labeled *B. burgdorferi* were grown in 7 mL of Barbour, Stoenner, Kelly (BSK) II medium with 6% rabbit serum in a 32^{o}C incubator for 5-6 days to log phase. The spirochetes were counted using a Petroff-Hausser counting chamber under dark field microscopy. For infection, bacteria were diluted in sterile BSK medium such that each mouse received $1x10^5$ bacteria. Mice were injected with 50uL of inoculum containing $5x10^4$ spirochetes in each hind footpad. This produces reliable arthritis and inflammation in our mice. Ankle swelling was measured throughout the infection at the thickest craniocaudal portion of the joint using a metric caliper. For the *in vivo* phagocytosis assay, previously infected mice were injected with $2.25x10^7$ GFP-labeled *B. burgdorferi* in the footpad in a 30ul volume or in the craniocaudal joint space in a 5uL volume.

3. Tissue homogenization for DNA Isolation

Tissues were harvested and snap-frozen in liquid nitrogen. Samples were stored at -80^{o} C until extraction. 750µL of 2.0mm zirconia beads and 1mL of TRIzol were

added to 2.0 mL microcentrifuge tubes. Tissues were placed into tubes and placed in the Bead Beater homogenizer for 2 minutes. After homogenization, each sample was transferred out of the bead tube into a 1.5 mL microcentrifuge tube and incubated at room temperature for 5 minutes. The homogenized samples were then processed further for DNA extraction.

4. *DNA extraction*

To the homogenized tissue, 200uL of chloroform was added and tubes were vortexed for 10 seconds. Samples were incubated at room temperature for 15 minutes, and spun at 12,000g, 4^{o}C, 30 minutes. The aqueous phase was then discarded and 500µL of Back Extraction Buffer was added to the organic and interphase. This was allowed to incubate at room temperature for 10 minutes before being centrifuged at 12,000g, 4^{o}C, 15 minutes. Upon removal from centrifuge, samples were immediately placed on ice and 400µL of isopropanol was added. Samples were immediately vortexed and incubated at room temperature for 5 minutes. All samples were centrifuged again at 12,000g, 4^{o}C, 15 minutes and resulting supernatant was removed. Pellets were washed with 75% ethanol, dried, and resuspended in HPLC grade H_2O.

5. *B. burgdorferi load determination using qRT-PCR*

Real-time PCR was performed on the ABI Prism 7700 Sequence Detection System using TaqMan Universal PCR Master Mix. The Master Mix consisted of 10uL HPLC grade H_2O, 12.5 µL 2x TaqMan mix, 0.5uL 15µM Nidogen 5'3' primer mix, 0.5µL 15uM Flagellin 5'3' primer mix, 0.25µL 10pM Nidogen specific TAMARA labeled probe, and 0.25µL 10pM Flagellin specific TAMARA labeled probe. A total of 24µL of master mix and 1µL of DNA was added for each reaction, equaling a total of 25µL.

The program used for the real-time PCR was as follows: 50°C for 2 minutes, 45 cycles at 95°C for 20 seconds, and 1 minute at 60°C. Flagellin copies represent copies of *B. burgdorferi* per sample, while Nidogen copies represented copies of mouse DNA. Bacterial loads were expressed as copies of Flagellin per 1000 copies of Nidogen.

6. *Determination of antibody levels*

Sera of infected animals were collected and *B. burgdorferi*-specific IgM and IgG levels were detected using enzyme-linked immunosorbent assays (ELISAs) on Immulon 2B ELISA plates. For the IgM ELISA, two columns were coated as standards with 20ug/mL goat anti-mouse IgM in coating buffer (0.1 M bicarbonate puffer, pH 9.4). The rest of the plate was coated with 0.5ug/mL of *B. burgdorferi* antigen in coating buffer. For the IgG ELISA, two columns were coated as standards with 20ug/mL rat anti-mouse IgG in coating buffer. The rest of the plate was coated with 0.5 ug/mL of *B. burgdorferi* antigen in coating buffer. Plates were coated overnight at 4°C and washed with ELISA wash buffer (0.05% Tween-20 in 1x PBS). The plates were then blocked with 3% BSA in 1x PBS at room temperature for 1.5 hours. Standard curves were prepared using a 1:3 dilution of purified mouse IgM or IgG. Sera from individual mice were diluted in 3% BSA in 1x PBS and added in duplicate to the plate. The plate was incubated for 2 hours at room temperature and washed with ELISA wash buffer. Either a secondary alkaline phosphatase-conjugated rat anti-mouse IgM or a donkey anti mouse IgG antibody was added at a 1:1000 dilution. The plate was incubated at room temperature for 45 minutes, washed with ELISA wash buffer, and phosphatase substrate in 10% diethanolamine

buffer was added. The substrate was left to develop the plate at room temperature for 20-50 minutes. The plates were read at 405nm on a SpectraMax Plus.

7. *Protein Isolation from Murine Joints and Hearts*

Tissue samples were obtained in liquid nitrogen and stored in a -80^{o}C freezer until use. 1 mL of Hanks Balanced Salt Solution (HBSS) containing a 1:1000 dilution of Protease Inhibitor Cocktail (PIC) was added to a 2 mL cryovial. Samples were removed from liquid nitrogen and wrapped in aluminum foil. Tissues were pulverized using a hammer and placed into cryovials containing the HBSS and PIC solution. The samples were sonicated using an ultrasonic processor for 20 seconds at an amplitude of 60%. The samples were then centrifuged at 8000 rpm, 4^{o}C, 10 minutes. The supernatant was then filtered through a 3mL syringe with an attached 45um filter into a new cryovial, and placed on ice. To quantify the amount of protein obtained, a BCA protein assay was run according to manufacturer's suggestions.

8. *Cell Isolation from Ankles and Hearts for Flow Cytometry*

Ankles were removed from each mouse by removing the toes and carefully cutting through the knee joint, particularly to avoid bone marrow contamination. Excess muscle tissue was trimmed to reduce blood contamination. Hearts were perfused with 1x PBS, removed and cut into fine pieces. Both ankles and hearts were placed in 15 mL conical tubes containing 5mL 1xPBS +4%FBS, 75uL diluted DNaseI (.03mg), and 50uL stock collagenase/dispase (100mg/mL). Both were placed on a rocker at room temperature for 1 hour before being placed into sterile petri dishes with 5 mL of additional RPMI supplemented with 10% FBS. Ankles were carefully flayed apart using sterile rat tooth forceps. Cells from joints and hearts were strained through a 70

micron filter (BD Falcon) into a 50 mL conical tube. Cells were spun at 300g, 4^{o}C, 8 minutes. Supernatant was removed and cells were washed with 5mL 1xPBS+4%FBS three times. Cells were counted using Trypan Blue exclusion.

9. *Cell Staining for Flow Cytometry*

A total of 1x10^{6} cells were stained in a 96 well U bottom plate (Corning, Inc.). All wells were blocked using a 1:50 dilution of Fc Block (anti CD16/CD32) for 15 minutes at 4^{o}C. Cells were then stained for cell specific markers in the dark for 30 minutes, 4^{o}C. After staining, cells were washed and fixed in 1% paraformaldehyde for 15 minutes. Cell type was analyzed using the Dako Cyan flow cytometer and Summit V5.0 software.

10. Bone Marrow Derived Macrophage Isolation and Stimulation with B. burgdorferi

Bone marrow derived macrophages (BMDM) were obtained from C3H/HeJ mice. Mice were euthanized and de-gloved using rat-tooth forceps. Excess muscle was removed from the bones and cuts were made directly above the ankle and right below the knee to extract bone marrow from the tibia. Cuts were also made above the knee and at the hipbone to remove femur bone marrow. A 27G needle and 1mL syringe full of 1x PBS were used to displace the bone marrow from the bone into a petri dish containing pre-warmed 1x PBS. Cells were transferred from the plate into a 50 mL conical tube, washed, and resuspended in RPMI (70%) and L929 supernatant (30%). After 6 days, cells were counted and 1x10^{6} macrophages were seeded into a 12 well plate. An MOI of 10 *B. burgdorferi* were added to half of the wells and allowed to

incubate overnight. The following day, flow cytometry was run to analyze macrophage polarization.

11. In vitro Cell Isolation and Polarization of BMDM

Bone marrow cells were isolated from C3H mouse femurs and tibias and differentiated on 100 x 30 plastic petri dishes in medium containing RPMI 1640 supplemented with 30% L929 cell-conditioned medium, 10% FBS, and 2% penicillin-streptomycin at 37°C in 5% CO_2 for 6 days. Adherent cells were removed, washed, and plated in a 12-well plate at $1x10^6$ per well overnight. The cells were then stimulated with 1ug/ml IL-4 (Peprotech) or LPS (Sigma) and IFNγ (Peprotech) for 24 hours. Supernatant nitrite concentrations were determined by the Greiss reaction. Arginase activity was determined by incubating cell lysate with L-arginine for 1 hour and determining the amount of urea produced.

12. Isolation of Bone Marrow Neutrophils and GFP-labeled B. burgdorferi phagocytosis

Mice were sacrificed, and tibia and femurs were removed and placed into sterile petri dish. The bone marrow was washed out using a 27G needle and complete DMEM media. Bone marrow cells and media were spun at 500g for 10 minutes at 4^oC and supernatant was removed. 5mL of Ammonium-Chloride-Potassium (ACK) lysis was added and cells were placed on a rocker at room temperature for 5 minutes. Cells were washed with HBSS, supernatant was removed and cells were resuspended in 3mL of HBSS. These cells were layered on top of a Percoll gradient. The bottom of the gradient consisted of 3mL of 75% Percoll, the middle layer consisted of 65% Percoll, and the top layer consisted of 55% Percoll. The Percoll gradient containing

cells were spun at 500g for 30 minutes at room temperature. The 75% and 65% interface was where the neutrophils were located, and these cells were carefully removed and counted using Trypan Blue exclusion. $1x10^6$ neutrophils per well were co-cultured in a 6-well plate with an MOI of 10 GFP-labeled *B. burgdorferi* for 2 hours. Phagocytosis of GFP-labeled *B. burgdorferi* was measured using flow cytometry.

13. *T Cell Depletion*

Mice were treated with 400μg CD8 depleting antibody, 300μg CD4 depleting antibody, or sterile saline intraperitoneally (i.p.) one day prior to infection. Every 7 days, CD8 or CD4 depletion was maintained by giving an additional i.p. injection of 250μg or 100μg antibody, respectively. T cell depletion was verified by flow cytometric analysis.

14. *Assessment of Arthritis and Carditis Pathology*

Ankle swelling was measured throughout infections at the thickest craniocaudal portion of the joint using a metric caliper. Zinc-formalin fixed, paraffin embedded sections of ankle joints and hearts were stained with Hematoxylin and eosin (H&E) and blindly evaluated on a scale of 0-4 with 0 representing no inflammation and 4 representing severe inflammation in more than half of the section evaluated.

15. *In Vivo Phagocytosis Assay*

Mice were infected with *B. burgdorferi* as previously described. At day 22 post-infection, mice were injected with $2.25x10^7$ GFP-labeled *B. burgdorferi* in the rear footpads (30μL/footpad) or in the craniocaudal joint space (5μL/joint). After 1 hour, joints were harvested for flow cytometric evaluation as previously described.

16. Cultivation of Biphenotypic B/Macrophage Cells

Spleens were removed from each animal and placed into a 70 μm nylon cell strainer in a 35 mm tissue culture dish. 10mL of Dulbecco's Modified Eagle medium (DMEM) was added to the dish. Spleens were pushed through the filter using the plunger of a 1 mL syringe, creating a single cell suspension. Cells were placed into 15 mL conical tubes and centrifuged at 300g, 4^{o}C, 8 minutes. Supernatant was discarded and 5 mL of ammonium chloride potassium (ACK) buffer was added. Cells were vortexed and placed on a rocker at room temperature for 5 minutes. Cells were centrifuged again at 300g, 4^{o}C, 8 minutes and supernatant was discarded. Splenocytes were washed 2 times with DMEM. $2x10^{8}$ cells were then run on a Miltenyi B cell isolation kit using magnetic separation. $3x10^{6}$ B cells were plated in each well of a 12-well plate with 3mL RPMI with 10% FBS, 5mM HEPES, 2% penicillin/streptomycin, 40ng/mL M-CSF, and 5ng/mL GM-CSF. After 5 days, cells were rinsed to eliminate non-adherent B cells. The media was changed every 7 days, or as needed. Cultivation in this media reliably produced Biphenotypic B/Macrophage cells.

CHAPTER III

CELLULAR CHARACTERIZATION OF LYME BORRELIOSIS USING FLOW CYTOMETRY

A. *Introduction*

An efficient inflammatory response is critical to control *B. burgdorferi* infection. In a murine model of experimental Lyme borreliosis, it is primarily the innate arm of the immune system that is responsible for the pathogenesis associated with the disease and the elimination of *B. burgdorferi* from tissues, but the adaptive immune response also has a role (10, 73-75). Neutrophil influx into joint tissue results in effective clearance of spirochetes, but can also cause inflammatory tissue damage (19, 76). It is postulated that within the joint, neutrophils phagocytose *B. burgdorferi* most effectively, while macrophages primarily phagocytose exhausted neutrophils (73). During carditis, macrophages are the predominant innate immune cell responsible for inflammation (7). In addition, an efficient B cell response ensures proper antibody-mediated clearance of the spirochetes (14-16). Although the importance of T cell responses during Lyme arthritis is debated, it is well understood that $CD4^+$ T helper cells aid in resolution of carditis (32).

The groundwork literature within the Lyme disease field relied heavily on immunohistochemistry to identify cell types recruited to joint and heart tissue as well as disease severity. Histological staining of inflamed tissue has allowed for a qualitative assessment of the cellular infiltrate as well as the spatial relationship of

cells within the tissue. However, immunohistochemical staining lacks the ability to quantify cell numbers and is limited in that cells can only be stained for a limited number of markers at a time. Flow cytometry is a powerful tool which allows for multiple and simultaneous cell staining and reliable, specific cell counts. To our knowledge, flow cytometry has never been utilized to look at both innate and adaptive immune cells infiltrating the tissues of *B. burgdorferi*-infected animals throughout the infection time course. Others in the field have used flow cytometry to assess cells within infected joint tissue, but have done so at a very limited number of time points (77, 78).

The study presented herein describes a novel technique in which flow cytometry was used to analyze cellular infiltration into both joint and cardiac tissue. Using this technique, we describe the cellular infiltration into the tissues throughout the time course of experimental murine Lyme borreliosis. We were also able to determine the percentage of innate and adaptive immune cells capable of phagocytosis in an *in vivo* system. We believe that by more thoroughly understanding the time of when immune cells infiltrate the tissue, and the numbers in which they do so, we will more thoroughly understand the microenvironment created in that tissue during infection.

B. *Results*

1. *Cellular Infiltration into the B. burgdorferi-infected ankle joint.*

WT C3H mice were infected with $1x10^5$ *B. burgdorferi* in each hind footpad. The progression of arthritis was monitored by measuring swelling at the thickest craniocaudal portion of the joint using metric calipers. Figure 3.1 shows the ankle swelling curve which is typical of *B. burgdorferi* infection, and is usually indicative of underlying inflammation (79). Joint swelling began as early as 7 days post-infection, peaked around day 28, and resolved shortly after (Figure 3.1). At specific time points during infection, ankles were removed, single cell suspensions were made, and cells were stained for flow cytometry. Cellular infiltration was quantified using flow cytometry and cell-specific markers (see Chapter 2). Mirroring the swelling curve, $CD45.2^+$ hematopoietic cells infiltrated the ankle joint as early as day 7 post-infection and numbers continued to increase within the joint until day 28 post-infection, and then decreased as resolution of the inflammation occurred (Figure 3.2A). $CD3e^+$ T cells made up the smallest population of hematopoietic cells within the joints at all time points during infection. Numbers of T cells were significantly elevated over uninfected controls at day 28 post-infection and as resolution occurred at days 45 and 60 (Figure 3.2B). Mature $Ly6g^{hi}$ neutrophils mediate disease pathogenesis in ankle joints (76) and were significantly increased at day 28 post-infection. The majority of $CD45.2^+$ hematopoietic cells within the ankle joint during infection were mature neutrophils. This population decreased as resolution occurred (Figure 3.2C). $Ly6g^{lo}$ cells, representing a combination of immature neutrophils and monocytes (80), followed a similar trend. Their numbers remained significantly

elevated over uninfected controls at day 28 post infection. (Figure 3.2D). The second largest cell population identified within the infected joint was F4/80^{+} macrophages, and their numbers peaked at day 28 post-infection (Figure 3.2E). B cells, identified based on expression of B220, were also significantly elevated at the peak of inflammation at day 28. At all other time points, their numbers were not statistically increased over those of uninfected controls (Figure 3.2F).

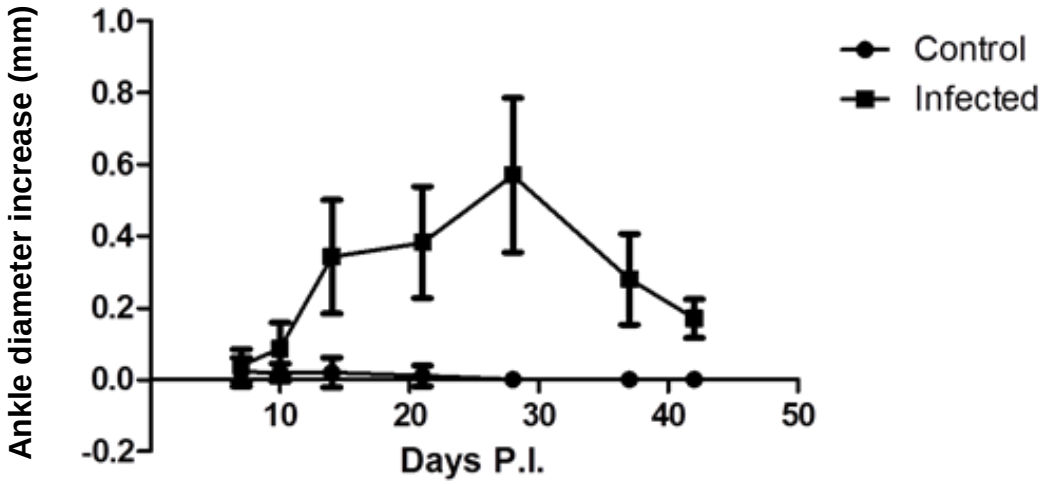

Figure 3.1: Ankle swelling was measured using metric calipers at the largest craniocaudal portion of the rear ankle joint over the infection time-course. n=5, representative of two separate experiments. Symbols represent means +/- SD.

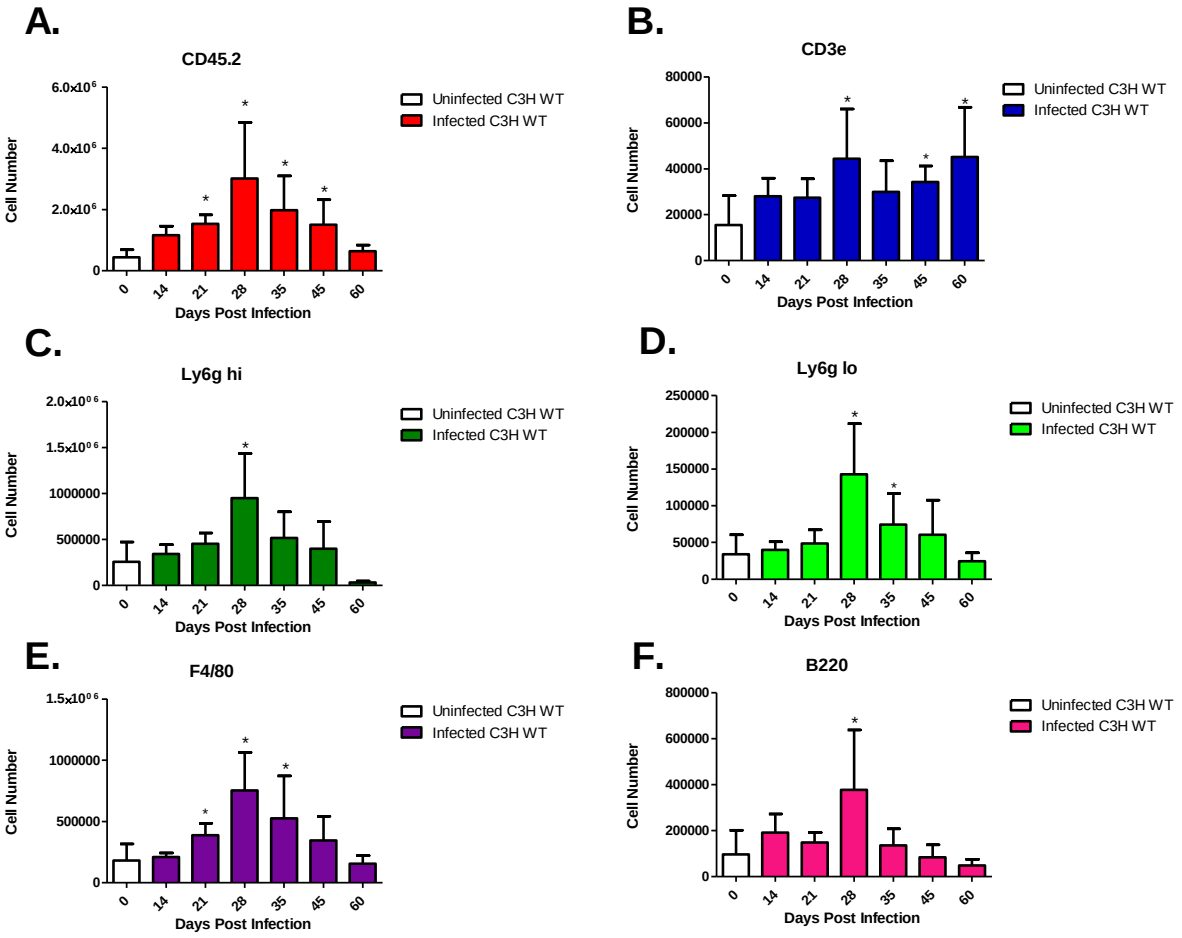

Figure 3.2: Innate and adaptive immune cells infiltrating the ankle joints were characterized using cell specific markers by flow cytometry. Cells were stained for $CD45.2^{+}$ hematopoietic cells (A), $CD3e^{+}$ T cells (B), $Ly6g^{hi}$ neutrophils (C), $Ly6g^{lo}$ monocytes/immature neutrophils (D), $F4/80^{+}$ macrophages (E), and $B220^{+}$ B cells (F). Cell numbers are representative of two joints. n=5, representative of two separate experiments. Bars represent means +/- SD.

2. *Phagocytosis of GFP-labeled B. burgdorferi.*

WT C3H mice were infected with $1x10^5$ *B. burgdorferi* in the hind footpads. At day 22 post-infection, mice were injected with GFP-labeled *B. burgdorferi* directly into the hind footpad. After one hour, mice were sacrificed and joint cells were isolated and stained for neutrophils, macrophages, and B cells as described earlier. Co-staining of GFP and cell-specific markers represented uptake of the bacteria. Neutrophils, the dominant cell type recruited to the joint after infection, showed the greatest uptake of GFP-labeled bacteria (Figure 3.3). Macrophages displayed a slightly lower uptake of bacteria when compared to neutrophils. B cells, while still able to take up bacteria, displayed a much reduced ability to do so (Figure 3.3). During *B. burgdorferi* infection, neutrophils are responsible for the majority of bacterial uptake.

3. *Cellular infiltration into the B. burgdorferi-infected heart.*

WT C3H mice were infected with $1x10^5$ *B. burgdorferi* in the hind footpads and infiltration of both innate and adaptive immune cells were monitored throughout a carditis time course. Hearts were removed, and cells were isolated and stained for cell-specific markers (see Chapter 2). $CD45.2^+$ hematopoietic cells peaked at day 21 post-infection and were significantly elevated over uninfected control populations (Figure 3.4A). $CD3e^+$ T cell numbers increased at day 7 post-infection, but were not significantly increased compared to uninfected control populations at any time point (Figure 3.4B). The number of infiltrating $Ly6g^{hi}$ mature neutrophils was significantly increased at day 21 post-infection over control animals, but by day 35, those numbers

had decreased to control levels (Figure 3.4C). $F4/80^+$ macrophage numbers were significantly elevated at days 14 and 21 post-infection, and were the dominant infiltrating cell population within the heart tissue throughout the infection (Figure 3.4D). $B220^+$ B cell numbers within the heart tissue were comparable to uninfected mice at all time points apart from day 21 post-infection when their numbers were significantly increased (Figure 3.4E).

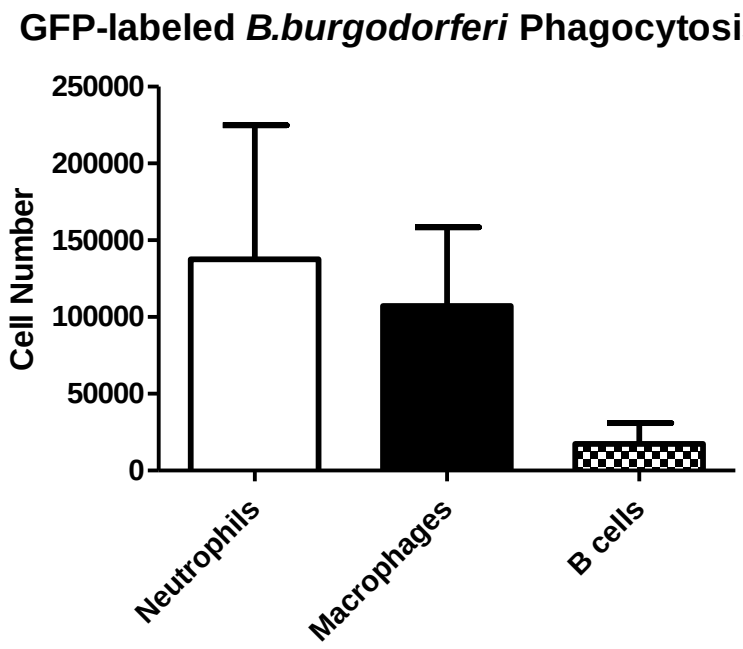

Figure 3.3: Phagocytosis of GFP-labeled *B. burgdorferi* in joint tissue was quantitatively measured using flow cytometry. Phagocytosis was measured by analyzing co-expression of GFP with a neutrophil specific marker (Ly6g), a macrophage specific marker (F4/80), or a B cell specific marker (B220). n=4, representative of 3 separate experiments. Bars representative of means +/- SD.

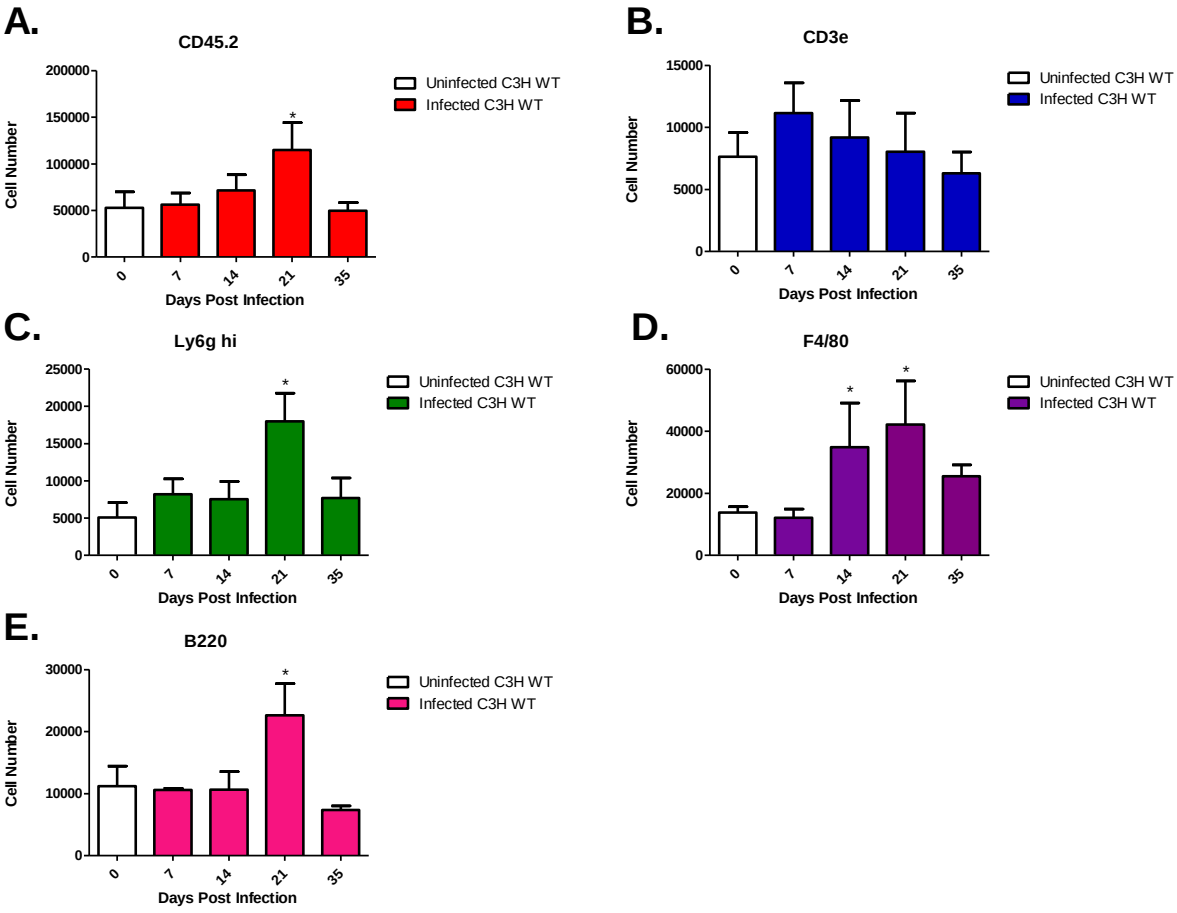

Figure 3.4: Innate and adaptive immune cells infiltrating the hearts of *B. burgdorferi*-infected mice were characterized throughout the infection using cell specific markers for flow cytometry. Cells were stained for $CD45.2^{+}$ hematopoietic cells (A), $CD3e^{+}$ T cells (B), $Ly6g^{hi}$ neutrophils (C), $F4/80^{+}$ macrophages (D), and $B220^{+}$ B cells (E). n=5, representative of two separate experiments. Bars represent means +/- SD.

C. *Conclusions*

Much work within the Lyme field has utilized immunohistochemistry to understand the immune response to *B. burgdorferi*. Here, we have established a method using flow cytometry to evaluate and quantify inflammatory cell infiltration into *B. burgdorferi*-infected murine ankle joint and heart tissue. The C3H/He mouse model of experimental Lyme disease has been used for years to study the inflammatory response to *B. burgdorferi* (11, 17). It is known that arthritis and carditis occur about two weeks after infection and both spontaneously resolve 6 to 8 weeks post-infection (10). Inflammation in response to *B. burgdorferi* infection is predominantly driven by neutrophils in the ankle joints and macrophages in the hearts. Shortly after peak infiltration of innate immune cells, spirochetes are cleared from the tissue and disease resolves; the entire process occurs in approximately 8 weeks (10). Ankle swelling measurements and histologic evaluation of tissues are both used to determine severity of experimental Lyme arthritis. In the current study, swelling began as early as 7 days post-infection and progressively increased through day 28, which agrees with previous literature (10). By day 45 post-infection, ankle diameter had nearly returned to pre-infection size, possibly indicating resolution had occurred (10). The first goal of our study was to use flow cytometry to characterize the cellular infiltrate in the ankle joint tissue throughout the infection time-course, as this method was new to the field and very little work had been done assessing cells directly from ankle tissue.

We began by assessing joints for hematopoietic cell infiltrates at day 14 post-infection, just as swelling was beginning. $CD45.2^{+}$ hematopoietic cells increased at day 14 post-infection, but were not significantly different from uninfected controls until day 21. Hematopoietic cell infiltration peaked in unison with ankle joint swelling at day 28 post-infection and decreased shortly after. Gating on hematopoietic cells, we also analyzed T cell, neutrophil, macrophage and B cell infiltrating populations. Of all the cells analyzed, $CD3e^{+}$ T cells made up the lowest fraction of the cellular infiltrate. Although it was known that innate immune cells mediate initiation of disease, it had long been hypothesized that T cells may exacerbate disease manifestations in experimental Lyme arthritis (28). The adoptive transfer of $CD4^{+}$ T cells into infected B6 RAG-1 mice exacerbated arthritis, indicating a role for T cells in disease manifestation (28). Our study, although in C3H/HeJ mice, demonstrated an elevated number of $CD3e^{+}$ T cells within the infected joint at day 28 post-infection and this population reduced again as resolution occurred. An elevation of T cells near the time of resolution is puzzling because it has been shown that resolution can be mediated in a T cell-independent manner, despite the potential benefit of having T-cell help in antibody production (35). The importance of T cells in *B. burgdorferi*-induced arthritis continues to be debated. Unlike T cells, neutrophils play an undeniable role in disease pathogenesis associated with Lyme arthritis. $CXCR2^{-/-}$ mice, which are unable to recruit neutrophils into the joint, had a significant reduction in arthritis severity (18). This demonstrated the importance of chemokine mediated recruitment of neutrophils in disease development (18). In the current study, neutrophils made up the majority of the joint cellular

infiltrate at each time-point assessed and numbers were significantly higher at day 28 post-infection, the peak of inflammation. Two populations of $Ly6g^{+}$ cells were found within the joint: $Ly6g^{hi}$ and $Ly6g^{lo}$. It has been determined that a high expression of Ly6g represents mature neutrophils while low expression represents immature neutrophils and monocytes (80). The number of low $Ly6g^{+}$-expressing cells was much reduced compared to the $Ly6g^{hi}$ population. Elucidating inflammatory and non-classical monocytes from this $Ly6g^{lo}$ population is an area of future study.

Macrophages were another innate immune cell known to be recruited to the ankle joints during *B. burgdorferi* infection, and it is thought that their main role is the clearance of exhausted and apoptotic neutrophils (22). The ability of macrophages to take up apoptotic cells is critical for the efficient resolution of arthritis (81). 5-lipoxygenase (5-LO)-deficient mice infected with *B. burgdorferi* displayed a defect in macrophage phagocytosis of apoptotic cells and developed persistent arthritis (81). $F4/80^{+}$ macrophages accounted for the second largest population of infiltrating immune cells identified within the ankle joints. From day 21 to day 35 post-infection, their numbers were significantly elevated compared to uninfected controls. Like macrophages, B cells are also critical in resolution of disease by producing *B. burgdorferi*-specific antibodies aiding in efficient clearance of spirochetes (74). Transfer of naïve B cells or antibodies, but not $CD4^{+}$ T cells into infected RAG-1 mice induced arthritis resolution (35). We found that during experimental Lyme arthritis, B cell numbers remained relatively low at all time points assessed apart from day 28, which was the peak of inflammation. At this point, B cell numbers were

significantly elevated above uninfected controls. It is likely that the B cells at this time-point are actively producing *B. burgdorferi*-specific antibodies, aiding in disease resolution.

During experimental Lyme borreliosis, efficient clearance of spirochetes appears to be critical in resolving inflammation in both ankle joint and heart tissue (74). Neutrophils efficiently phagocytose and destroy *B. burgdorferi* (19), but both macrophages and B cells are also capable of bacterial clearance (82-84). To better understand the role of these immune cells in spirochete clearance, we performed an *in vivo* phagocytosis assay in *B. burgdorferi*-infected joints. C3H WT mice were infected with $1x10^5$ *B. burgdorferi* in the hind footpads and at day 22 post-infection, $2.25x10^7$ GFP-expressing *B. burgdorferi* were injected directly into each hind footpad. Uptake of *B. burgdorferi* by each cell type was measured by GFP fluorescence using flow cytometry. Although neutrophils were potent phagocytes, macrophages were also highly efficient in bacterial uptake. It is unknown whether macrophages had phagocytosed the bacteria alone or neutrophils containing GFP-labeled *B. burgdorferi*. Using confocal microscopy, we witnessed no evidence of macrophage uptake of phagocytic neutrophils, but this is still a possibility. It has been demonstrated that B cells are capable of both antigen presentation to $CD4^+$ T cells and phagocytosis of bacteria (82, 83). In experimental Lyme arthritis, we found that B cells were capable of phagocytosis of *B. burgdorferi* spirochetes, but did so very poorly compared to neutrophils and macrophages. We also investigated whether injection of the same number of GFP-expressing *B. burgdorferi* directly into the joint

capsule would alter cellular uptake of the bacteria, but the trend was identical to that of the footpad injection. Overall, the only detectable difference was that fewer cells took up the bacteria. We believe this was due to the limited volume that can be injected into each joint (5uL). To our knowledge, this was the first *in vivo* phagocytosis assay to be performed in joint tissue. Currently, phagocytosis assays are typically performed using an *in vitro* system. Phagocytic cells are derived from bone marrow and co-cultured with bacteria or beads. After a set amount of time, phagocytosis can then be measured by either flow cytometry or confocal microscopy. Our method may prove to be a more physiologically relevant way in which to determine cellular phagocytosis efficiency or phagocytic defects, as in the 5-LOX-deficient mice in which macrophages display a defect in phagocytosis *in vitro* (81).

Lyme carditis is an often overlooked manifestation of Lyme disease, but is just as relevant to human disease as arthritis (4). Approximately 2-8% of humans chronically infected with *B. burgdorferi* develop carditis (2). Humans that develop Lyme carditis suffer varying severity of atrioventricular blocks, ventricular tachycardia and bradycardia (6, 7). In biopsies taken from patients of both fatal and non-fatal *B. burgdorferi*-induced carditis, spirochetes were detected within the myocardium (6). The potential for fatality in Lyme carditis patients makes studying the immune response and spirochete clearance with the hearts important.

Our final goal of this current study was to determine the cellular makeup of the inflammatory infiltrates into the *B. burgdorferi* infected heart over time. Similar to

experimental Lyme arthritis, development of carditis is innate immune cell driven and disease resolution is primarily mediated by the adaptive immune system (20, 32). To better understand the most appropriate time points in which to study different cellular infiltrates, we stained for innate and adaptive immune cells in *B. burgdorferi*-infected mice at time-points corresponding to the induction, peak and resolution of carditis (85). $CD45.2^{+}$ hematopoietic cells became significantly elevated at day 21 post-infection, indicating the peak of the inflammatory cell infiltrate. Although T cells were elevated on days 7, 14, and 21 post-infection, their numbers were not elevated over control animals. This was unexpected as TNF-α-producing $CD4^{+}$ Th1 cells were shown to facilitate disease resolution in murine Lyme carditis (32). As in experimental Lyme arthritis, neutrophil recruitment into cardiac tissue is thought to partially mediate disease pathogenesis (76). C3H $KC^{-/-}$ mice, which cannot signal through the CXCR2 receptor, failed to recruit neutrophils into the *B. burgdorferi*-infected heart. This resulted in significantly decreased disease severity at day 21 post-infection (76). In another study, mice deficient in the macrophage chemokine receptor CCR2 displayed a defect in macrophage recruitment to the *B. burgdorferi*-infected heart (22). As a compensatory mechanism, these mice displayed significantly elevated numbers of neutrophils in heart tissue and developed more severe carditis (22). In the current study, we found a significant increase in $Ly6g^{hi}$ neutrophils at day 21 post-infection, which correlated with the peak of disease. We did not find two separate populations of Ly6g expressing cells within the infected heart tissue. This suggested that there were no immature neutrophils recruited to the heart tissue. Neutrophils are potent inflammatory cells, but previous studies have

shown that macrophages were the predominant cellular infiltrate during carditis and drove much of the inflammation (7). In our study, F4/80^{+} macrophages were the predominant cell type within the heart throughout the infection time course. At day 35 post-infection, macrophage cell numbers had decreased but were still well above all other cellular infiltrates. As in experimental Lyme arthritis, *B. burgdorferi*-specific antibody production by B cells was critical in clearance of spirochetes from infected heart tissue (74). Similar to what we described during experimental Lyme arthritis, a significant increase in B220^{+} B cells was seen at the peak of inflammation during experimental Lyme carditis. At no other time point were B cell numbers significantly elevated. It has been established that B cells are not required for the resolution of experimental Lyme carditis (32). While transfer of immune mouse serum is effective in resolving experimental Lyme arthritis, it does not aid in carditis resolution (32).

Prior to this study, the conventional method of studying the cellular infiltrate and inflammation of the tissues during experimental Lyme borrreliosis was using histological techniques. While histology has increased our understanding of what is occurring at the site of inflammation, it is limited to a qualitative analysis of a small section of tissue. Flow cytometry allows for a more quantitative assessment of the whole tissue. By perfecting a new technique for the field, we are able to assess deeper questions about the cellular make-up of the infiltrating population of inflammatory cells during Lyme borreliosis.

CHAPTER IV

MACROPHAGE POLARIZATION IN MURINE LYME BORRELIOSIS

A. *Introduction*

Macrophages play a dynamic role in the immune system as both inflammatory and anti-inflammatory mediators. Their phenotype is highly flexible and dependent on the cytokine stimulus of the microenvironment they infiltrate (66). They are routinely classified as proinflammatory and immunomodulatory (M1) or anti-inflammatory and remodeling (M2) macrophages, but their phenotype actually lies within a spectrum of inflammatory to anti-inflammatory polarization (86). The language within the field is currently being modified to ensure that the macrophages being studied have a clear phenotypic description. Within the last fifteen years, much work has been done to phenotypically characterize each subset. Identifying unique surface and intracellular markers, as well as understanding transcriptional regulation, has allowed the importance of macrophage phenotype in infectious and autoimmune models to begin to be uncovered.

Despite increasing interest in macrophage polarization in infectious disease models, macrophage phenotype has not been fully appreciated within the Lyme disease field. Although it is known that the inflammatory response in the joints to *B. burgdorferi* infection is mediated by neutrophils, macrophages appear to drive inflammation during Lyme carditis (22). Understanding the polarization status of macrophages throughout a Lyme disease time course may help us understand the mechanisms that

drive both the development of inflammation and its resolution. Currently, we know that macrophages are capable of phagocytosing and degrading *B. burgdorferi* within lysosomes (87). Their numbers become elevated near the onset of disease resolution and they actively eliminate exhausted neutrophils, potentially inducing resolution (81). It is yet unclear as to whether polarization into M1, M2, or resolution phase macrophages (rM) correlates to different stages of the immune response to *B. burgdorferi*. In order to understand this, we used flow cytometry to analyze macrophage phenotype at key time-points representing the induction, peak, and resolution of inflammation during experimental Lyme disease.

B. *Results*

1. *Macrophage polarization in vitro with B. burgdorferi.*

Bone marrow derived macrophages (BMDM) are commonly used in Lyme disease research to study *in vitro* macrophage responses to *B. burgdorferi* (45, 88-90). Following their culture and differentiation in our laboratory, unstimulated cells appeared to take on an uncommitted or M2 phenotype as determined by flow cytometry expression of CD206 and a lack of NOS2 expression (Figure 4.1A). NOS2 and CD206 are commonly used markers to identify M1 and M2 macrophages, respectively. Upon co-culture with *B. burgdorferi* for 24 hours, BMDM from C3H WT mice became primarily M1-like cells, down-regulating their expression of CD206 and increasing their expression of NOS2 (Figure 4.1A). They also acquired the M1-like ability to produce NO (Figure 4.1B). Interestingly, a small population of cells appeared to express both NOS2 and CD206. Whether these cells were in the

process of transitioning from the M2 to M1 phenotype or represent a separate macrophage state, such as the rM described by Bystrum et. al (71), is unclear at the present time. However, it is clear that BMDM adopt an M1-like phenotype when cultured with *B. burgdorferi in vitro*.

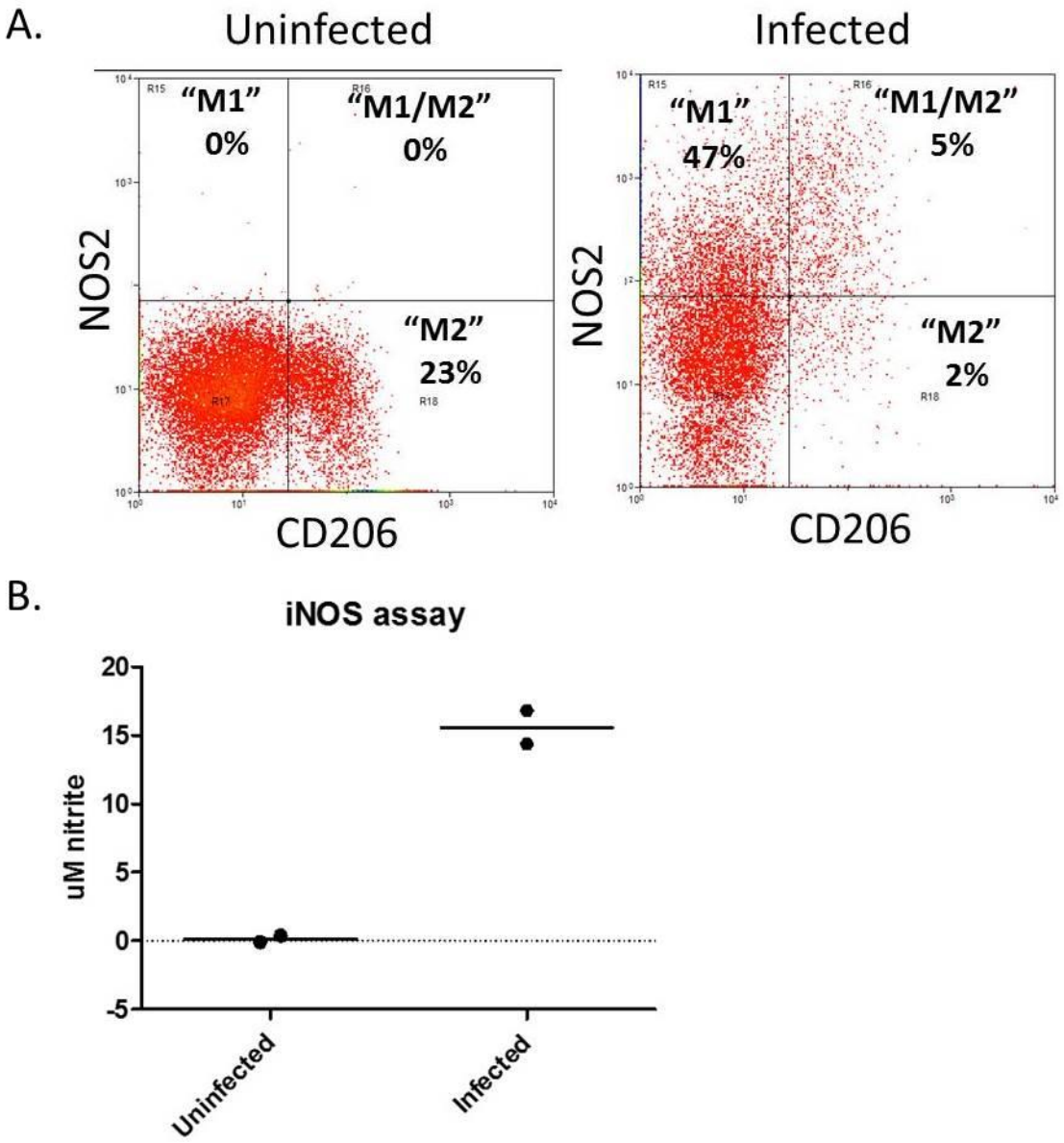

Figure 4.1: *In vitro* characterization of BMDM from C3H WT mice. BMDM were cultured with (infected) or without (uninfected) *B. burgdorferi* spirochetes (MOI 10:1) for 24 hours. Cell suspensions were gated on live, F4/80^{+} macrophages and then assessed for expression of CD206 and NOS2. Representative flow plots are shown. Percentage of F4/80^{+} cells expressing NOS2 (M1), CD206 (M2), or both NOS2 and CD206 (M1/M2) are presented (A). Levels of endogenous nitrite produced in uninfected and infected BMDM were analyzed using the Greiss reagent method (B). Each symbol represents a single culture, dotted line represents the limit of detection of the assay. Results are indicative of one trial.

2. *Flow cytometric evaluation of macrophage phenotype.*

In a murine model of Lyme disease, inflammation occurs within the ankle joints and the heart (11, 17, 91). While several researchers have used flow to analyze cellular infiltrates within cardiac tissue, very few have used flow cytometry to analyze cells from joint tissues. The large amount of non-hematopoietic cells and cellular debris within joint tissue can make cellular infiltrates into joint tissue difficult to analyze by flow cytometry. To overcome this unique challenge, we developed a gating strategy that allowed us to hone in on the primary macrophage subsets of interest. We began by setting a live gate around cells of interest on a forward versus side scatter plot (Figure 4.2A). Using this gate, we then identified hematopoietic cells using a CD45.2 stain (Figure 4.2B). Maintaining both the live and CD45.2 gates, we analyzed cellular infiltrates for $F4/80^{+}$ macrophage infiltration. This gate represented the percentage of macrophages within the total joint tissue (Figure 4.2C). Maintaining the previous three gates, the macrophages within the infected joints were further assessed using the M2 and M1 markers CD206 and NOS2, respectively (Figure 4.2D). It was readily apparent that macrophage polarization within joint tissue was not as clean or straightforward as that described *in vitro*. However, at d21 post-infection we were able to distinguish both M1-like ($F480^{+}NOS2^{+}CD206^{-}$) and M2-like ($F4/80^{+}NOS2^{-}CD206^{+}$) macrophages in the joints of *B. burgdorferi*-infected C3H WT mice. In addition, we noticed a small population of macrophages that expressed both CD206 and NOS2. At day 21 post-infection we expected these cells to be macrophages in an intermediate stage. However, by day 56 post-infection we saw a dramatic increase in $CD206^{+}NOS2^{+}$ macrophages. This time point coincides with

resolution of the inflammatory response in the joint. Other groups have shown that rM peak as inflammation resolves and they possess a phenotype expressing both M1 and M2 macrophage subset markers. Based upon the time of infiltration and the shared surface expression, we believe this dual marker expressing population represents resolution phase macrophages that may possess a pro-resolution phenotype (Figure 4.2E and 4.2F).

3. *Macrophage phenotype over the course of murine Lyme arthritis.*

To our knowledge, there are no reports analyzing how macrophage phenotype changes over the course of Lyme arthritis. Although neutrophils are known to dominate the early immune response (10), it has been suggested that M1 macrophage polarization may aid in early inflammation. We and others have hypothesized that M1-like ($F4/80^{+}NOS2^{+}CD206^{-}$) macrophages would be seen early during the initiation of inflammation and M2-like ($F4/80^{+}NOS2^{-}CD206^{+}$) macrophages would be seen near the time of disease resolution. C3H WT mice infected with $1x10^{5}$ *B. burgdorferi* developed swelling of the ankle joints, which was measured every 7 days throughout the infection time course. Ankle swelling peaked at day 28 post-infection and tapered off shortly after (Figure 4.3F). Hematopoietic cell numbers ($CD45.2^{+}$) in the joints of *B. burgdorferi*-infected mice gradually increased until day 21 post-infection and then slowly dissipated as the infection was cleared. This influx and outflow of inflammatory cells mirrored the ankle swelling curve (Figure 4.3A). A similar trend was seen for the $F4/80^{+}$ macrophages (Figure 4.3B). In contrast to our hypothesis, $CD206^{+}NOS2^{-}$ M2-like macrophages dominated the macrophage pool

throughout the infection in the joint, even at early time points. Their numbers peaked at day 14 post-infection as the inflammatory response was building (Figure 4.3D). Throughout the time-course, M2-like ($F4/80^{+}NOS2^{-}CD206^{+}$) macrophages always outnumbered their M1-like ($F4/80^{+}NOS2^{+}CD206^{-}$) counterparts. NOS2 expressing M1-like macrophage numbers peaked at day 21 post-infection, directly before the peak of ankle joint swelling (Figure 4.3C). M1 ($F4/80^{+}NOS2^{+}CD206^{-}$) macrophages are capable of producing high levels of nitric oxide species and other pro-inflammatory cytokines, so despite their presence in lower numbers, it may be possible that they remain capable of initiating or prolonging the inflammatory response seen in experimental Lyme arthritis. It is also possible that neutrophils, not M1 ($F4/80^{+}NOS2^{+}CD206^{-}$) macrophages, are largely responsible for the inflammatory response seen. Many of the cellular and molecular drivers of inflammation within Lyme arthritis are understood. However, the cellular mechanisms that drive the spontaneous resolution seen in this model are not known. Resolution phase macrophages are now being appreciated in some infectious disease models, but have not been examined within the Lyme disease field. Here, we define resolution phase macrophages as macrophages that express both NOS2 and CD206. We identified a larger population of NOS2/CD206 co-expressing macrophages within the joints at the time of disease resolution. The microenvironment created within the joint after day 35 post-infection may contribute to the emergence of this unique phenotype (Figure 4.3E). Although future research is necessary, our data suggests that rM may have an unappreciated role in the resolution of Lyme arthritis.

4. Macrophage phenotype over the course of murine Lyme carditis.

Lyme carditis differs from that of arthritis in that macrophages are considered to be the primary inflammatory cell (22). We therefore hypothesized that macrophage polarization would play a more prominent role in the hearts of *B. burgdorferi*-infected mice. We stained for $CD45.2^{+}$ hematopoietic cells, which we found peaked at day 21 post-infection (Figure 4.4A). High numbers of $F4/80^{+}$ macrophages were seen in the infected heart tissue at days 14 and 21 post-infection (Figure 4.4B). Unlike what we discovered in the ankle joints, M1-like ($F4/80^{+}NOS2^{+}CD206^{-}$) macrophages were found to be present in slightly greater numbers than M2-like ($F4/80^{+}NOS^{-}CD206^{+}$) macrophages (Figure 4.4C and 4.4D). Within the heart, M1-like polarized macrophages may be initiating much of the inflammation seen. M2-like ($F4/80^{+}NOS2^{-}CD206^{+}$) macrophages increased in number at day 56 post-infection, indicating a role in resolution. What is evident is that rM accounted for a low number of macrophages within the heart at any time point, especially at the time of resolution. It appeared that they did not play a significant role in the resolution of carditis, although their presence at days 14 and 21 post-infection may indicate a macrophage in transition from an M1-like ($F4/80^{+}NOS2^{+}CD206^{-}$) cell to an M2-like ($F4/80^{+}NOS2^{-}CD206^{+}$) cell (Figure 4.4E).

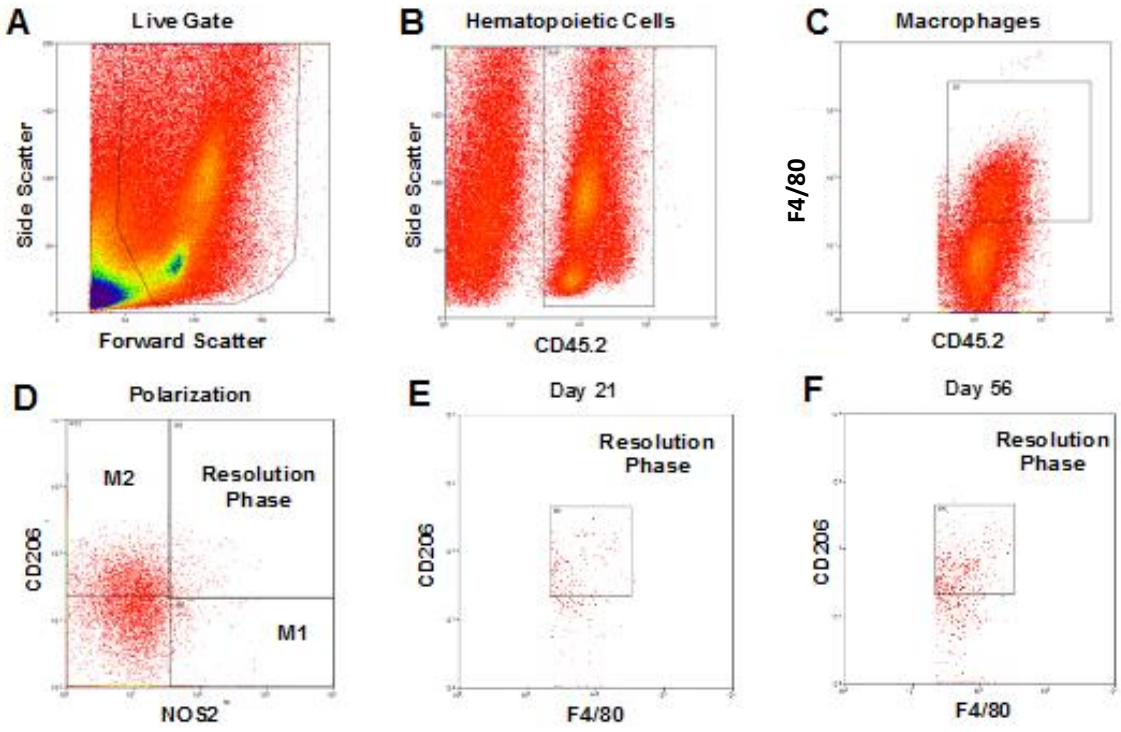

Figure 4.2: Cells from ankle joints were isolated. Hematopoietic cells were determined (B) from live gated cells (A). Macrophages ($F4/80^{+}$) were selected using previously set live and hematopoietic cell gates (C). Macrophage phenotype was further investigated by surface expression of NOS2 and/or CD206 (D). Resolution phase macrophage numbers (NOS2/CD206 double-positive cells) increased from day 21 (E) to day 56 (F). n=4, results representative to two separate experiments.

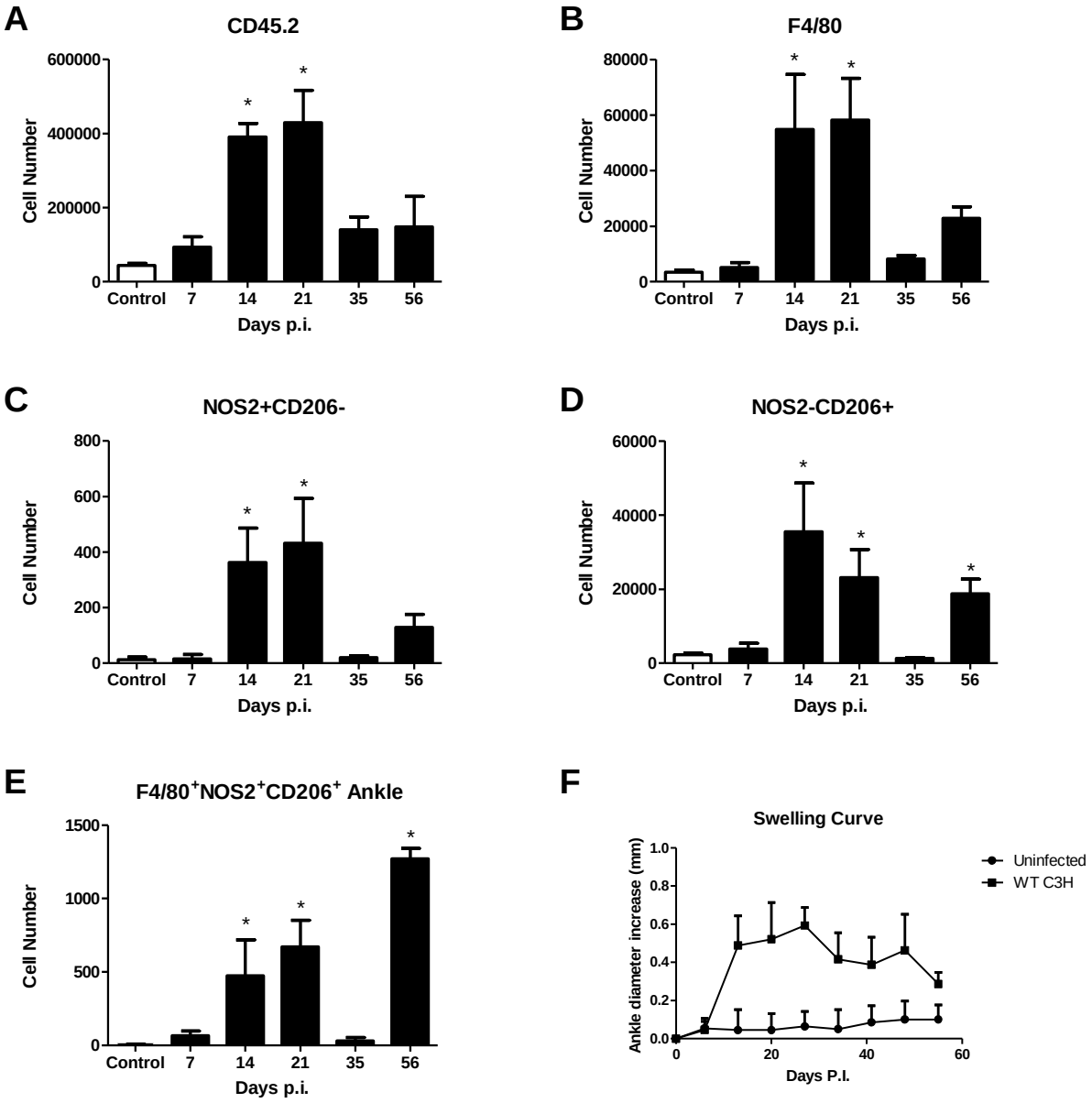

Figure 4.3: Macrophage phenotype was characterized in *B. burgdorferi*-infected ankle joints throughout the infection time-course. Swelling of the ankle joints were measured using metric calipers on a weekly basis (F). Joints were harvested at specific time points throughout the infection and cells were isolated and gated as described in Figure 2. Hematopoietic cell numbers (A) and macrophage numbers (B) were determined at each time point. The number of NOS2+CD206- (C), $NOS2^{-}CD206^{+}$ (D) and $NOS2^{+}CD206^{+}$ (E) cells within the joints were described throughout the infection. n=4, results representative of two separate trials. Bars represent means +/- SD. * indicate data is significantly different from control data at the $p<0.05$ level determined by ANOVA followed by Dunnett's test.

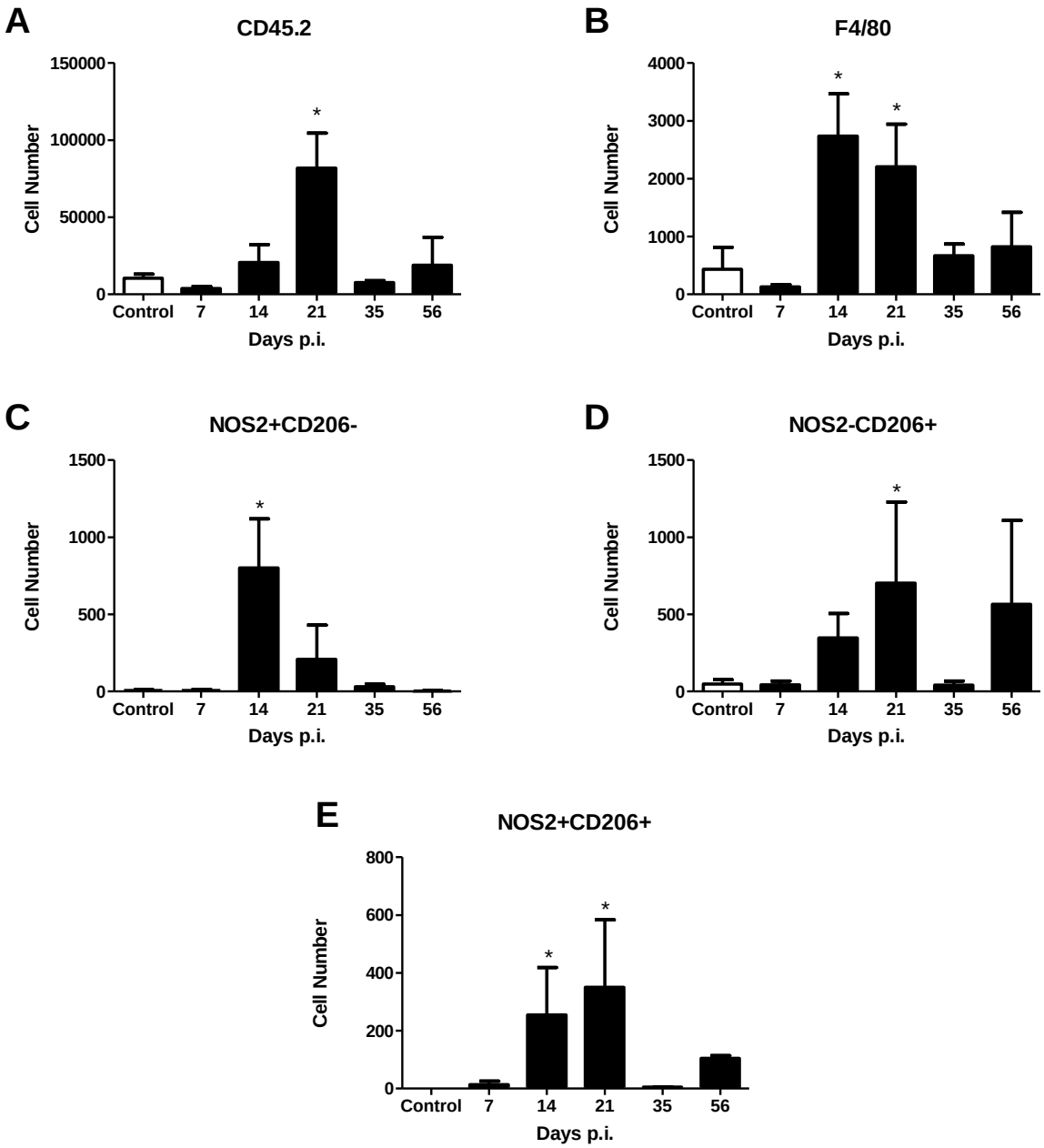

Figure 4.4: Macrophage phenotype was characterized in *B. burgdorferi*-infected heart tissue throughout the infection time-course. Hearts from control and infected mice were perfused and cells were isolated. Infected hearts were analyzed for the number of hematopoietic cells (A), macrophages (B), $NOS2^{+}CD206^{-}$ M1 macrophages (C), $NOS2^{-}CD206^{+}$ M2 macrophages (D), and $NOS2^{+}CD206^{+}$ resolution phase macrophages (E). n=4, results representative of two separate trials. Bars represent means +/- SD. * indicate data is significantly different from control data at the $p<0.05$ level determined by ANOVA followed by Dunnett's test.

5. *5-Lipoxygenase (5-LOX)-deficient animals display fewer M2 and resolution phase macrophages during arthritis.*

Our lab has previously shown that 5-Lipoxygenase-deficient (5-LOX$^{-/-}$) mice developed arthritis similar to WT controls, yet failed to resolve their inflammation (81). Macrophages from 5-LOX$^{-/-}$ mice displayed reduced ability to phagocytose opsonized spirochetes (81). Macrophage polarization and phenotype switching in these mice has not been previously described. We found that 5-LOX$^{-/-}$ mice stimulated *in vitro* under M1-polarizing conditions made comparable levels of nitrite to WT mice (Figure 4.5A). Under M2-polarizing conditions, 5-LOX$^{-/-}$ animals also displayed no difference in arginase activity when compared to WT controls (Figure 4.5B). This demonstrated that macrophages from 5-LOX$^{-/-}$ mice had no intrinsic defects in macrophage polarization capacity. Upon analysis of marker expression of *in vitro* M1-and M2-polarized macrophages from 5-LOX$^{-/-}$ and WT mice, we noticed some variation. 5-LOX$^{-/-}$ macrophages polarized under M1 conditions displayed a slightly higher percentage of NOS2^{+} cells (Figure 4.5C). Increased NOS2 could lead to greater inflammation in these mice, but *in vitro* studies are not always indicative of what occurs *in vivo*. To determine if NOS2 was increased in 5-LOX$^{-/-}$ macrophages *in vivo*, we infected mice with 1x10^{5} *B. burgdorferi* in the hind footpads and sacrificed them at two separate time points: day 21 and day 56 post-infection. These time points are indicative of the peak and resolution of inflammation. At both time points, macrophage numbers in the ankle joints were not significantly different between WT and 5-LOX$^{-/-}$ mice (Figure 4.6A). Additionally, numbers of NOS2^{+} macrophages were not significantly different between the WT and 5-LOX$^{-/-}$ mice.

This suggested that NOS2 does not play a role in the lack of resolution seen in these mice (Figure 4.6B). Although NOS2 appeared to play no role in the delayed resolution in 5-LOX$^{-/-}$ mice, a lack of M2 polarization or fewer resolution phase macrophages still could influence disease resolution. To analyze this, BMDM from WT and 5-LOX$^{-/-}$ animals were polarized under M2 conditions. We found that 5-LOX$^{-/-}$ mice had a reduced percentage of CD206 expressing macrophages (Figure 4.5D). Resolution phase macrophages were analyzed *in vitro*, but were only induced under M1-polarizing conditions. 5-LOX$^{-/-}$ mice showed a lower percentage of NOS2^{+}CD206^{+} resolution phase macrophages (Figure 4.5E). In order for relevance to be made, we analyzed this phenomenon in our *in vivo* model. At day 21 post-infection, there were fewer CD206^{+} M2 macrophages and NOS2^{+}CD206^{+} resolution phase macrophages in the ankle joints of 5-LOX$^{-/-}$ mice (Figure 4.6C and 4.6D). At day 56, this was no longer true. Both M2 macrophage and resolution phase macrophage numbers in the 5-LOX$^{-/-}$ joints were comparable to WT controls (Figure 4.6C and 4.6D).

6. *5-Lipoxygenase-deficient animals display fewer M2 macrophages during carditis.*

The role of 5-LOX in experimental Lyme carditis has not been studied, but because macrophages predominately drive early inflammation in carditis, we were interested to see if macrophage phenotype was different in the hearts of these mice. At days 21 and 56 post-infection, hearts were perfused with sterile saline to eliminate blood contamination. Single cell suspensions were made and stained for M1 and M2 appropriate markers for analysis by flow cytometry. Hearts of 5-LOX$^{-/-}$ mice

contained significantly fewer macrophages at day 21 compared to WT controls (Figure 4.7A). Since macrophages drive the development of murine Lyme carditis, 5-LOX$^{-/-}$ mice may have had less severe inflammation at this time point. It would be interesting to analyze 5-LOX$^{-/-}$ hearts at day 21 post-infection histologically to determine the severity of carditis. Macrophage numbers, however, did not remain decreased and by day 56 post-infection, their numbers were comparable to WT controls (Figure 4.7A). Similar to the joint tissue, we found no significant differences in the number of NOS2^{+} M1-like macrophages between the WT and 5-LOX$^{-/-}$ mice at either time point (Figure 4.7B). At day 21, the 5-LOX$^{-/-}$ mice displayed significantly reduced numbers of CD206^{+} M2-like macrophages in their hearts (Figure 4.7C). Although not significantly different, they also had fewer numbers of NOS2^{+}CD206^{+} resolution phase macrophages at this same time point (Figure 4.7D). During resolution, both CD206^{+} M2 macrophages and NOS2^{+}CD206^{+} resolution phase macrophage populations were similar between the WT and 5-LOX$^{-/-}$ mice (Figure 4.7C and 4.7D).

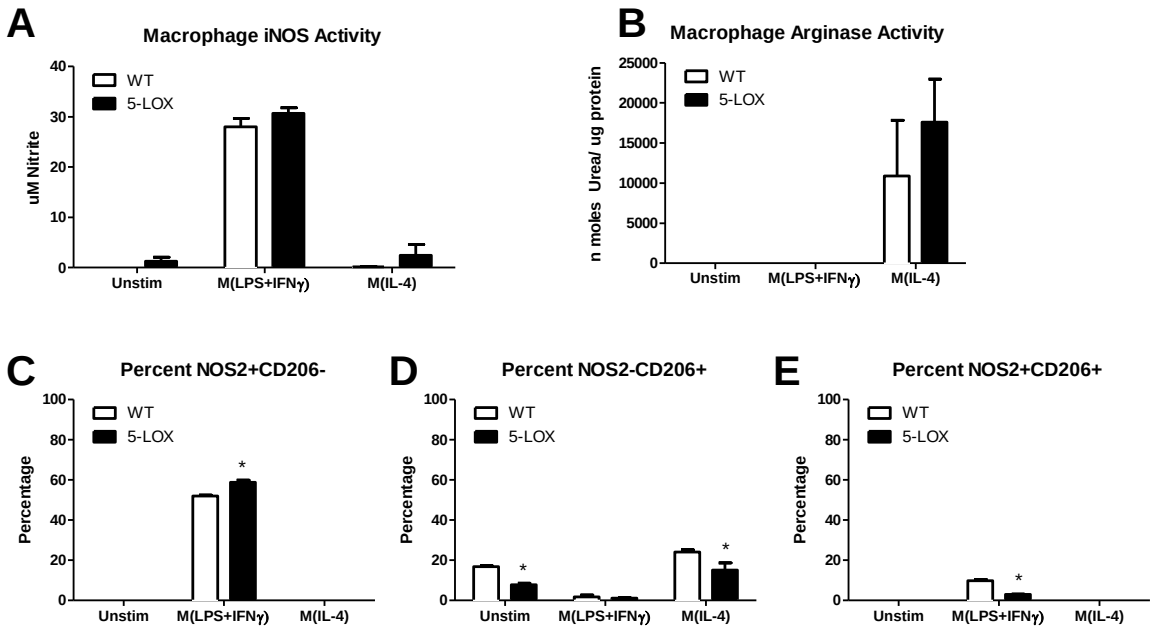

Figure 4.5: BMDM from 5-LOX$^{-/-}$ mice were isolated and polarized into either M1 or M2 macrophages. Both iNOS (A) and arginase (B) activity were identical between wild type in 5-LOX$^{-/-}$ mice. The percentage of NOS2^{+} M1 macrophages was slightly, but significantly higher in the 5-LOX$^{-/-}$ mice (C), whereas the percentage of CD206^{+} M2 macrophages were significantly lower (D). Resolution phase macrophages expressing both NOS2 and CD206 were significantly lower in the 5-LOX$^{-/-}$ mice (E). n=3, data representative of two separate trials. Bars representative of the mean +/- SD. * indicates statistically significant difference between the 5-LOX$^{-/-}$ cells compared with WT controls from the same group at the $p<0.05$ level.

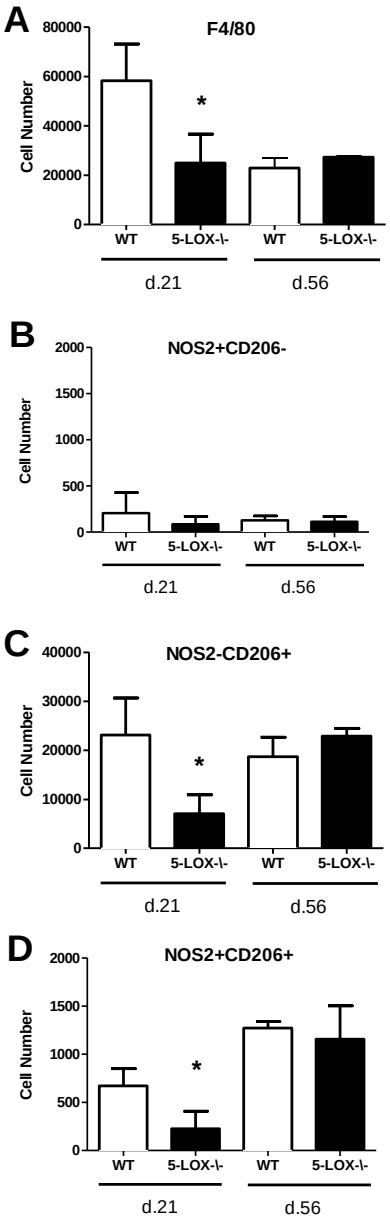

Figure 4.6: Macrophage phenotype was analyzed from cells isolated from the joints of *B. burgdorferi*-infected 5-LOX$^{-/-}$ mice. Macrophage infiltration was similar between the WT and 5-LOX$^{-/-}$ mice at days 21 and 56 (A) post-infection. NOS2^{+} macrophages also showed no significant changes at day 21 or 56 (B). However, the 5-LOX$^{-/-}$ mice showed decreased numbers of CD206^{+} M2-like macrophages at day 21, but numbers recovered by day 56 (C). Resolution phase macrophages expressing both NOS2 and CD206 were significantly decreased in the 5-LOX$^{-/-}$ mice at day 21 post-infection, but rebounded by the time of resolution (D). n=2, results representative of one trial. Bars represent means +/- SD. * indicate data is significantly different from control data at the $p<0.05$ level determined by ANOVA followed by Dunnett's test.

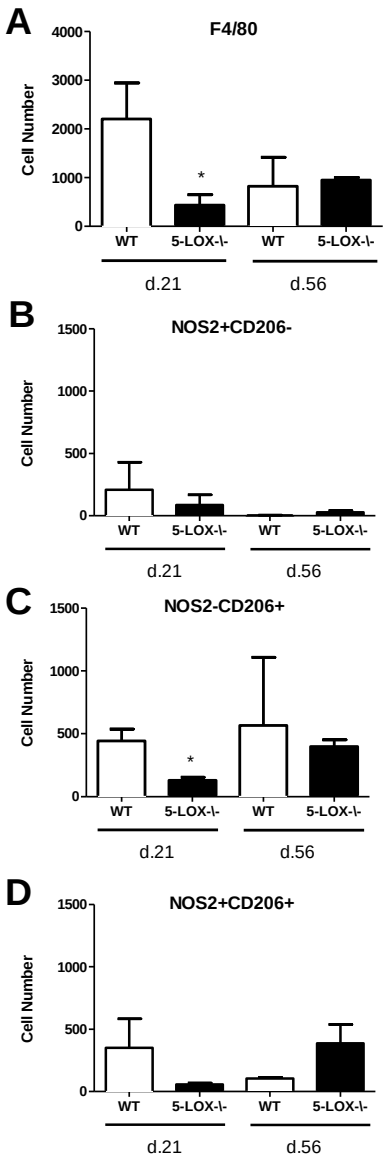

Figure 4.7: Macrophage phenotype was analyzed from cells isolated from hearts of *B. burgdorferi*-infected 5-LOX$^{-/-}$ mice. At day 21 and 56 post-infection, macrophage numbers were quantified in the 5-LOX$^{-/-}$ and WT mice (A). No significant difference was found in the number of NOS2^{+} M1-like macrophages between 5-LOX$^{-/-}$ and WT mice at either day 21 or 56 post-infection (B). CD206^{+} M2-like macrophages were significantly lower in the 5-LOX$^{-/-}$ mice at day 21 post-infection, but not at day 56 post-infection (C). Resolution phase macrophage populations were similar between the two mouse strains at both time points (D). n=2, results representative of one trial. Bars represent means +/- SD. * indicate data is significantly different from control data at the $p<0.05$ level determined by ANOVA followed by Dunnett's test.

C. *Conclusions*

Macrophage polarization and phenotype plasticity has been implicated in the onset and resolution of inflammation in a variety of infectious disease models. Following bacterial infection, monocytes are recruited to the site of infection where they mature into macrophages (92). These macrophages, along with resident macrophages, are polarized by the surrounding microenvironment into either proinflammatory M1-like macrophages or anti-inflammatory M2-like macrophages (50). Bacteria are detected by innate immune cells through a variety of pathogen associated molecular patterns (PAMPS) and toll-like receptors (TLR's). This recognition induces the activation of key transcriptional factor pathways, resulting in the development of nitric oxide-producing M1-like macrophages (93). The ability to form M1 macrophages was shown to be critical in clearing infection of *Listeria monocytogenes*, *Mycobacterium tuberculosis*, and *Salmonella typhimurium* (61, 94, 95). After the bacteria are cleared, the environment becomes more anti-inflammatory. The plasticity of the macrophage allows for re-polarization into an anti-inflammatory M2-like state which further controls the once exuberant immune response (50). When a defect in repolarization occurs, the result is chronic inflammation (96). Chronic brucellosis occurs when too much IL-10 is produced and an M2 activated state is maintained (97). This same phenomenon can occur in Mycobacterial infections, preventing clearance of bacteria (98). The importance of macrophage subset plasticity is also seen in many autoimmune diseases (99, 100).

During a study of obesity, adipose tissue macrophages from mice fed a high-fat diet underwent a subset polarization change from their normal anti-inflammatory M2-like phenotype to a pro-inflammatory M1-like phenotype (100). Similar results were found during a human study of macrophage polarization and obesity (101). Obese human patients displayed an increase in M1-like polarized adipose tissue macrophages. Three months following gastric bypass surgery, the adipose tissue macrophage phenotype shifted from that of a predominantly M1 to a predominantly M2 population suggesting a less inflammatory profile overall (101). In a model of relapsing EAE in Dark Agouti rats, the first clinical attack showed balanced levels of M1 and M2 macrophages. However, upon relapse there was a strong bias toward the proinflammatory M1 phenotype. By adoptively transferring *in vitro* polarized M2 macrophages, the EAE severity was lowered at relapse (102). These results indicated that modifying macrophage polarization could potentially be used as a therapeutic.

In experimental models of both Lyme arthritis and carditis, macrophages have been shown to play a role in the inflammatory process. Macrophages, although to a lesser extent than neutrophils, are capable of phagocytosing *B. burgdorferi*, as was shown in the previous chapter. In the Lyme carditis model, macrophages are thought to drive the inflammatory response and are the predominant infiltrating cell type (21, 22). In the current study, we were interested in defining the phenotype of the macrophages within the joints and hearts of *B. burgdorferi*-infected mice. After *in vitro* co-culture of BMDM with *B. burgdorferi*, we found the macrophages primarily adopted an M1-like phenotype. Thus, we hypothesized that M1-like macrophages expressing NOS2

would predominate during the onset of and peak of inflammation. We found that this model was too simplistic, and that macrophage polarization is much more complex within an *in vivo* model. This study emphasizes that conclusions about macrophage polarization should not be made solely by working in an *in vitro* system alone. Many labs would benefit from steering away from such an artificial system when working with cells that are so highly dependent upon multiple stimuli from their microenvironment.

Using an *in vivo* system, we tracked macrophage infiltration into the joints of *B. burgdorferi*-infected mice during the onset, peak, and resolution of disease. Macrophage numbers within the ankle joint peaked at day 21 post-infection. The majority of macrophages throughout the infection were $CD206^{+}$ M2-like macrophages regardless of the time-point analyzed. Very few $NOS2^{+}$ M1-like macrophages were seen even at the peak of inflammation. It appears that M1 macrophages are either highly potent and very few are needed to aid in disease progression, or they are not important in the development of disease. Earlier work demonstrated that Nitric oxide (NO) inhibition or deficiency had little effect on the development or severity of Lyme arthritis. This suggests that NO- producing macrophages do not play a significant role in the development of arthritis (103, 104). The resolution of Lyme arthritis occurs spontaneously, and is thought to be mediated by antibody-induced spirochete clearance (15). We found that during disease resolution at day 56 post-infection, there was a large increase in $NOS2^{+}CD206^{+}$ resolution phase macrophages. This unique macrophage could play an unrecognized

role in disease resolution (71, 72). Resolution phase macrophages are neither classically nor alternatively activated; their phenotype is a combination of the two (71). Until now, resolution phase macrophages have not been implicated in the resolution of Lyme arthritis. Further study may lead to the development of pharmaceuticals to target this unique cell type, and help control chronic inflammation.

Lyme carditis is unique from arthritis in that macrophages are the driving force in disease progression (22). Despite this, macrophage polarization has not been assessed in experimental Lyme carditis. We found that $NOS2^{+}$ M1-like macrophages were the predominant cell type during the peak of inflammation and M2 macrophages predominated at resolution. A very small number of resolution phase macrophages were identified within the *B. burgdorferi*-infected hearts. This indicates that macrophage phenotype may play a role in the development and resolution of Lyme carditis.

To better understand the role of macrophage polarization in the experimental Lyme borreliosis model, we also studied a non-resolving mouse model. 5-LOX-deficient mice are susceptible to arthritis, but fail to resolve their inflammation (81). 5-LOX is the enzyme responsible for converting arachidonic acid into leukotrienes (105). The leukotrienes are proinflammatory lipid mediators responsible for chemotaxis of neutrophils and increased vascular permeability (105, 106). $5\text{-LOX}^{-/-}$ mice showed no defect in recruitment of macrophages into *B. burgdorferi*-infected ankle joints at

either the peak or resolution of inflammation. At day 21 post-infection, 5-LOX$^{-/-}$ mice had significantly fewer CD206^{+} M2-like macrophages and NOS2^{+}CD206^{+} resolution phase macrophages in the joint tissue which could indicate a more inflammatory environment. However, during disease resolution, both M2 and resolution phase macrophage numbers were comparable between the WT and 5-LOX$^{-/-}$ mice. 5-LOX may play a small role in M2-like macrophage polarization early in disease, but it is unlikely that this resulted in their failure to resolve inflammation. During Lyme carditis, 5-LOX$^{-/-}$ mice had significantly reduced numbers of macrophages recruited at day 21 post-infection. This suggested that these mice would have less severe carditis at this time point, but those studies still need to be undertaken. By the time resolution occurred, macrophage numbers were comparable to WT mice. As was seen in the ankle joints, CD206^{+} M2-like macrophages were significantly reduced in the hearts of the 5-LOX$^{-/-}$ mice at day 21 post-infection, but this was likely a result of the reduced number of total macrophages at this timepoint.

In conclusion, macrophage phenotypes can be identified within the ankle joints and hearts of *B. burgdorferi*-infected mice. In the joints, CD206^{+} M2-like macrophages outnumber NOS2^{+} M1-like macrophages 10:1, while in the heart tissue the numbers of M1/M2 like macrophages are similar but with slightly different kinetics. At the time of disease resolution, a resolution phase macrophage expressing both NOS2 and CD206 appears to be present, but more work is necessary to elucidate its exact function. Non-resolving 5-LOX$^{-/-}$ mice show a defect in the production of both M2 and resolution phase macrophages in both the ankle joints and hearts at the peak of

inflammation. This may drive the chronic inflammation by exacerbating the strength and persistence of pro-inflammatory signals, or by the failure of initiating a pro-resolution program. These possibilities are currently under investigation. This study lays the groundwork for future studies of macrophage phenotype in other *in vivo* models of infectious disease.

CHAPTER V

CHARACTERIZATION OF BIPHENOTYPIC B/MACROPHAGE CELLS *IN VITRO* AND IN EXPERIMENTAL LYME BORRELIOSIS

A. *Introduction*

The current model of hematopoietic cell lineage dictates that lymphocytes and myeloid cells are distinct cell types and distantly related. However, over the past few decades it has become readily apparent that lineage promiscuity and plasticity occurs, and lymphoid cells can alter their phenotype into that of a myeloid-like cell (107). Many papers have reported a breakdown in B lymphocyte lineage commitment into that of a myeloid cell lineage (108-111). This was first reported in a murine lymphoblastic lymphoma model where lymphocytes underwent a transition to macrophage-like cells (112). It was initially thought that this phenomenon was strictly due to inappropriate gene transcription from malignancy, and was ignored. It was later discovered that these cells were a distinctive cell type, and their presence in tumors indicated a poor prognosis (112, 113).

Biphenotypic B/Macrophage cells are a unique cell type that are derived from B cells and co-express both B cell and macrophage cell surface markers (109). It was discovered that these cells could be propagated *in vitro* by purifying splenic B-cells and culturing them with Macrophage Colony-Stimulating Factor (M-CSF)-secreting fibroblasts (108). M-CSF induced differentiation and GM-CSF enhanced proliferation; addition of these cytokines alone to either B1a or B1b cells caused a

phenotypic switch into a macrophage-like cell (114). Murine markers for biphenotypic cells include F4/80 and CD11b as macrophage specific and B220, IgD, IgM and CD5 as B-cell specific markers (109, 115). Using PCR analysis, these cells have also been shown to undergo heavy chain gene rearrangement, confirming that they are of B cell origin (109). Biphenotypic B/Macrophage cells were also capable of phagocytosis; it has been demonstrated *in vitro* that they can take up both opsonized sheep erythrocytes and latex beads (109).

Biphenotypic B/Macrophage cells have not been previously studied in an infectious or inflammatory model aside from cancer. All previous studies have identified and assessed the cells by cultivating murine B cells and growing them *in vitro* (108). To our knowledge this is the first report of Biphenotypic B/Macrophage cells in an *in vivo* model of experimental Lyme disease. Using flow cytometric analysis, we have identified and quantified these cells throughout the infection time-course in both ankle joint and heart tissue. In the ankle joint, the number of Biphenotypic B/Macrophage cells peak during the resolution phase of inflammation, leading us to hypothesize that these cells actively play a role in resolving inflammation. It is currently unknown whether these are an intermediate cell with a specialized intermediary function or a definitive cell stage with a defined purpose.

B. Results

1. *Biphenotypic B/Macrophage cells grown in vitro are derived from B lymphocytes and alter cell surface expression over time.*

To grow Biphenotypic B/Macrophage cells in *in vitro* culture, we first purified B2 cells from uninfected C3H WT spleens using negative selection magnetic separation. They were then cultured for 21 days in complete DMEM containing 40ng/mL M-CSF and 5ng/mL GM-CSF, as reported elsewhere (108). After 14 days in culture, it became apparent that the lymphocytes had begun to physically transform into macrophage-like cells. The normally small, round cells became much larger, granular, and developed pseudopodia-like structures (Figure 5.1A). This data supported previous reports and confirmed that fully differentiated B cells were able to transform into myeloid-like cells (108, 109). The B cell isolation kit used normally yields about 97% purity, so we wanted to ensure that these cells were not simply an outgrowth of contaminating macrophages. We isolated purified B cells and cultured Biphenotypic B/Macrophage cells and assessed them for heavy chain gene rearrangement using PCR . Only lymphocytes are capable of gene rearrangement so if the Biphenotypic B/Macrophage cells are derived from B cells, they will display rearranged Immunoglobulin genes. Both Biphenotypic B/Macrophage cells and B cells displayed gene rearrangement proving these cells were derived from a B cell lineage (Figure 5.1B). Although Biphenotypic B/Macrophage cells have been reported from *in vitro* cultures, data concerning cell surface expression over time was lacking. To understand how these cells changed as they transitioned from B cells into Biphenotypic B/Macrophage cells, we stimulated purified B cells with M-CSF and

GM-CSF as previously described and analyzed cell surface expression of both B cell and macrophage-specific markers over time (Figure 5.2). On day 7 of culture, the B cell specific marker CD19 was still expressed, but was no longer expressed by day 21. Both B cell-specific IgM and B220 were maintained as the cells transitioned from B cells to Biphenotypic B/Macrophage cells throughout the three weeks of culture. Expression of the monocyte marker CD11b continually increased over time, indicating a switch from the lymphocyte to myeloid cell lineage. In addition, as the B cells differentiated into Biphenotypic B/Macrophage cells they increased and maintained expression of F4/80. It is apparent that upon stimulation with M-CSF and GM-CSF, B cells were phenotypically altered. By analyzing changes in surface marker expression from *in vitro* cultures, we were then able to identify these cells in an *in vivo* model of experimental Lyme disease.

2. *Biphenotypic B/Macrophage cells can be identified from ankle joint and heart tissue of B. burgdorferi-infected mice.*

To determine if biphenotypic cells could be identified during an immune response *in vivo*, C3H WT mice were infected with $1x10^5$ *B. burgdorferi* in the hind footpads. Mice were sacrificed at days 7, 14, 21, 28, and 49 post-infection and single cell suspensions were made from both ankle joint and heart tissue as described earlier. Cell suspensions were stained for the Biphenotypic B/Macrophage cell-specific markers B220, IgM, F4/80 and CD11b, as was previously determined from *in vitro* work. Flow cytometry was used to identify the Biphenotypic B/Macrophage cell populations within the infected tissues. First, doublets were eliminated from the

analysis to ensure that co-expression of myeloid and lymphoid specific markers was not simply due to an inappropriate reading by the cytometer of multiple events (Figure 5.3A). Dead cells, stained with Annexin V, were eliminated from the forward/side scatter plot (Figure 5.3 B&C). The remaining cells were gated on $B220^{+}IgM^{+}$ classical B cells (Figure 5.3 D). Biphenotypic B/Macrophage cells were finally identified by overlaying the classical B cell population onto an F4/80/CD11b macrophage plot (Figure 5.3E). Cells that possessed both B cell and macrophage specific markers were enumerated (Figure 5.3F). Within the ankle joints, a small number of Biphenotypic B/Macrophage cells were identified from uninfected control animals. The numbers of Biphenotypic B/Macrophage cells increased during infection, and were significantly elevated at day 49 post-infection compared to uninfected controls (Figure 5.4). The timing of this peak of Biphenotypic B/Macrophage cells in the infected joint suggested that they may play a potential role in disease resolution. Far fewer biphenotypic cells were found in infected heart tissue. Their numbers were statistically higher than controls at day 14 post-infection, but their overall cell numbers remained quite low (Figure 5.5). Although it was possible that such a small number of cells could influence the course of disease, their exact role is still under investigation. To our knowledge, this was the first time Biphenotypic B/Macrophage cells have been identified *in vivo* in an infectious disease model. Their presence led us to question whether they are actively recruited to, or made at, the site of infection.

3. *Biphenotypic cells are capable of trafficking to the ankle joint during B. burgdorferi infection.*

To determine whether Biphenotypic B/Macrophage cells could traffic to the joint tissue upon infection, we isolated peritoneal cells from an uninfected C3H WT mouse and labeled them with CFSE. CFSE is a fluorescent cell-staining dye that can be used to track cell migration. These cells were adoptively transferred into *B. burgdorferi*-infected C3H WT mice by intraperitoneal injection. After 21 days of infection, cells from ankle joint tissue were harvested and stained for Biphenotypic B/Macrophage cell-specific markers. We were able to identify Biphenotypic B/Macrophage cells within the ankle joint tissue that expressed CFSE (Figure 5.6A). Because the adoptively transferred peritoneal cells were not purified, it was not clear whether these cells were Biphenotypic B/Macrophage cells from the peritoneum that trafficked to the infected joints or whether they were B cells that migrated to the joints and converted into a Biphenotypic B/Macrophage cell. To determine whether the environment within the infected joint was permissive to Biphenotypic B/Macrophage cell formation, we assessed the concentration of M-CSF within *B. burgdorferi*-infected joint tissue. M-CSF is responsible for converting B cells to Biphenotypic B/Macrophage cells (108). We determined that at day 23 post-infection, M-CSF levels were significantly elevated over uninfected controls, suggesting that the phenotypic switch may occur at the site of inflammation (Figure 5.6B). It is possible that Biphenotypic B/Macrophage cells are both recruited to and made at the site of inflammation, but further studies are needed to elucidate whether both occur.

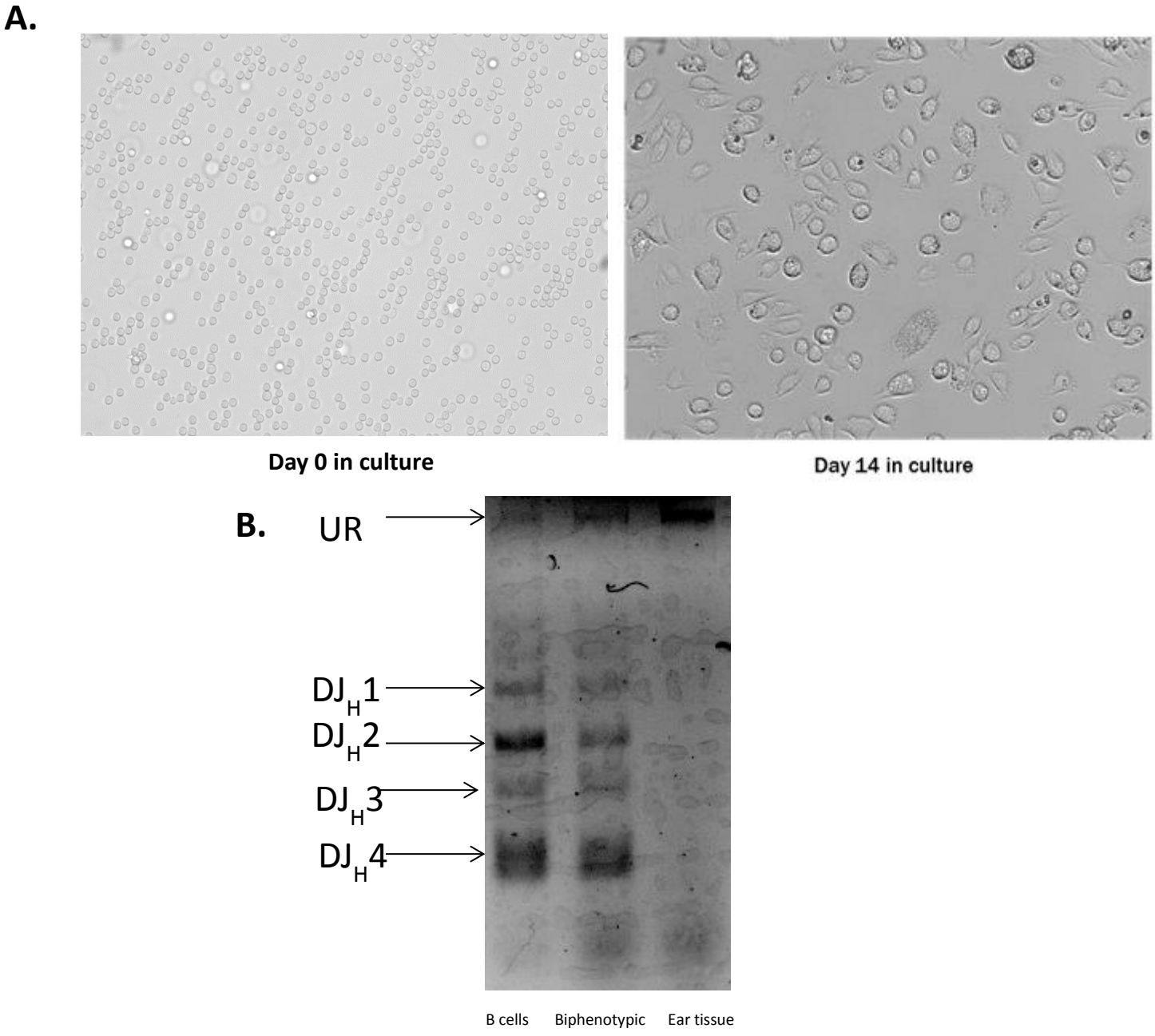

Figure 5.1: Splenic B cells were isolated and stimulated with M-CSF and GM-CSF for 14 days. Small, round B cells convert to larger, highly granular macrophage-like cells in just two weeks in culture (A). After 21 days in culture, we show that Biphenotypic B/Macrophage cells have undergone heavy chain gene rearrangement, identical to purified B cells (B). UR (un-rearranged). n=3, representative to two separate experiments.

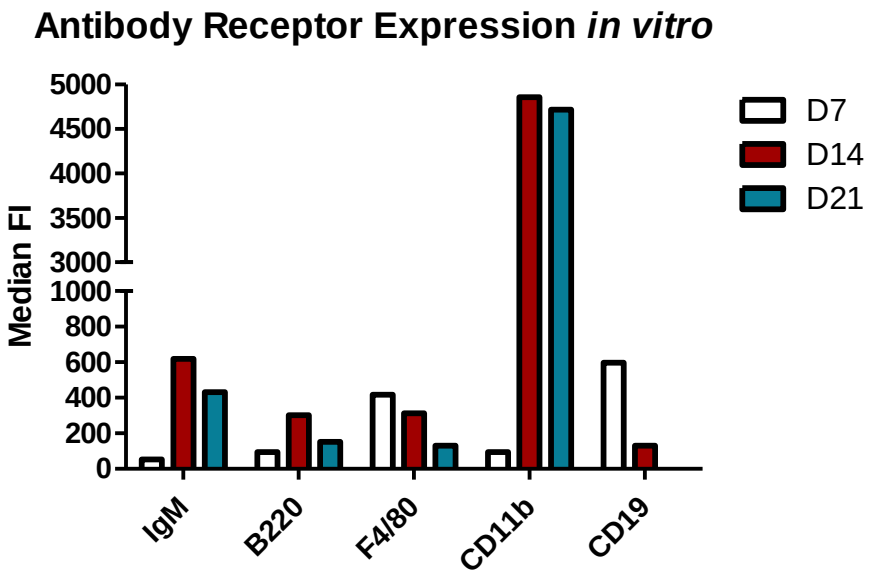

Figure 5.2: Using flow cytometry, surface marker expression of *in vitro* grown Biphenotypic B/Macrophage cells was analyzed over time. N=3, data representative of one trial.

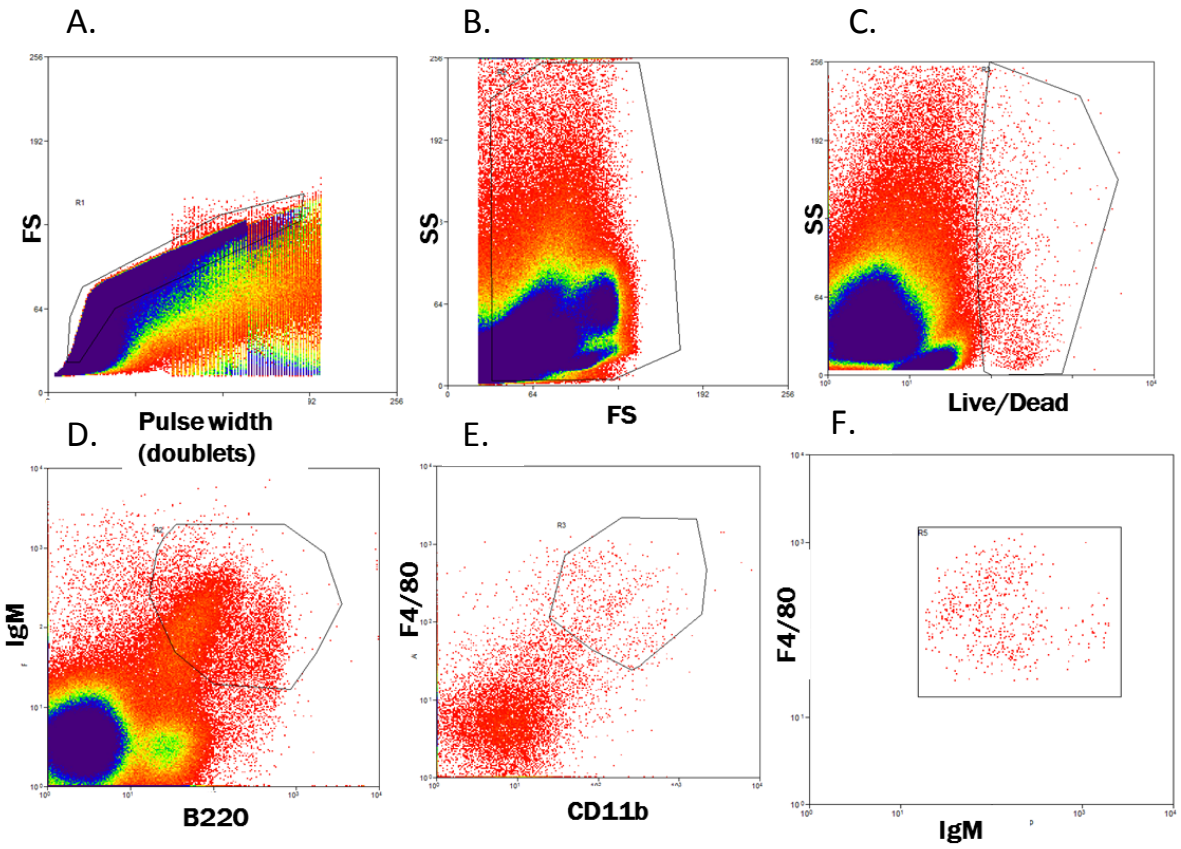

Figure 5.3: Flow cytometry of Biphenotypic B/Macrophage cells. All gates shown are cumulative. Using flow cytometry, doublets were eliminated to ensure we were assessing individual cells (A). Cells were then gated on a forward/side scatter plot (B). Dead cells were eliminated based on expression of Annexin V staining (C). Classical B cells were selected based on expression of both B220 and IgM. Biphenotypic B/Macrophage cells were selected based on the additional expression of F4/80 and CD11b (E). An example population of typical Biphenotypic B/Macrophage cells is represented (F). n=5, results representative of three separate experiments.

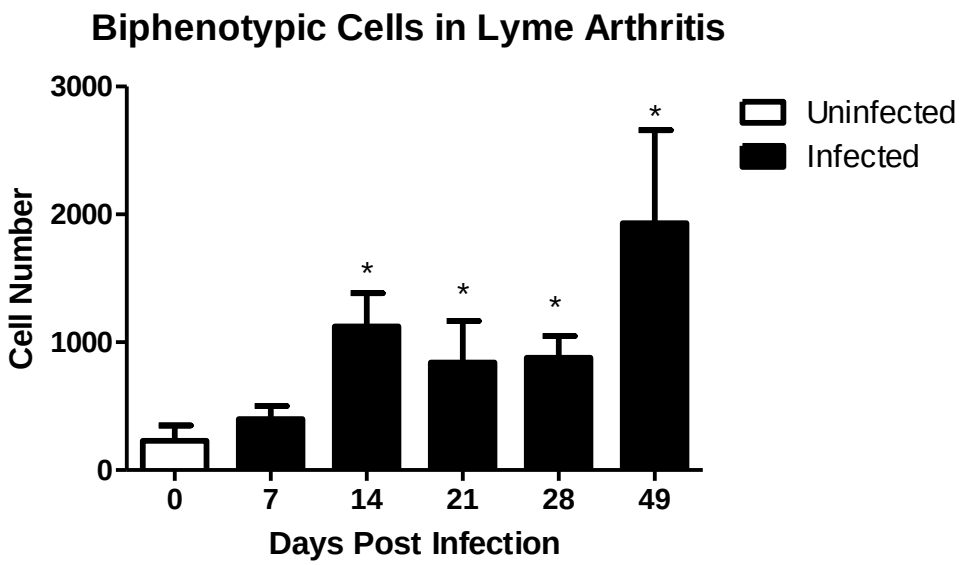

Figure 5.4: C3H WT mice were infected with $1x10^5$ *B. burgdorferi* in rear footpads and Biphenotypic B/Macrophage ($B220^+IgM^+F4/80^+CD11b^+$) cells were identified from ankle homogenates throughout the infection time-course. n=3, data representative of three separate experiments. Bars represent means +/- SD. * indicate data is significantly different from control data at the $p<0.05$ level determined by ANOVA followed by Dunnett's test.

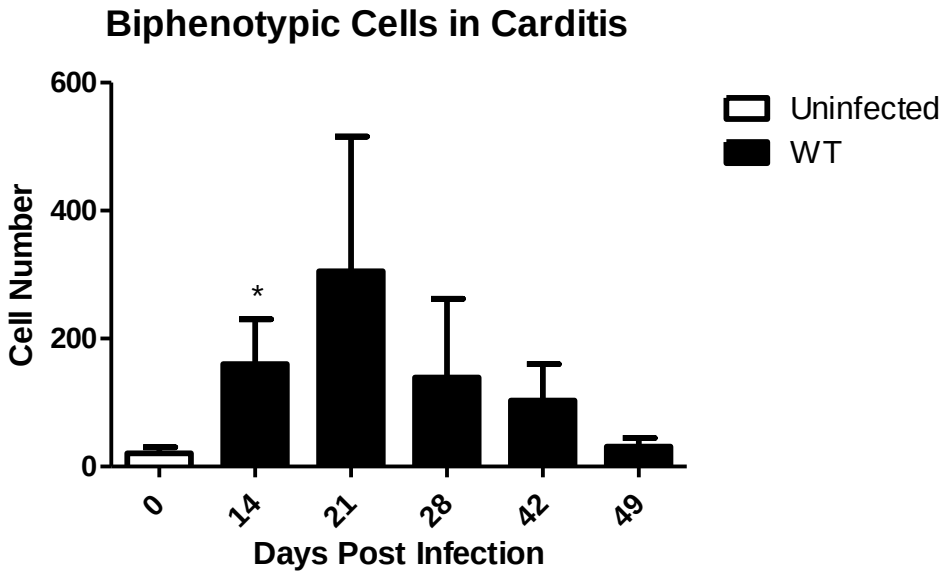

Figure 5.5: C3H WT mice were infected with $1x10^5$ *B. burgdorferi* in rear footpads and Biphenotypic B/Macrophage cell infiltration into heart tissue was tracked throughout the infection time-course. n=3, data representative of three separate experiments. Bars represent means +/- SD. * indicate data is significantly different from control data at the $p<0.05$ level determined by ANOVA followed by Dunnet's test.

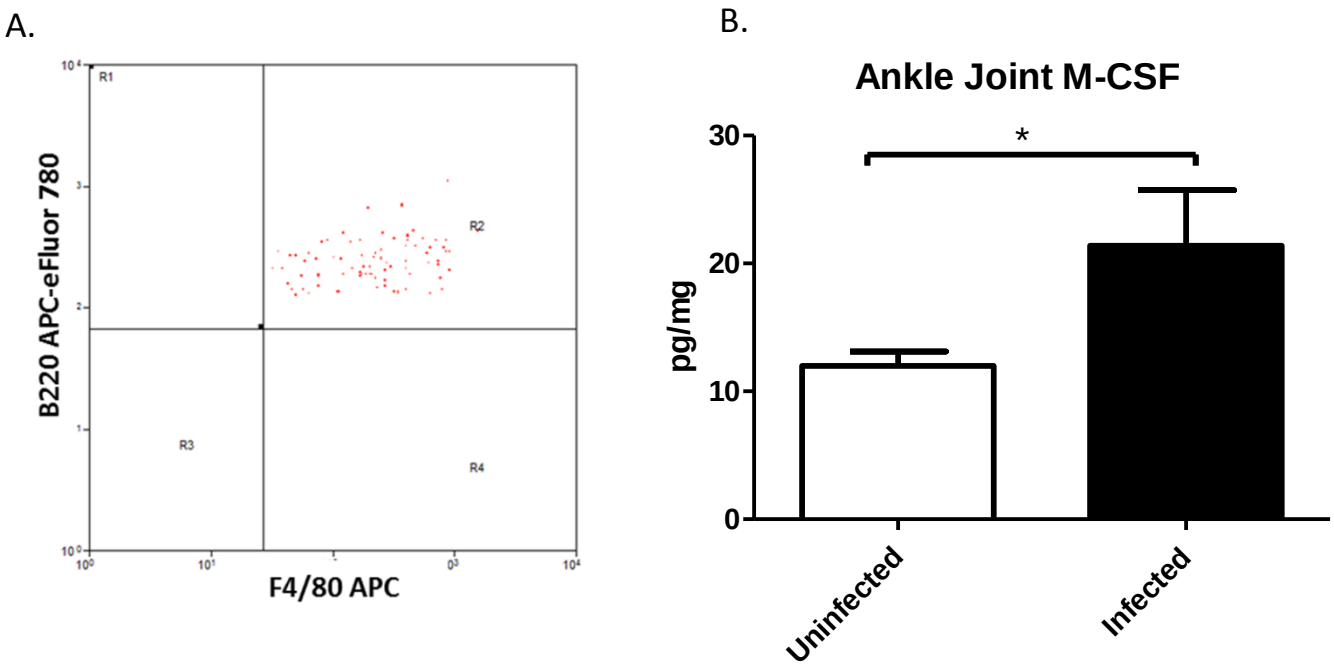

Figure 5.6: Cells isolated from the peritoneum of an uninfected C3H WT mouse were labeled with CFSE and adoptively transferred into the peritoneum of *B. burgdorferi*-infected mice. 21 days post-infection, joints were harvested and stained for Biphenotypic B/Macrophage cell-specific markers. $CFSE^{+}$ cells were selected and identified for expression of Biphenotypic B/Macrophage cell-specific markers. CFSE-labeled Biphenotypic B/Macrophage cells are shown (A). M-CSF levels are increased in *B. burgdorferi*-infected joints at day 23 post-infection (B). n=4, representative of two separate experiments. Bars represent mean +/- SD. * indicates data is significantly different from control data at the $p<0.05$ level determined by Student's T-test.

C. Conclusions

Biphenotypic B/Macrophage cells are hybrid cells that express surface markers unique to both B cells and macrophages. They were originally defined in $CD5^+$ B cell lymphomas and were indicative of a poorer prognosis (116). The cells were originally thought to be a caused by a transcriptional defect unique to malignant B cells and lymphoma B cell lines. Studying how the cells transitioned from B cells also proved to be difficult. Culturing the cells using macrophage culturing methods was unsuccessful (113). It was later discovered that co-culturing purified splenic B1 cells with splenic fibroblasts could produce a bi-potential cell possessing a phenotype similar to both B cells and macrophages, termed a Biphenotypic B/Macrophage cell (109). The *in vitro*-differentiated Biphenotypic B/Macrophage cells were capable of phagocytosis of both *B. abortus* and latex beads. In addition, they possessed Ig gene rearrangements, but failed to secrete IgM or IgG1 in response to LPS treatment (109). Later studies uncovered that fibroblast secreted M-CSF was responsible for the generation of Biphenotypic B/Macrophage cells and GM-CSF aided in their proliferation (108). Addition of M-CSF and GM-CSF to purified and cultured B cells generated Biphenotypic B/Macrophage cells (108). The development of this technique allowed for the simple differentiation and culturing of Biphenotypic B/Macrophage cells and provided a model for studying their potential role in inflammatory processes.

Biphenotypic cells possess unique cell surface markers, but studies describing their phenotype over time in culture as they transition from B cells to Biphenotypic B/Macrophage cells were lacking. We grew Biphenotypic B/Macrophage cells from isolated splenic B cells and stimulated with M-CSF and GM-CSF, as previously described (108). By day 14, they had morphologically changed from small, rounded lymphocytic cells to larger, more granular macrophage-like cells. This is consistent with data obtained in the Phipps lab (109). Current B cell isolation kits yield approximately 97% purity, so it was possible that a small population of macrophages grew out in the culture. To ensure that the cells being studied were not a result of contaminating cells, we analyzed cells for DJ heavy chain gene rearrangement. At day 21 in culture, it is apparent that Biphenotypic B/Macrophage cells have the same gene rearrangement seen in purified B lymphocytes, verifying that these cells were not an outgrowth of macrophages. Interestingly, only about 10% of B cells in culture will actually convert to a Biphenotypic B/Macrophage cell. At day 7, all non-adherent B cells are removed, and the few remaining will differentiate and proliferate into the Biphenotypic B/Macrophage population studied. It is currently unknown what predisposes some B cells, but not others, to become Biphenotypic B/Macrophage cells. Recent studies suggest that the early transcription factor network affects lineage outcome in lymphoid progenitors. It was found that in fully committed pre-B cells, CEBP-α bound upstream regions of Tet2 and de-repressed myeloid genes, allowing an efficient conversion into macrophages (110, 111). This does not explain, however, how fully differentiated B cells convert to a macrophage-like phenotype. It is possible that stimulation of B cells through the M-CSF receptor

stimulates C/EBP-α activity, allowing them to partially differentiate into myeloid-like cells (117). However, this hypothesis has not yet been tested, and further work is required to elucidate the mechanism behind the differentiation.

Surface marker expression of Biphenotypic B/Macrophage cells differentiated in culture has been assessed by others at day 15 (109), but how the markers change in culture over time is still unknown. To this end, we analyzed expression of CD19, CD11b, IgM, F4/80 and B220 on B cells stimulated with Biphenotypic B/Macrophage-producing cytokines (M-CSF and GM-CSF) from day 7 to day 21 in culture. By day 21, CD19 expression had completely disappeared. Previous studies analyzing Biphenotypic B/Macrophage cells at day 15 in culture reported and characterized these cells based on expression of CD19 (113). Our findings suggest that this may not be a reliable marker in which to characterize these cells due to significant down-regulation. Our analysis identified four appropriate markers for evaluating Biphenotypic B/Macrophage cells *in vivo*: CD11b, IgM, F4/80 and B220. Using this staining scheme, we were able to assess the presence of Biphenotypic B/Macrophage cells during experimental Lyme disease.

Despite numerous observations of B cells transitioning into macrophage-like cells *in vitro*, there was no data showing that this phenomenon actually occurred in an *in vivo* infectious model. We discovered that WT C3H mice have very low resting numbers of Biphenotypic B/Macrophage cells in both joint and heart tissue. Once infected with *B. burgdorferi*, these numbers increased in both locations. During carditis,

Biphenotypic B/Macrophage cell numbers were only significantly elevated at day 14 post-infection but did not reach numbers greater than 200 cells. Although possible, it is unlikely that they play a significant role in the development or resolution of disease. In Lyme arthritis, Biphenotypic B/Macrophage cell numbers were significantly elevated at nearly all time points assessed, but were dramatically increased at day 49 post-infection. At this point, mice were resolving disease, and we hypothesized that Biphenotypic B/Macrophage cells play a role in disease resolution. Further studies need to be undertaken in order to assess whether these cells are capable of inducing a pro-resolution phenotype.

Biphenotypic B/Macrophage can be identified within *B. burgdorferi*-infected joint tissue, but it is unknown how they get there. To study whether they actively migrated, we CFSE-labeled splenic cells and adoptively transferred them intraperitoneally into a *B. burgdorferi*-infected host. After 21 days, the ankle joints were harvested and single cell suspensions were made. Biphenotypic B/Macrophage cells expressing CFSE could be identified within the joint. This indicated that either B cells or Biphenotypic B/Macrophage cells from the spleen trafficked to the joint upon infection. Additionally, we found significantly elevated levels of M-CSF in infected ankle joint tissue, suggesting that B cells within the joint could potentially transition to Biphenotypic B/Macrophage cells. Future studies will elucidate how Biphenotypic B/Macrophage cell numbers become elevated within *B. burgdorferi*-infected tissue.

In conclusion, we have identified a novel cell type in the joints and hearts of *B. burgdorferi*-infected mice. Biphenotypic B/Macrophage cells are unique cells that may play multiple roles during disease, including the initiation of resolution. Future studies need to be performed to determine the role of these cells during Lyme borreliosis. The mechanism by which fully mature B cells are re-programmed into myeloid-like cells will also be elucidated to develop potentially pro-resolution therapeutics.

CHAPTER VI

T CELLS EXACERBATE LYME BORRELIOSIS IN TLR-2-DEFICIENT MICE

A. Introduction:

In a murine model of experimental Lyme borreliosis, infection with *B. burgdorferi* results in acute arthritis and carditis with symptoms similar to those found in Lyme disease patients (91). Mice develop both cellular and humoral immune responses to the outer surface proteins (OSP) of *B. burgdorferi* (14). Upon migration from the tick to the mammalian host, *B. burgdorferi* modifies its normal OspA antigen to OspC (118). OspC is readily recognized by the immune system by Toll-like receptor 2 (TLR-2) (119).

Due to the importance of TLR-2 in immune recognition of *B. burgdorferi*, it was hypothesized that TLR-2-deficient mice would display an attenuated disease phenotype following infection. However, TLR-2-deficient mice developed a more severe arthritis and had higher bacterial burdens in tissues than did WT control mice (78). This phenomenon was not unusual; increased inflammation during absence of TLR-2 occurred in several other infectious disease models including *Mycobacterium tuberculosis* (120), *Paracoccidioides brasiliensis* (121) and *Streptococcus pneumoniae* (122) TLR-2-deficient mice had increased numbers of T cells recruited to ankle joints following *B. burgdorferi* infection, perhaps due to increased CXCL9 and CXCL10 expression (78). It was also postulated that this early influx of T cells may be important for recruitment of innate immune cells that drive the increased inflammation seen in these mice (78).

In the current study, we found that depletion of specific T cell subsets lessened both Lyme arthritis and carditis severity in TLR-2-deficient mice. This depletion directly resulted in decreased recruitment of both neutrophils and macrophages to the site of infection, emphasizing the importance of early TLR-2-independent T cell responses for innate immune cell recruitment and disease development. Our study also demonstrated the importance of $CD8^+$ T cells in the production of CXCL9 by synovial fibroblasts. These results suggest that TLR-2-independent responses to *B. burgdorferi* are much more complicated than once thought.

B. Results

1. TLR-2-deficiency results in increased T cell infiltration into ankle and heart tissue following B. burgdorferi infection.

C3H WT and C3H TLR-2-deficient mice were infected with $1x10^5$ *B. burgdorferi* in both rear footpads and ankle swelling was measured throughout the infection time-course. As was typical for an experimental Lyme infection, swelling began at day 7 and peaked around 14-21 days post-infection. It was evident by day 14 post-infection that TLR-2-deficient mice displayed greatly increased ankle swelling compared to WT controls (Figure 6.1). As WT mice were beginning to resolve disease at day 35 post-infection, swelling remained elevated in the TLR-2-deficient mice (Figure 6.1). Mice were sacrificed on days 14, 21, 28, 42 and 49 post-infection and joints were analyzed for T cell infiltration. Throughout the infection time-course, $CD3e^+$ T cells were elevated in the TLR-2-deficient mice, with numbers reaching significance at day 28 post-infection (Figure 6.2A). This data supports earlier findings reported by the

Weis lab which found increased numbers of T cells within the joints of *B. burgdorferi* infected TLR-2-deficient mice (78). Similarly, hearts were harvested at days 14, 21, 28, 35, and 60 post-infection and analyzed for T cell infiltration. At days 35 and 60 post-infection, T cells were significantly elevated in inflammatory infiltrates isolated from the hearts of TLR-2-deficient mice (Figure 6.2B). To our knowledge, the phenotype of these T cells has never been assessed.

2. T cell phenotype in B. burgdorferi-infected TLR-2-deficient mice is tissue specific. C3H WT and C3H TLR-2-deficient mice were infected with $1x10^5$ *B. burgdorferi* in both rear footpads and T cell phenotype into both joint and heart tissue was assessed using flow cytometry. $CD4^+$ and $CD8^+$ T cells were selected from $CD45.2^+$ $CD3e^+$ T cells. Expression of CD45.2, CD3e and CCR6 was used to identify inflammatory Th17 cells (123). We also assessed both the joint and heart cellular infiltrates for the presence of $Foxp3^+$ T regulatory cells, but these cells could not be identified in either tissue (data not shown). Within the ankle joint, $CD4^+$ T cells made up the majority of the T cells in both WT and TLR-2-deficient mice. However, TLR-2-deficient mice showed a reduced number of $CD4^+$ T cells compared to their WT counterparts (Figure 6.3A). $CD8^+$ T cells within the joints were significantly elevated in the TLR-2-deficient mice at day 28 post-infection and the numbers of these cells trended higher at all time points evaluated (Figure 6.3B). $CCR6^+$ Th17 cell numbers were significantly higher in WT mice at days 14 and 21 post-infection. As resolution occurred, the number of Th17 cells decreased dramatically, possibly indicating a less inflammatory environment (Figure 6.3C).

Within the heart tissue, infiltrating $CD4^+$ T cell numbers in the TLR-2-deficient mice trended higher on day 28 and were significantly elevated by day 35 post-infection (Figure 6.3D). $CD4^+$ T cells have been shown to be important in carditis resolution, so the TLR-2-deficient mice could potentially resolve their carditis much faster (32). $CD8^+$ T cells were elevated in the TLR-2-deficient mice within the heart tissue infiltrates on days 28 and 35 post-infection, but their numbers did not reach statistical significance (Figure 6.3E). $CCR6^+$ Th17 cells were significantly higher in WT mice at day 28 post-infection and their numbers were reduced by day 35 post-infection. Interestingly, Th17 cell numbers in TLR-2-deficient mice peaked at day 35 and were significantly increased compared to WT controls possibly indicating a delayed recruitment (Figure 6.3F). This data suggests that specific T cell subsets may play a role in *B. burgdorferi* infection in TLR-2-deficient mice.

It was also possible that the increased $CD3e^+$ T cells within the joint or heart tissue could be attributed to recruitment of Natural Killer T (NKT) cells. Others have suggested a role for NKT cells during Lyme arthritis (124). We therefore looked for both Natural Killer (NK) ($CD45.2^+NKp46^+CD122^+CD3e^-$) and NKT ($CD45.2^+NKp46^+CD122^+CD3e^+$) cells in the infected tissues at day 21 post-infection. Within the ankles, both NK and NKT cells were significantly elevated in WT mice compared to the TLR-2-deficient mice (Figure 6.4A). Within the infected heart tissue, we were unable to detect any NKT cells, and NK cell numbers were very low in both WT and TLR-2-deficient mice. In either tissue, populations were not

significantly different (Figure 6.4B), and it was therefore unlikely that either NKT or NK cells could account for the increased disease severity seen in the TLR-2-deficient mice.

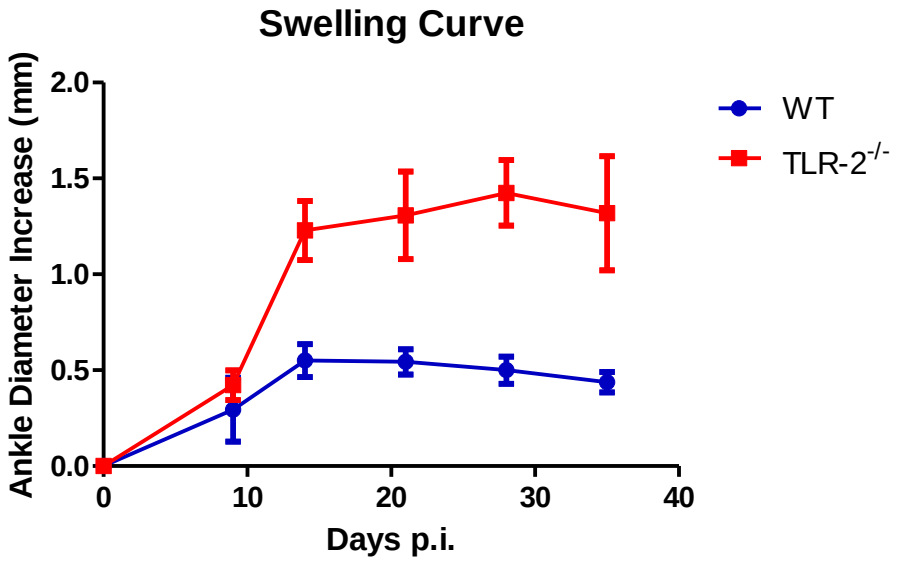

Figure 6.1: Ankle swelling curve of WT and TLR-2-defiicent mice. C3H WT and C3H TLR-2-deficient mice were infected with $1x10^5$ *B. burgdorferi* in the hind footpads and ankle swelling was monitored throughout the infection time-course. N=3, data representative of two separate experiments. Symbols represent means +/- SD.

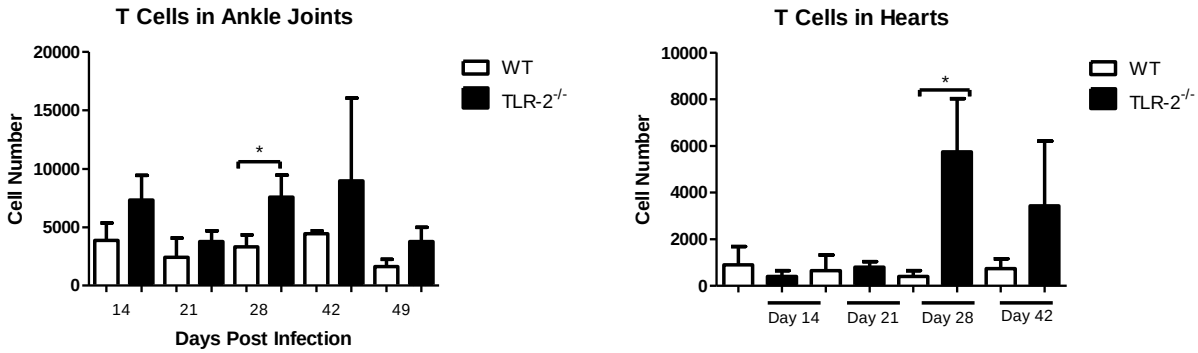

Figure 6.2: Quantification of $CD3e^+$ T cells in inflammatory infiltrates of *B. burgdorferi*-infected WT and TLR-2-deficient mice. C3H WT and C3H TLR-2-deficient mice were infected with *B. burgdorferi* and numbers of infiltrating $CD3e^+$ T cells were monitored from both ankle joint tissue and hearts using flow cytometry. n=3, data representative of two separate trials. Bars represent means +/- SD. * indicate data is significantly different from control data at the $p<0.05$ level determined by ANOVA followed by Tukey test.

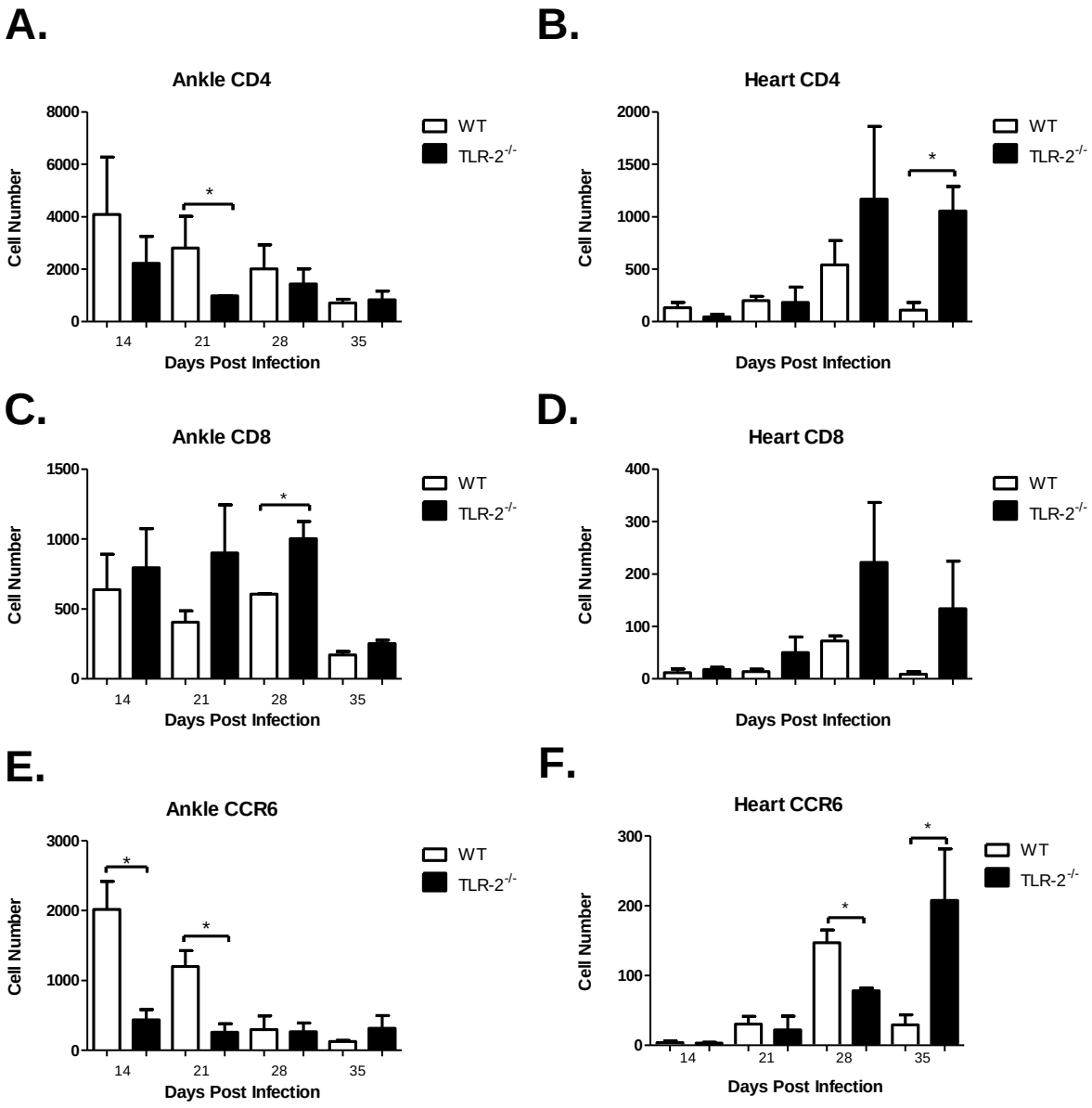

Figure 6.3: Populations of T cells in ankle and heart tissue were assessed using flow cytometry. C3H WT and C3H TLR-2-deficient mice were infected with *B. burgdorferi* and T cell phenotype in ankle and heart tissue was characterized using CD4 (A&B), CD8 (C&D), and Th17 (E&F) cell specific markers. T cells were characterized at days 14, 21, 28 and 35 post-infection. n=3, data representative of one trial. Bars represent means +/- SD. * indicate data is significantly different from control data at the $p<0.05$ level determined by ANOVA followed by Tukey test.

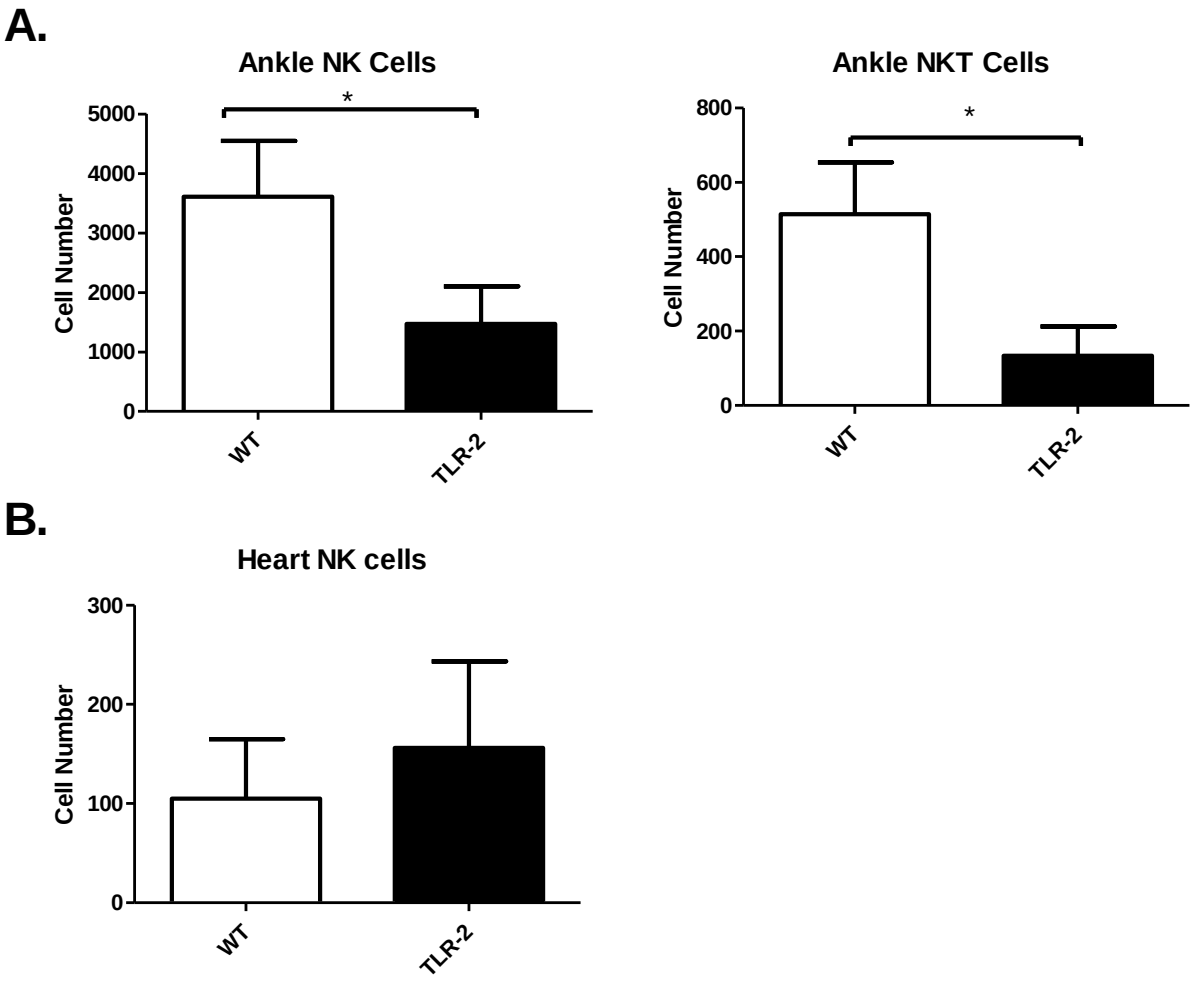

Figure 6.4: C3H WT and C3H TLR-2-deficient mice were infected with *B. burgdorferi* and NK ($CD45.2^{+}NKp46^{+}CD122^{+}CD3e^{-}$) and NKT ($CD45.2^{+}NKp46^{+}CD122^{+}CD3e^{+}$) cells were enumerated in ankle and heart tissue at day 21 post-infection. n=3, data representative of one trial. Bars represent means +/- SD. * indicate data is significantly different from control at the $p<0.05$ level determined by Student T-test.

3. $CD4^+$ or $CD8^+$ T cell depletion reduces ankle joint swelling in TLR-2-deficient mice and innate immune cell recruitment.

C3H WT and C3H TLR-2-deficient mice were depleted of either $CD4^+$ or $CD8^+$ T cells using intraperitoneal injections of either $CD4^+$ or $CD8^+$ T cell-depleting antibodies. One day after administration of depleting antibodies, mice were infected with $1x10^5$ *B. burgdorferi* in both rear footpads. T cell depletion was maintained by weekly administration of depleting antibody throughout the infection time-course. Ankle swelling was monitored every 7 days. WT mice depleted of either $CD4^+$ or $CD8^+$ T cells had slightly reduced swelling at all time points assessed compared to saline-treated controls (Figure 6.5A). TLR-2-deficient mice depleted of $CD4^+$ T cells had significantly reduced ankle swelling compared to untreated controls, but all of the mice died after day 21 post-infection. Like their $CD4^+$ T cell depleted counterparts, anti-CD8-treated TLR-2-deficient mice showed significantly reduced ankle swelling, but survived the infection (Figure 6.5B). Figure 6.5C shows a representative ankle from a TLR-2 deficient CD8-depleted mouse and a saline treated TLR-2-deficient control mouse at day 14 post-infection. $CD8^+$ T cell depleted TLR-2-deficient mice had dramatically reduced ankle joint swelling compared to saline-treated TLR-2-deficient mice. Sections of both ankle joint (Figure 6.6A) and heart (Figure 6.6B) tissue from untreated and T cell-depleted TLR-2-deficient mice were analyzed for disease severity histologically by H&E staining. Upon analysis, it was evident that TLR-2-deficient mice displayed significantly worse arthritis and carditis compared to WT controls (Figure 6.6C). In addition, TLR-2-deficient animals depleted of $CD8^+$ T cells had less severe inflammation in both ankle joint and heart tissue compared to

their untreated counterparts. $CD4^+$ T cell-depletion resulted in slightly reduced severity in the TLR-2-deficient mice, but this was not significant. In order to obtain quantitative values for inflammatory cell infiltrates, we used flow cytometry to evaluate innate immune cell recruitment into the joints.

Untreated and T cell-depleted WT and TLR-2-deficient mice were sacrificed at days 21 and 35 post-infection. Ankle joints were harvested and analyzed for neutrophil and macrophage infiltration using flow cytometry. $Ly6g^{hi}$ cells, representative of mature neutrophils, were increased in untreated TLR-2-deficient mice compared to untreated WT mice on both day 21 and 35 post-infection (Figure 6.9A&B) in agreement with a previous report (78). However, following either $CD4^+$ or $CD8^+$ T cell depletion, neutrophil numbers were significantly lower (Figure 6.9A&B). This change in neutrophil infiltration was not seen in $CD4^+$ or $CD8^+$ T cell-depleted WT mice. Instead, T cell depletion in WT mice actually increased neutrophil recruitment on day 21. By day 35, neutrophil numbers within the joints of untreated TLR-2-deficient mice were reduced compared to day 21 levels, possibly indicating the beginning of resolution. Neutrophil numbers in untreated and T cell-depleted WT mice were not significantly different at this time point. Surprisingly, $CD8^+$ T cell-depleted TLR-2-deficient mice had significantly elevated numbers of neutrophils on day 35 post-infection (Figure 6.9A). This indicated that the innate immune response was either delayed or T cell depletion was not maintained for the full five weeks. To check for the maintenance of T cell depletion, the mice were stained for $CD4^+$ and $CD8^+$ T cells at each time point. A very small number of $CD8^+$ T cells were present in the joint tissue on day 35 post-infection, but remained significantly reduced

compared to saline treated controls (data not shown). $CD4^+$ T cells maintained complete depletion for five weeks of consistent treatment.

Similar to neutrophils, macrophage numbers were significantly decreased in both CD4 and CD8-depleted TLR-2-deficient mice on day 21 post-infection. WT mice depleted of $CD8^+$ T cells showed a significant increase in macrophages compared to their untreated counterparts. On day 35 post-infection, macrophage numbers were similar in depleted or saline-treated WT and TLR-2-deficient mice (Figure 6.9B). In TLR-2-deficient mice, early T cell responses appeared to be important for recruitment and/or maintenance of the innate immune response.

4. T cell depletion in TLR-2-deficient mice results in more efficient bacterial clearance despite a poor B. burgdorferi-specific antibody response.

TLR-2-deficient mice depleted of $CD4^+$ T cells become moribund and die shortly after the peak of infection. We initially hypothesized that these mice would display a defect in *B. burgdorferi*-specific antibody production and have even higher bacterial loads compared to their untreated litter-mates. We collected serum at day 21 and day 35 post-infection from all animals and determined that *B. burgdorferi*-specific IgM levels were unchanged in either T cell-depleted or saline-treated WT and TLR-2-deficient animals (Figure 6.7). However, *B. burgdorferi*-specific IgG levels were reduced in both TLR-2-deficient and WT mice depleted of $CD4^+$ T cells. $CD4^+$ T cells are important to help B cells produce an adequate antibody response (125), so it was expected that both sets of mice would make a poorer *B. burgdorferi* specific IgG response (Figure 6.7). We also tested mice for bacterial clearance to insure that very high bacterial levels were not responsible for the death of the $CD4^+$ T cell-depleted

TLR-2-deficient mice. Untreated TLR-2-deficient mice at day 21 post-infection have significantly elevated bacterial numbers compared to their WT counterparts (Figure 6.8A). This has been previously reported and agrees with our preliminary data (78). Interestingly, after either $CD4^+$ or $CD8^+$ T cell-depletion in the TLR-2-deficient mice, bacterial numbers in the tissues were dramatically reduced (Figure 6.8). The reason for this is unclear, but does not appear to be due to a better antibody response (Figure 6.7) or a stronger recruitment of innate immune cells (Figure 6.9).

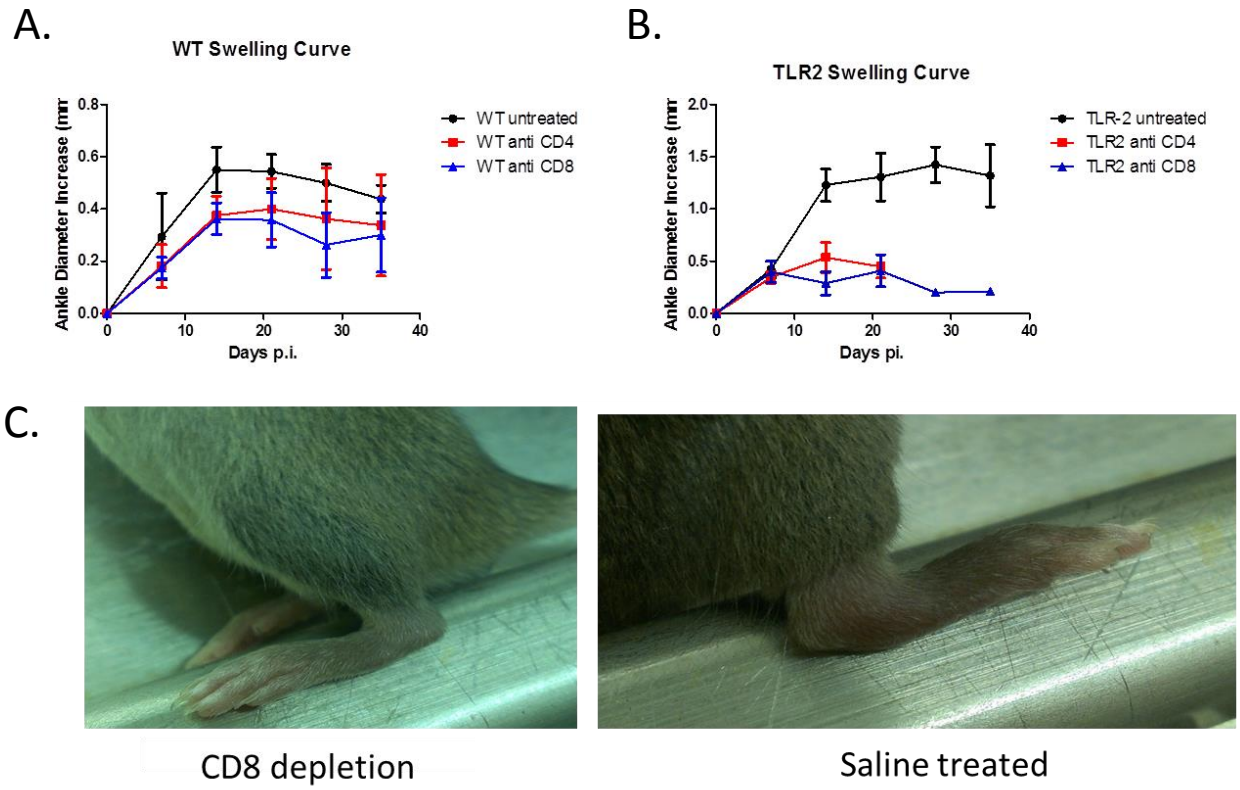

Figure 6.5: C3H WT and C3H TLR-2-deficient mice were treated with saline, CD4 depleting antibody or CD8 depleting antibody and infected with *B. burgdorferi*. Ankle swelling was monitored over the infection time-course for both WT (A) and TLR-2-deficient (B) mice. Representative pictures of TLR-2-deficient mice depleted of CD8 T cells or saline-treated were taken at day 14 post-infection (C). n=3, data representative of one trial. Symbols represent means +/- SD.

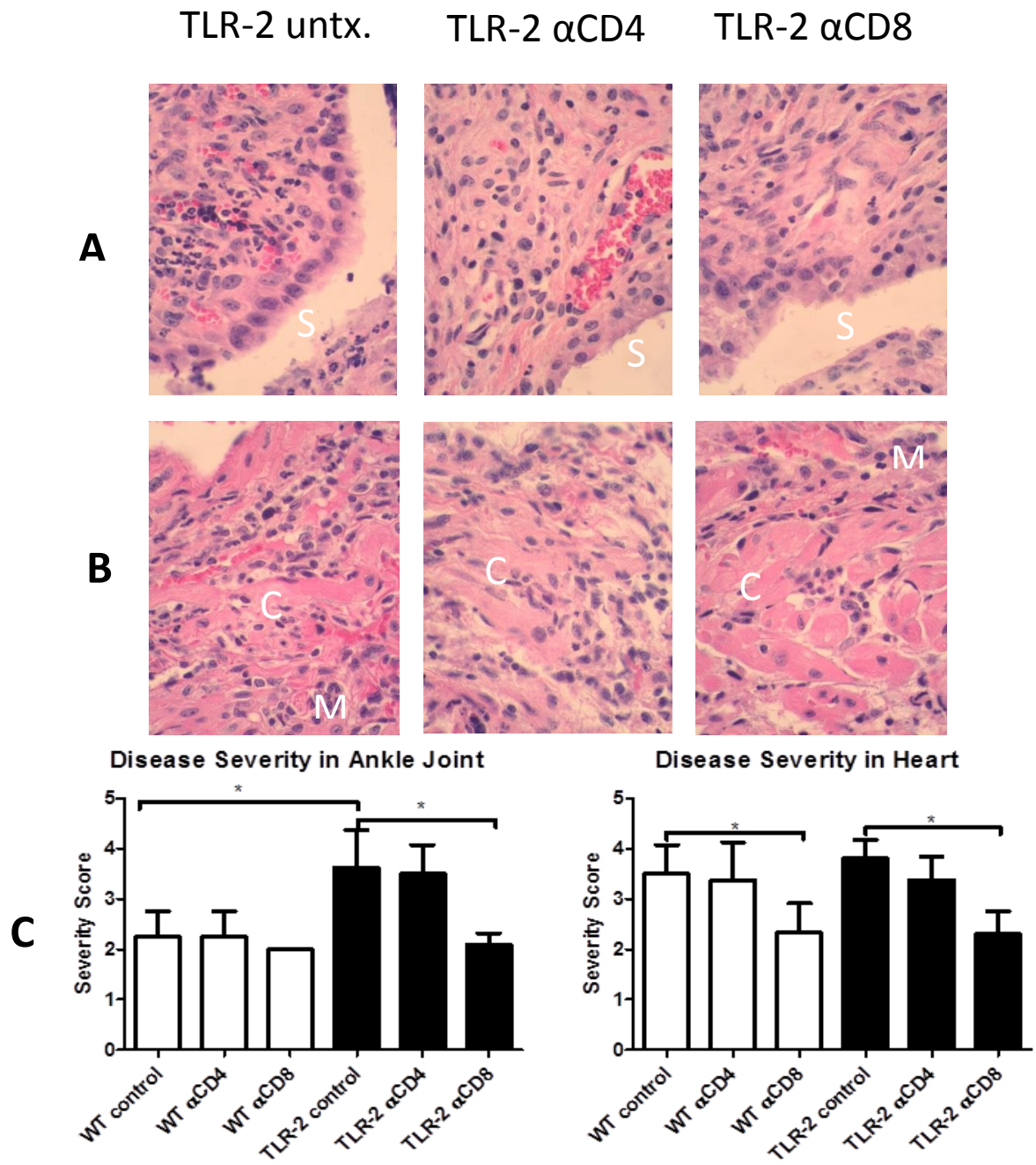

Figure 6.6: C3H WT and C3H TLR-2-deficient mice were treated with saline, CD4 depleting antibody or CD8 depleting antibody and infected with *B. burgdorferi*. Ankle (A) and heart (B) sections were evaluated for each mouse by histopathology and scored for lesion severity (C). The following scale was used: 0 = none (no inflammation); 1 = minimal inflammation involving < 5% of tissue; 2= moderate with focally extensive areas of inflammation 3 = moderate to severe with focally extensive areas of inflammation; 4 = severe with large confluent areas of inflammation. C=cardiomyocyte, M=macrophage, S=synovial membrane. n=8, bars represent means +/- SD. * indicate data is significantly different with $p<0.05$ using unparametric ANOVA with Dunnet post-test. Results indicative of one trial.

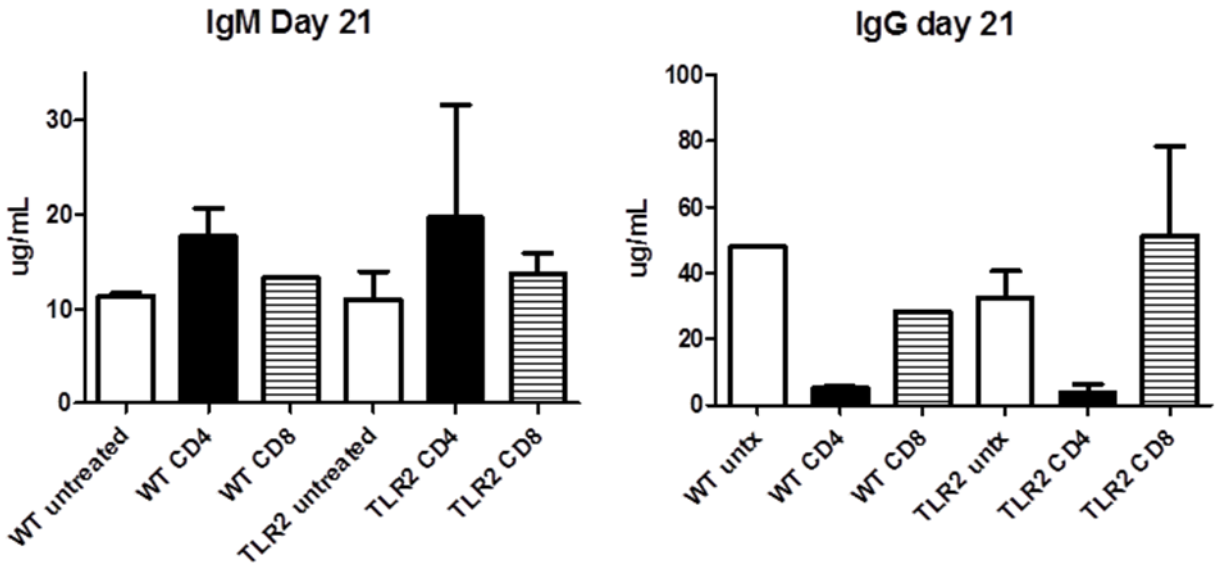

Figure 6.7: C3H WT and C3H TLR-2-deficient mice treated with saline, CD4 depleting antibody or CD8 depleting antibody were assessed for *B. burgdorferi*-specific IgM and IgG levels in sera. Serum was collected at day 21 post-infection, and was assessed for antibody levels using an ELISA. n=3, data representative of one trial. Bars represent means +/- SD.

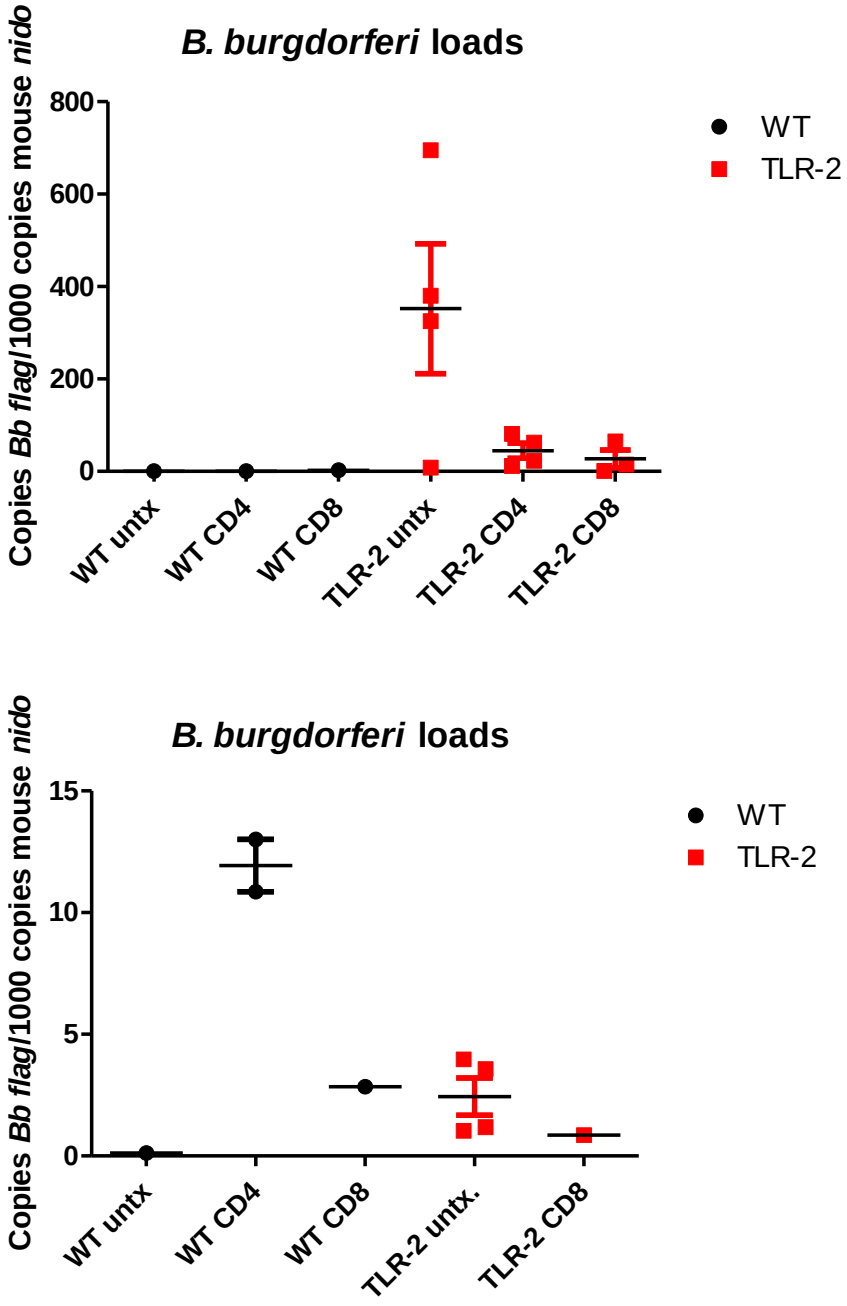

Figure 6.8: *B. burgdorferi* loads in tissues from TLR-2 and WT mice with and without specific T cell depletion. Bladders were harvested at day 21 (A) and day 35 (B) post infection and *B. burgdorferi* numbers were determined using RT-PCR analysis. n=3, data representative of one trial. Bars represent means +/- SD.

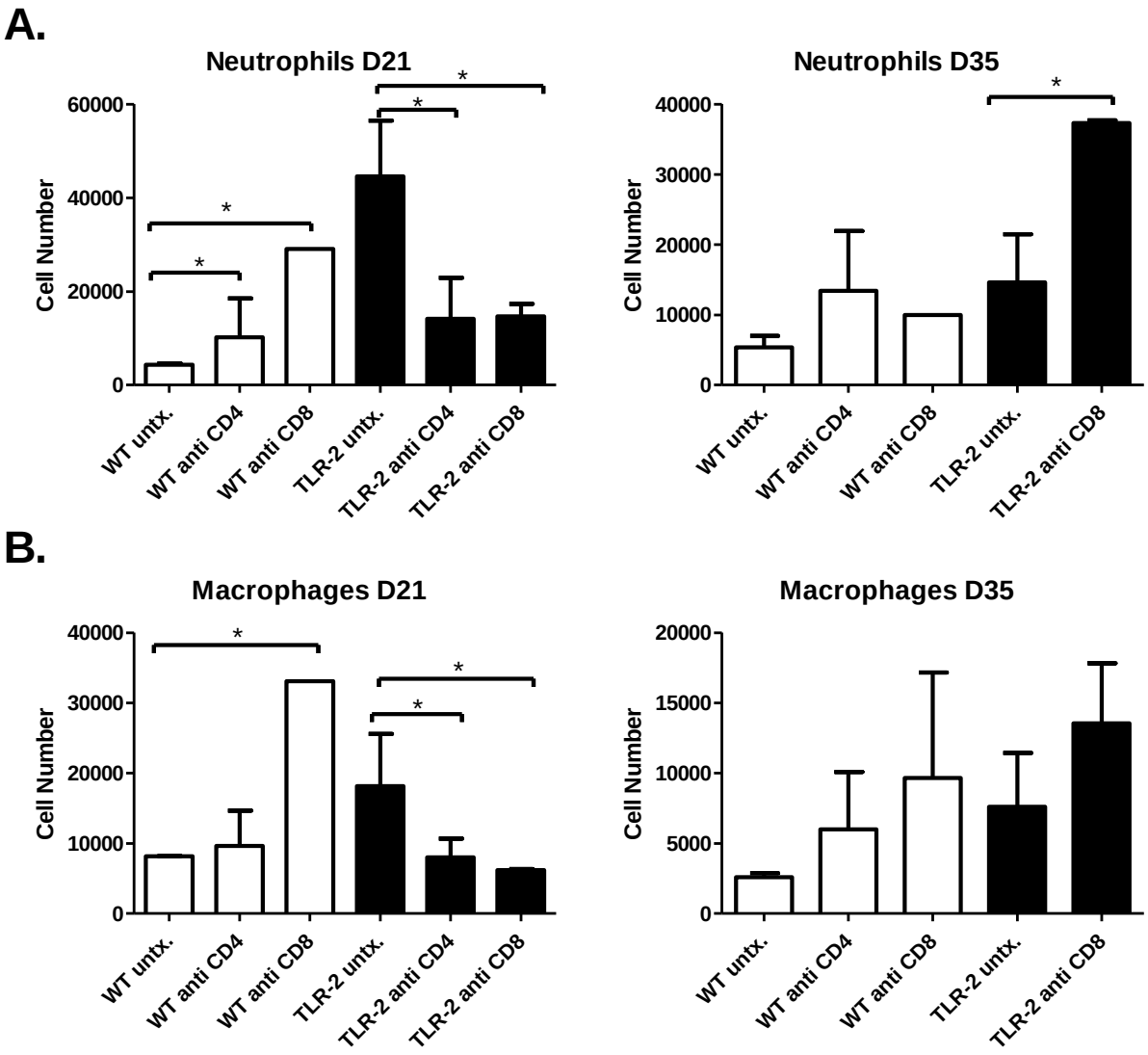

Figure 6.9: Analysis of neutrophil and macrophage recruitment into ankle joint tissue using flow cytometry. C3H WT and C3H TLR-2-deficient mice were treated with saline, CD4 depleting antibody or CD8 depleting antibody and infected with *B. burgdorferi*. Neutrophil ($Ly6g^{hi}$) numbers were assessed from joint tissue at day 21 and 35 post-infection (A). Similarly, macrophage ($F4/80^{+}$) numbers were also evaluated at these time points (B). n=3, data representative of one trial. Bars represent means +/- SD. * indicate data is significantly different from untreated control at the $p<0.05$ level determined by ANOVA followed by Tukey test.

5. TLR-2-deficient mice display a defect in innate immune cell function.

BMDM were obtained from C3H WT or C3H TLR-2-deficient mice and stimulated with either IFN-γ and LPS or IL-4 to polarize them to either an M1 or an M2 phenotype, respectively. TLR-2-deficient macrophages displayed a defect in both M1 and M2 polarization compared to WT controls (Figure 6.10). The mechanism behind this defect still needs to be elucidated, but may indicate a reason why, although more macrophages are recruited to the joint, *B. burgdorferi* titers are still elevated in the TLR-2-deficient mice. To test neutrophil function, neutrophils were isolated from the bone marrow of both WT and TLR-2-deficient animals using a Percoll gradient (126). The cells were co-cultured with GFP-labeled *B. burgdorferi* for 1 hour and stained for a neutrophil specific marker (Ly6g). Uptake of bacteria was measured using flow cytometry. There was no significant defect in spirochete uptake by TLR-2-deficient neutrophils; only a 1% decrease was noted (data not shown). Bactericidal studies still need to be undertaken to assess whether neutrophils, upon uptake of bacteria, can efficiently kill them.

6. Cytokine differences are seen between WT and TLR-2-deficient mice.

We initially hypothesized that $CD4^+$ or $CD8^+$ T cell depletion would result in less IFN-γ production, and therefore less inflammation. To address this, we analyzed saline-treated and T cell-depleted WT and TLR-2-deficient mice for IFN-γ levels from ankle joint tissue at day 21 and day 35 post-infection. No significant differences were seen between untreated or T cell-depleted WT and TLR-2-deficient mice (Figure 6.11). We decided to look at an earlier timepoint, as other pro-inflammatory

mediators peak early during Lyme arthritis (127). Analysis of IFN-γ at day 7 post-infection yielded no difference between untreated or T cell-depleted TLR-2-deficient mice (data not shown). To delve further into potential cytokine differences, a Luminex inflammatory cytokine panel was run on harvested joint samples. The only detectable cytokine difference between WT and TLR-2-deficient mice was MIG (CXCL9), which signals through the chemokine receptor CXCR3 (128). Untreated TLR-2-deficient mice had significantly elevated levels of MIG compared to WT controls. In addition, $CD8^+$ T cell depletion in these mice dramatically reduced the level of MIG produced at both day 21 and day 35 post-infection. Others have suggested that MIG production in TLR-2-deficient mice was mediated by synoviocytes (78). This finding suggests a role $CD8^+$ T cells in stimulating MIG production by synoviocytes (Figure 6.12). Preliminary data suggested that $CD8^+$ T cell depletion, specifically, resulted in reduced production of MIG from ICAM-1^+ V-CAM-1^+CD14^- synoviocytes in joint tissue at day 14 post-infection (Figure 6.13). $CD8^+$ T cells likely secrete IFN-γ early, increasing production of MIG by synoviocytes which causes additional recruitment of T cells. This data suggests that early T cell responses within the joint stimulate recruitment of additional T cells by inducing MIG production in synoviocytes.

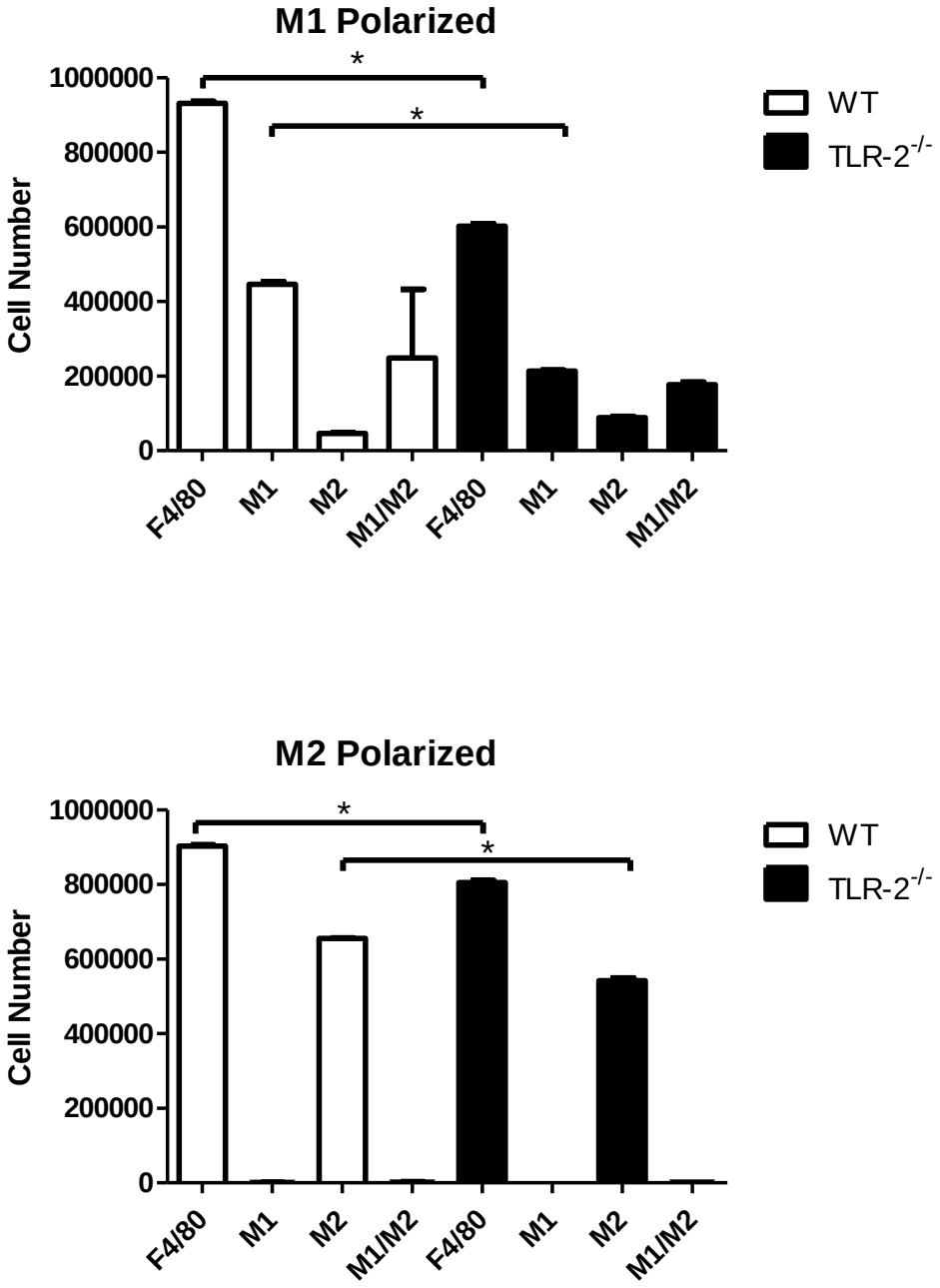

Figure 6.10: Macrophage polarization in WT and TLR-2-deficient mice. BMDM from C3H WT and C3H TLR-2-deficient mice were cultured and polarized to either the M1 (IFN-y, LPS) or M2 (IL-4) phenotype. Ability to phenotype switch was assessed using flow cytometry. n=3, data representative of one trial. Bars represent means +/- SD. * indicate data is significantly different from control data at the $p<0.05$ level determined by ANOVA followed by Tukey test. Figure made in collaboration with Rachel Olson.

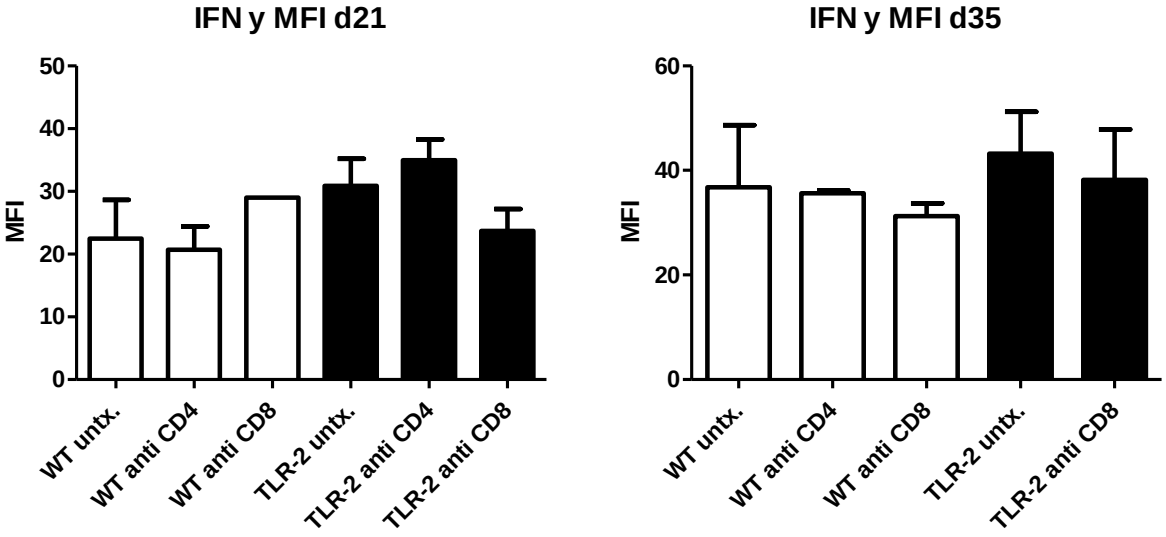

Figure 6.11: MFI of IFN-γ in *B. burgdorferi*-infected joint tissue from WT and TLR-2-deficient mice. Using flow cytometry, untreated and T cell-depleted WT and TLR-2-deficient mice were analyzed for IFN-γ production. Mean fluorescent intensities are given at day 21 and day 35 post-infection. n=3, data representative of one trial. Bars represent means +/- SD.

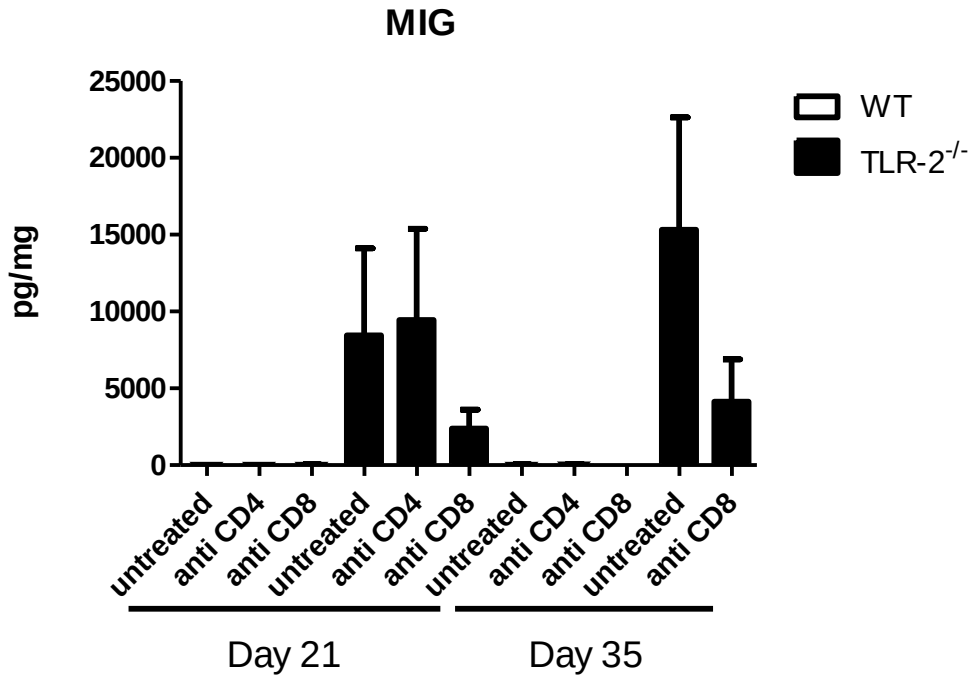

Figure 6.12: A murine cytokine panel was run on joints of untreated and T cell-depleted WT and TLR-2-deficient mice using a Luminex assay. MIG (CXCL9) protein levels were significantly different between WT and TLR-2-deficient mice at both days 21 and 35 post-infection. n=3, data representative of one trial. Bars represent means +/- SD.

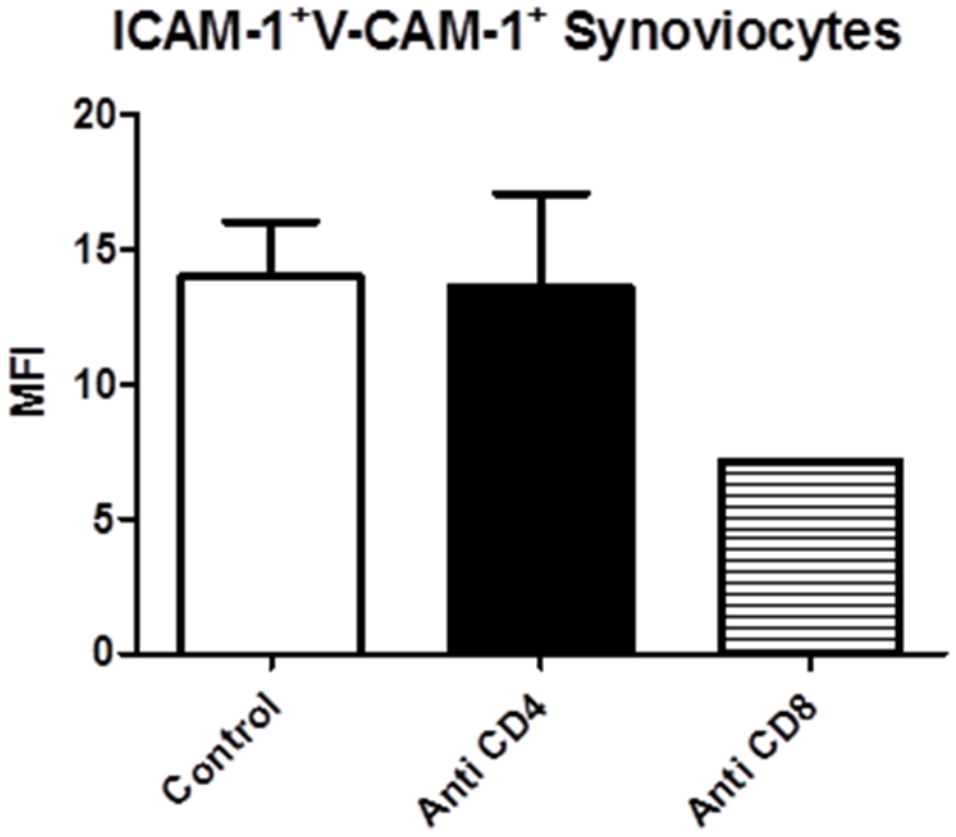

Figure 6.13: MIG levels within ICAM-1^{+}V-CAM-$1^{+}$$CD14^{-}$ synoviocytes were assessed from TLR-2-deficient mice. TLR-2-deficient mice were treated with saline or depleted of $CD4^{+}$ or $CD8^{+}$ T cells and infected with *B. burgdorferi*. 14 days post-infection, mice were sacrificed and synoviocytes were intracellularly stained for CXCL9. n=3, data representative of one trial. Bars represent means +/- SD.

Conclusions:

B. burgdorferi is an extracellular bacterium that expresses immunostimulatory outer surface proteins (OSPs) (37, 38). Upon entry into the mammalian host, *B.burgdorferi* switches its OspA dominant lipoprotein to the OspC lipoprotein (129). Pattern recognition receptors (PRRs), including NOD-like receptors (NLR) and toll-like receptors (TLR), have been implicated in the recognition of *B. burgdorferi* (39, 46). It has been demonstrated that TLR-2 is the primary recognition receptor for *B. burgdorferi* OspC and is important in bacterial clearance (44, 45).

Both C57BL/6 and C3H TLR-2-deficient mice infected with *B. burgdorferi* display significantly worse arthritis and carditis (45, 78). SCID mice lacking TLR-2 display reduced arthritis severity compared to mice lacking only TLR-2, indicating that the increased severity in the TLR-2-deficient mice was due to either B or T lymphocytes (47). It was later clarified that it was T cell infiltration that predisposed TLR-2-deficient mice to more severe arthritis, as T cell numbers within arthritic lesions were significantly elevated (78). This increase in T cell numbers in the joints was associated with increased levels of CXCL9 and CXCL10, giving a potential mechanism for the increased T cell recruitment (78). In addition, other immune cells populations such as neutrophils and mononuclear cells were also significantly elevated within the joint tissue of TLR-2-deficient mice (78). It was suggested that dysregulated chemokine production resulted in this innate immune cell increase. Despite this increased cellular immune response, *B. burgdorferi* levels remained approximately 7-fold higher in the TLR-2-deficient mice compared to WT control mice despite an apparently efficient antibody response (45). In

the current study, we sought to further address the role of T cells in TLR-2-independent response to *B. burgdorferi* infection.

Similar to previous publications, we found that TLR-2-deficient mice infected with *B. burgdorferi* displayed both increased ankle swelling and elevated numbers of $CD3e^+$ T cells within joint tissue at all timepoints assessed. In infected WT mice, T cells typically make up about 2% of the hematopoietic cell population within the joints. In infected TLR-2-deficient mice, this percentage jumped to 10%. In the hearts, we found a similar phenomenon; T cell numbers were elevated during carditis. As resolution began in the infected hearts, TLR-2-deficient mice showed a greater recruitment of T cells compared to their WT counterparts. To our knowledge, the identity of these T cells has not been previously published. Upon analysis of T cell phenotype, we found that the T cells consisted of $CD4^+$, $CD8^+$, and Th17 T cells; T regulatory cells could not be found in either joint or heart tissue. We initially thought that NKT cells may account for a portion of the $CD3e^+$ T cells identified within the infected ankle joint and heart tissue. Fewer than 1,000 NKT cells could be identified within infected joint tissue and none were found within heart tissue of the TLR-2-deficient mice. This indicated that, although NKT cells may play a role in Lyme arthritis in WT mice (124, 130), they do not appear to make up a significant portion of the T cell infiltrate in the tissues of TLR-2-deficient mice. $CD4^+$ T cells made up the majority of T cells within the joint tissue of both WT and TLR-2-deficient mice infected with *B. burgdorferi*, but the joints of TLR-2-deficient mice had significantly less compared to WT controls. Similarly, TLR-2-deficient mice had significantly fewer Th17 cells within the joints at day 21 post-infection. In this study, we did not further investigate the phenotype of the $CD4^+$ T cells as either Th1 or Th2 cells,

but this may prove useful in the future as a balance of Th1 and Th2 cells has been implicated in the development and resolution of Lyme arthritis (23, 131-133). We also found that the infiltration of $CD4^+$ and $CD8^+$ T cells was tissue specific. During carditis, TLR-2-deficient mice recruited more $CD4^+$ T cells compared to WT mice and had elevated numbers of $CD8^+$ T cells, but this difference did not reach statistical significance. On day 21 post-infection, Th17 cells were elevated in WT mice, but as resolution occurred TLR-2-deficient mice had significantly more Th17 cells within infected heart tissue. These cells may partially account for the dramatic increase in $CD4^+$ T cells at day 35 within the infected hearts. In models of fungal or *Staphylococcus aureus* infection, an increased population of Th17 cells and increased inflammation was associated with an absence of TLR-2. However, innate immune cell numbers were not elevated (121, 134).

The innate immune response following *B. burgdorferi* infection of TLR-2-deficient mice has been poorly studied. It is known that both neutrophils and mononuclear leukocyte infiltration are increased in the absence of TLR-2 (78). Here, we show that both neutrophil and macrophage infiltration into both joint and heart tissue following *B. burgdorferi* infection were increased in the TLR-2-deficient mice. It appeared that both $CD4^+$ and $CD8^+$ T cells played a role in the recruitment of these cells. Both $CD4^+$ and $CD8^+$ T cell-depleted TLR-2-deficient mice showed significantly decreased numbers of both innate immune cells at day 21 post-infection compared to untreated controls. This phenomenon did not occur in T cell-depleted WT mice. The effectiveness of the neutrophil and macrophages in killing *B. burgdorferi* following their recruitment into the joints and hearts of TLR-2-deficient mice has not been examined. BMDM from TLR-2-

deficient mice stimulated with sonicated *B. burgdorferi* antigen failed to produce nitric oxide (NO), IL-6, or TNF-α (45). However, neutrophil function was not studied. In *Porphyromonas gingivalis* pulmonary infection, TLR-2-deficient innate immune cell recruitment was unchanged, however the bactericidal function of neutrophils was reduced by 54% compared to WT cells (49). Due to the importance of innate immune cells in the clearance of *B. burgdorferi (18),* we sought to analyze the function of the innate immune cells in the TLR-2-deficient mice. We showed that BMDM from TLR-2-deficient mice were less capable of producing a reliable M1 or M2 response after *in vitro* stimulation with either LPS and IFN-γ or IL-4, respectively. This suggested that macrophages *in vivo* may be less capable of phagocytosing *B. burgdorferi* or exhausted neutrophils and potentially less able to induce resolution. It may also explain the reduced NO, IL-6 and TNF-α seen after the addition of sonicated spirochetes as discussed above (45). Neutrophils isolated from the bone marrow of TLR-2-deficient mice did not show a reduced ability to take up GFP-labeled *B. burgdorferi*. However, this does not mean that they are able to efficiently kill the engulfed spirochetes, and future bactericidal studies will be undertaken. Although TLR-2-deficient mice recruited a more intense innate immune response, it may be less functional due to a failure to signal appropriately. Surprisingly, we found that in the absence of either $CD4^+$ or $CD8^+$ T cells, TLR-2-deficient mice had lower bacterial loads despite a reduced recruitment of innate immune cells. Both neutrophil and macrophage numbers in these treated mice resembled that of a WT mouse. Thus, it is likely that the overwhelming innate immune response seen in the TLR-2-deficient mice actually hindered bacterial clearance more than it helped.

The mechanism of increased T cell recruitment in the TLR-2-deficient mice is not clear, but the increased production of IFN-inducible CXCL9 and CXCL10 by synoviocytes has been suggested to drive this response (78). TLR-2-deficient mice have increased transcripts of CXCL9 and CXCL10 following infection with *B. burgdorferi* (78). We found only CXCL9 was upregulated in the joints of *B. burgdorferi*-infected TLR-2-deficient mice, in our hands. We did not find elevated levels of CXCL10 as others have found (78), but it is possible this cytokine undergoes a post-transcriptional modification (135). In the absence of $CD8^+$ T cells, CXCL9 levels were dramatically reduced, suggesting that $CD8^+$ T cells activate synoviocytes to produce CXCL9, thereby recruiting addition T cells into the joint. To investigate this possibility, we depleted TLR-2-deficient mice of $CD8^+$ T cells, infected them with *B. burgdorferi*, and assessed CXCL9 production by ICAM-1^+V-CAM-1^+CD14^- synoviocytes from ankle joint tissue. Our preliminary data showed that synoviocytes from $CD8^+$ T cell-depleted TLR-2-deficient mice produced lower levels of CXCL9 compared to $CD8^+$ T cell-sufficient TLR-2-deficient controls. *Mig* is an IFN-γ-responsive gene (136), and this data suggested that early production of IFN-γ by $CD8^+$ T cells potentially modifies the synoviocyte chemokine response, causing the increased recruitment of T cells.

The pathogenesis of Lyme arthritis and carditis has been assessed in the absence of T cells (35). *Rag*-1 mice, deficient in both B and T cells, reconstituted with T cells alone developed more severe arthritis and carditis than non-reconstituted mice (28). This indicated a role for T cells in the pathology of Lyme borreliosis (28). Because the number of T cells was elevated in the TLR-2-deficient mice, we hypothesized that depletion of either $CD4^+$ or $CD8^+$ T cells would modify the inflammatory response. We

found that $CD8^+$ T cells stimulated synoviocytes to produce CXCL9. An increase in CXCL9 most likely recruits additional T cells to the infected joint (128). Depletion of either T cell subset in TLR-2-deficient mice reduced ankle swelling, severity and innate immune cell recruitment. Both swelling and innate immune cell recruitment in the TLR-2-deficient mice was returned to WT levels after T cell depletion. This reduction in inflammatory infiltrates enabled the TLR-2-deficient mice to more effectively clear the spirochetes. However, the results shown are preliminary and representative of just one trial; they need to be repeated to strengthen our hypotheses. Our preliminary results indicated that the overly exuberant immune response in the TLR-2-deficient mice is primed by T cells and hinders bacterial clearance.

CHAPTER VII

THE EFFECT OF IL17RA ABLATION ON DEVELOPMENT AND SEVERITY OF EXPERIMENTAL LYME DISEASE

A. *Introduction*

The role of IL-17 in the development of Lyme disease has been in question as early as 2000. It was discovered that T cells primed in the presence of whole *B. burgdorferi* or synthetic peptides representative of the bacteria's outer surface proteins, preferentially expressed IL-17 (137). A later study showed that blocking endogenous IL-17 in a vaccination and challenge model, protected mice from Lyme arthritis development (138). Serum from *B. burgdorferi*-infected patients showed increased levels of IL-23, IL-6, TGF-β, and IL-1β, which were capable of activating a Th17 response (139). Additional *in vitro* studies indicated that *Borrelia* species activated caspase-1 which, in turn, induced the production of IL-17 (40). However, these results have come from the use of unique experimental models of Lyme disease, and the applicability of these results to human Lyme Disease is unclear. The importance of IL-17 in the pathogenesis of Lyme arthritis depends entirely upon which model system is used, and how this relates to human disease has yet to be determined. In the current study, we infected C3H mice deficient in the IL-17RA subunit with *B. burgdorferi* and followed arthritis and carditis development over time to assess whether there was a role for IL-17 in the development of experimental Lyme disease.

IL-17 is a proinflammatory cytokine associated with chronic inflammatory conditions including rheumatoid arthritis and multiple sclerosis (140, 141), as well as experimental collagen induced arthritis (142). The majority of IL-17 is produced by Th17 cells, but innate immune cells including γδ T cells, iNKT cells and mast cells are also capable of producing it (143, 144). The IL-17 family consists of 6 members: IL-17A-F, with IL-17A and IL-17F as the most well-studied members. All IL-17 cytokines signal through homo- or hetero-dimers of a family of IL-17 receptors. Similar in naming to the cytokines themselves, the receptors are IL-17RA, IL-17RB, IL-17RC, IL-17RD, and IL-17RE. IL-17RA is a common heterodimer for signaling of IL-17A, IL-17F, and IL-17E, so ablation of this gene compromised signaling of the most common IL-17 cytokines produced (145). IL-17RA signaling stimulated the production of neutrophilic chemokines such as CXCL1 (KC), CXCL2, CXCL5, CXCL6, and CXCL8 (146). IL-17RA-deficient mice infected with *Klebsiella pneumonia* quickly succumbed to infection due to a failure to recruit a sufficient number of neutrophils (147). This phenomenon is not unique to *Klebsiella* infection; an additional report using IL-17RA-deficient mice infected with influenza also recruited significantly fewer neutrophils and suffered less severe lung injury (146). Because experimental Lyme arthritis pathology is highly dependent on recruitment of neutrophils (76), it has been hypothesized that IL-17RA-deficient mice would have less severe arthritis. Our studies indicate that absence of IL-17RA signaling had little impact on the development of either Lyme arthritis or carditis. In addition, no IL-17 was detectable in joint tissue from *B. burgdorferi*-infected mice. These results are similar to those reported by Nardelli et al. (148). Modest levels of IL-17 were found

within the serum, but the significance of this to the immune response or bacterial clearance is not clear.

B. *Results*

1. *IL-17RA deficiency does not alter ankle swelling or disease severity.*

To determine whether IL-17 played a role in development of experimental Lyme borreliosis, we infected C3H WT and C3H IL-17RA-deficient mice with $1x10^5$ *B. burgdorferi* in the hind footpads. Ankle swelling was monitored throughout the infection time-course and joints and hearts were harvested at days 21 and 42 post-infection. Despite an inability to respond to IL-17, *B. burgdorferi*-infected IL17RA-deficient mice displayed no difference in ankle swelling development or resolution compared to WT controls (Figure 7.1A). To determine if there were differences in disease development, we examined H&E stained histology sections of infected ankles and hearts from WT and IL-17RA-deficient mice. The tissue sections were evaluated and scored for their overall level of inflammation (severity score) and for the ratio of neutrophils to macrophages (type score). Histological analysis showed no difference in disease severity in either ankle or heart tissue using severity (Figure 7.1B) or type scoring (Figure 7.1C). All scores were higher at day 21 post-infection, which is typically near the peak of inflammation. Lower scores were associated with the resolution of inflammation at day 42 post-infection. These results indicated that IL-17RA-deficient mice developed Lyme arthritis and carditis, and resolved disease similarly to WT mice.

2. *Cellular infiltration into ankle joint tissue during experimental Lyme arthritis.*

It is known that IL-17RA-deficient mice have lower levels of circulating neutrophils (149). Our lab has previously shown that altering circulating neutrophil levels can impact Lyme arthritis development (150). Additionally, IL-17 can induce the production of the chemokine KC, regulating neutrophil recruitment (151). Neutrophil recruitment is critical to Lyme arthritis development (76). Using flow cytometry, we analyzed cellular infiltration into the joint tissue following infection with *B. burgdorferi*. Ankle joints were analyzed for infiltration of macrophages (F4/80), mature neutrophils ($Ly6g^{hi}$), B cells (B220/IgM), and T cells (CD3e). The majority of the inflammatory cells within the tissue at both day 21 and day 45 post-infection were neutrophils. However, there was no significant difference in neutrophil recruitment between the WT and the IL-17RA-deficient mice (Figure 7.2B). There was also no difference in macrophage (Figure 2A), B cell (Figure 7.2C), or T cell (Figure 7.2D) recruitment between the WT and IL-17RA-deficient mice. Recruitment of inflammatory cells to the site of infection did not appear to be compromised in the absence of IL-17 signaling.

3. *IL-17RA-deficient mice efficiently clear B. burgdorferi.*

The clearance of *B. burgdorferi* from infected tissues is thought to mediate disease resolution (152). Our lab has found that cyclooxygenase (COX)-1-deficient mice infected with *B. burgdorferi* made an efficient *B. burgdorferi*-specific IgM response, but failed to effectively class switch to IgG (153). The failure to class switch was

associated with low levels of IL-17 and IL-6 in the serum. By administering exogenous IL-17, the phenotype was rescued. We were interested in determining the *B. burgdorferi*-specific antibody response in the IL-17RA-deficient mice and the ability of these mice to clear spirochetes from tissue. *B. burgdorferi*-specific IgM (Figure 7.5B) and IgG (Figure 7.5C) antibody levels were analyzed by ELISA. We found that IL-17RA-deficient mice made the same level of both *B. burgdorferi*-specific IgM and IgG as WT controls. In addition, spirochete loads from ear tissue in the IL-17RA-deficient mice were no different than WT mice (Figure 7.4). IL-17 has been shown to increase phagocytosis in neutrophils (154), therefore we tested whether neutrophils from IL-17RA-deficient mice would have a decreased ability to uptake *B. burgdorferi*. Peripheral neutrophils were isolated from IL-17RA-deficient mice and WT mice and co-cultured with GFP-labeled *B. burgdorferi*. Uptake of spirochetes was analyzed using flow cytometry. We found that neutrophils from WT and IL-17RA-deficient mice phagocytosed GFP-labeled *B. burgdorferi* at similar levels (Figure 7.5), indicating that IL-17 signaling had no effect on neutrophil phagocytosis. Our results indicate no functional defects in the host response to *B. burgdorferi* infection in IL-17RA-deficient mice.

4. *IL-17 production in B. burgdorferi-infected mice.*

IL-17 has been shown to be important in the vaccination and challenge model of Lyme disease (155). Our lab has previously published that IL-17 is detectable in serum of *B. burgdorferi*-infected mice (153), but we have not detected it in infected joint tissue (unpublished data). Here, we were able to recapitulate previous data and

found IL-17 in the serum of both WT and IL-17RA-deficient mice (Figure 7.6). The IL-17RA-deficient mice had higher levels compared to WT mice, but this was not significant. This was likely due to their inability to utilize IL-17. We also found low levels of IL-17 in the heart tissue of both WT and IL-17RA-deficient mice at both day 21 and 42 post-infection (Figure 7.6). However, the hearts were not perfused and it is possible that this was due to blood contamination and not production of IL-17 directly within the tissue itself. IL-17 was completely undetectable within the joints of either WT or IL-17RA-deficient mice (data not shown). We found that IL-17 is produced systemically in the serum of mice infected with *B. burgdorferi*, but little to none at the sites of disease.

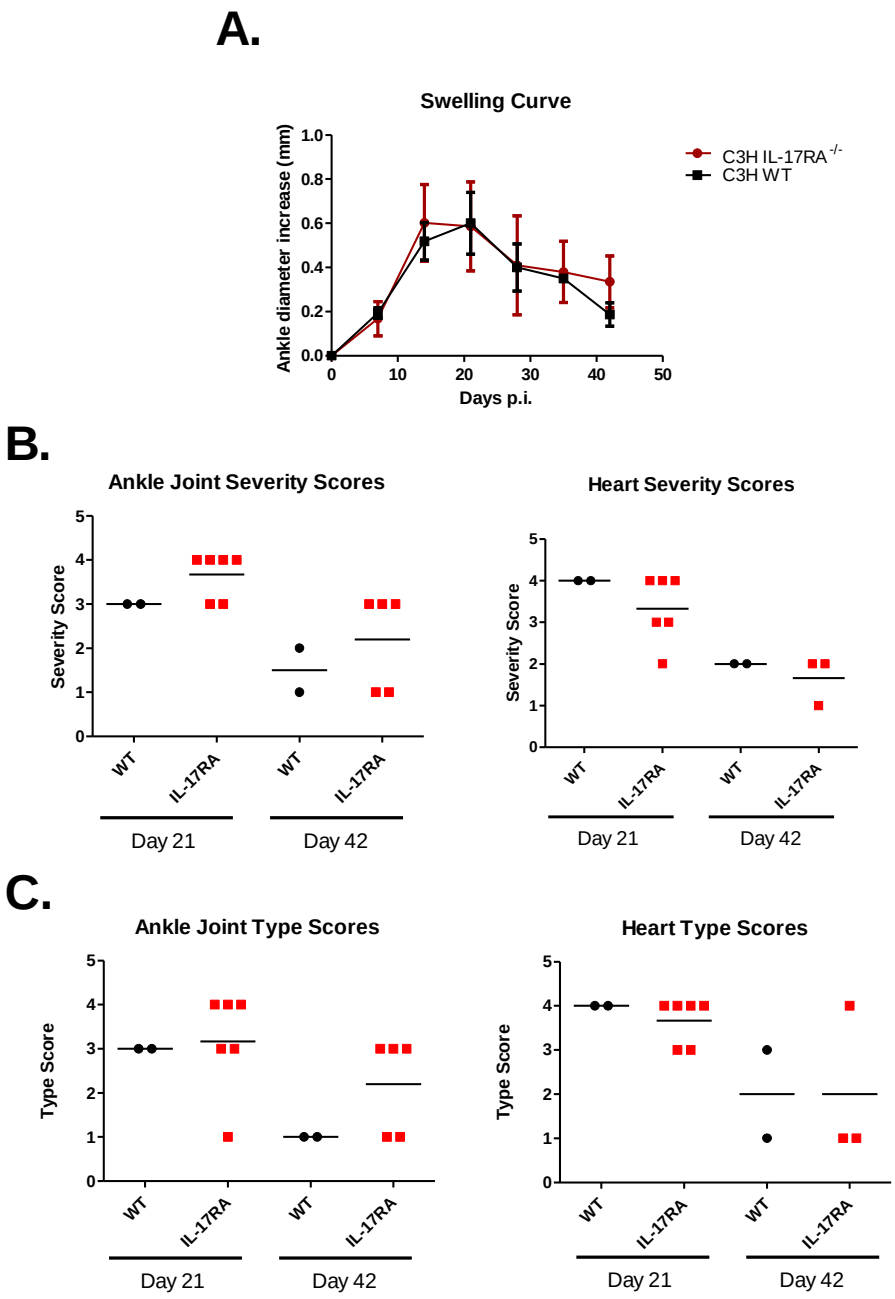

Figure 7.1: C3H WT and C3H IL-17RA-deficient mice were infected with *B. burgdorferi* and ankle swelling was monitored throughout the infection time course (A). Ankle joint and heart tissues were harvested at days 21 and 42 days post-infection and assessed histologically for both severity scores (B) and type scores (C) on a scale of 0-4. n=5, data representative of two separate trials. Each symbol represents an individual animal and bars represent the mean.

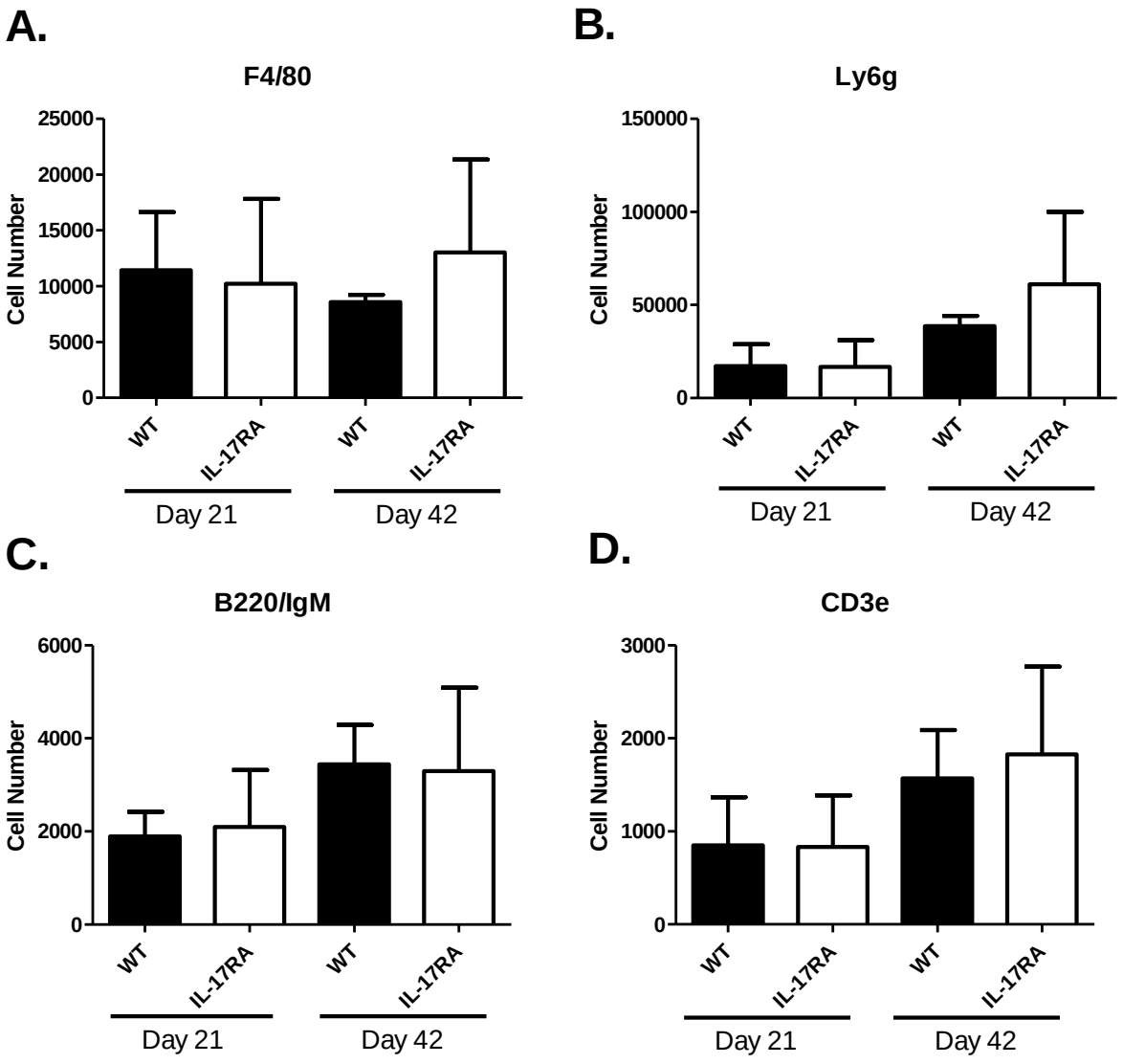

Figure 7.2: Joints of *B. burgdorferi*-infected C3H WT and C3H IL-17RA-deficient mice were analyzed for cellular infiltration using flow cytometry. Numbers of macrophages (A), neutrophils (B), B cells (C) and T cells (D) were evaluated at days 21 and 42 post-infection using cell-specific markers. n=5, data representative of two separate trials. Symbols represent means +/- SD.

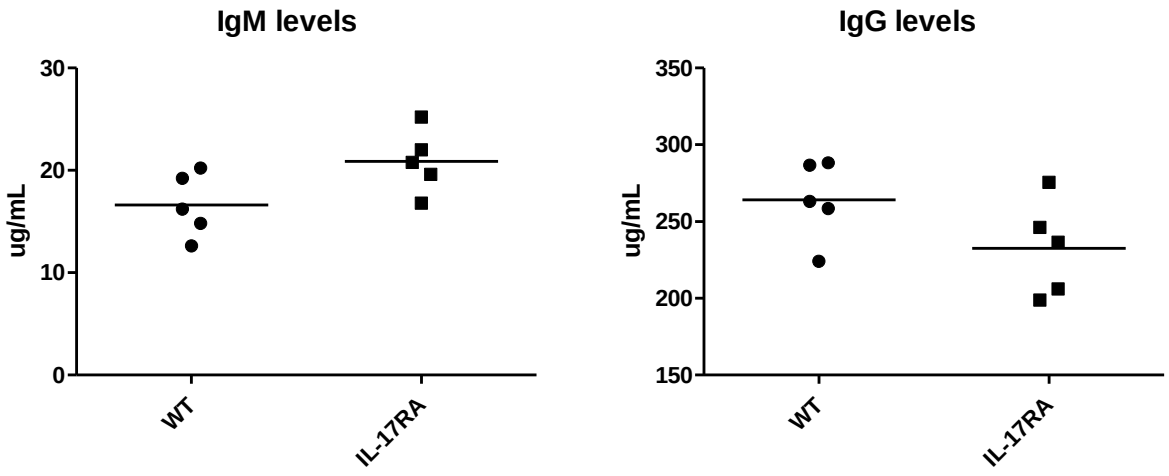

Figure 7.3: Serum from *B. burgdorferi*-infected C3H WT and C3H IL-17RA-deficient mice was obtained at 24 days post-infection. *B. burgdorferi*-specific IgM and IgG levels were determined using ELISA assay. n=5, data representative of two separate trials. Each symbol represents an individual animal, bars represent means.

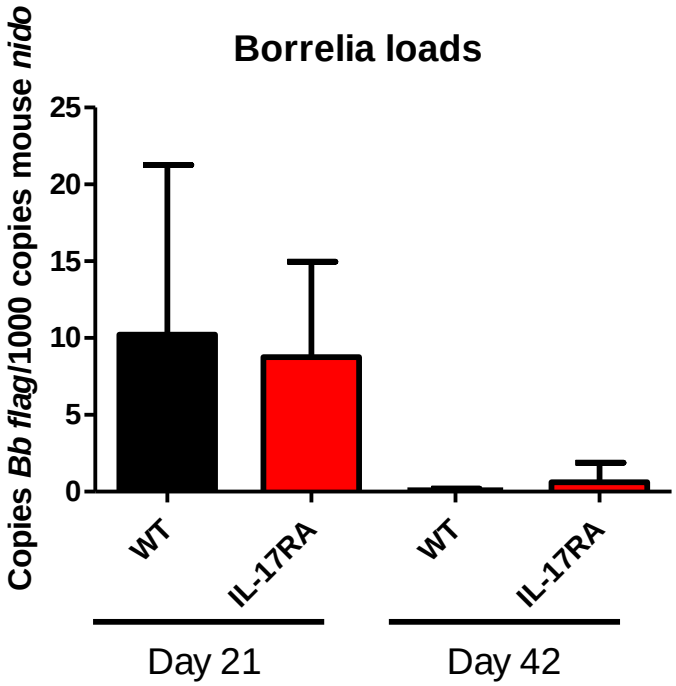

Figure 7.4: *B. burgdorferi* loads quantified from ear tissue from WT and IL-17RA-deficient mice. DNA was isolated from ear tissue of *B. burgdorferi*-infected C3H WT and C3H IL-17RA-deficient mice at days 21 and 42 post-infection. qRT-PCR analysis was used to determine bacterial numbers remaining within the tissue. n=5, data representative of two separate trials. Bars represent the mean +/- SD.

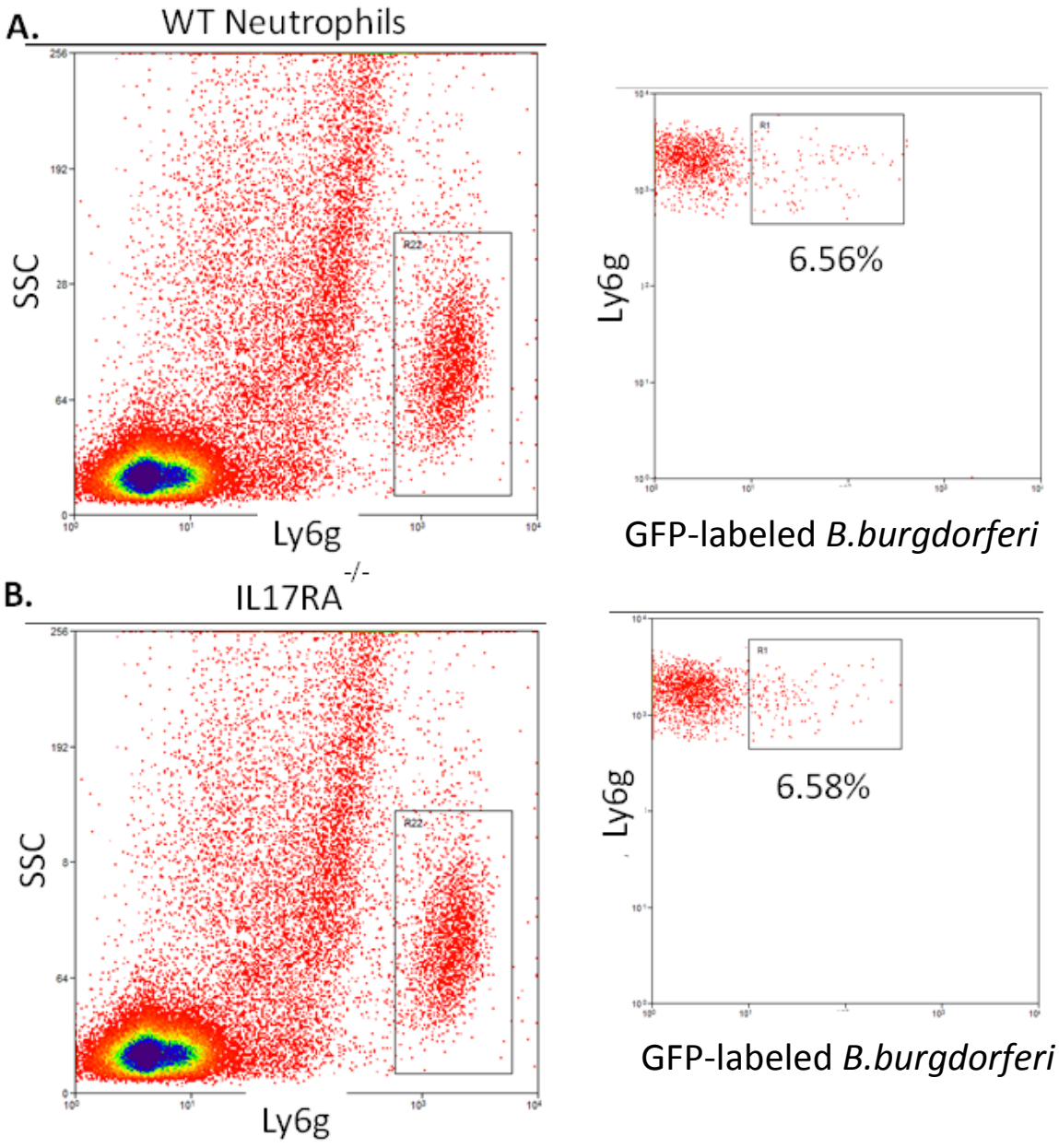

Figure 7.5: Flow cytometry of isolated cells from WT and IL-17RA-deficient neutrophils from peripheral blood using a Ficoll gradient. Neutrophils were co-cultured with GFP-labeled *B. burgdorferi* for two hours and stained for the neutrophil specific marker, Ly6g. Neutrophils that uptook spirochetes co-expressed Ly6g and GFP. Both WT (A) and IL-17RA (B) neutrophils were able to phagocytose *B. burgdorferi*. n=2, data representative of two separate trials.

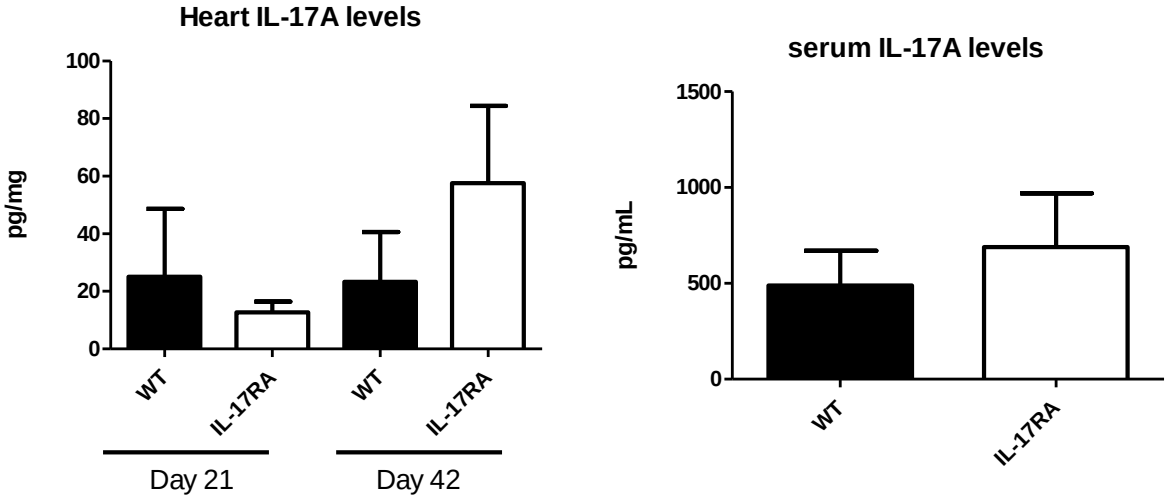

Figure 7.6: IL-17 levels in serum and heart tissue were quantified from infected mice using ELISA. IL-17A levels from *B. burgdorferi*-infected WT (open bars) and IL-17RA-deficient (closed bars) mice were determined from heart tissue at day 21 and 42 post-infection or serum at day 21 post-infection. n=5, data representative of two separate trials. Symbols represent means +/- SD.

C. *Conclusion*s

IL-17 is an important pro-inflammatory cytokine produced by Th17 cells and select innate immune cells (143). Although several studies have proposed that IL-17 may play a role in chronic and intermittent Lyme disease, this had never been tested under normal experimental conditions. In a vaccination and challenge model, IL-17 appeared to directly impact arthritis development in *B. burgdorferi*-infected mice. When IFN-γ-deficient mice were infected and challenged with *B. burgdorferi* in the presence of IL-17 neutralizing antibodies, arthritis onset was delayed (155). If treatment was combined with administration of anti-TGF-β and anti-IL-6, arthritis development could be eliminated. This suggested that IL-17 and its related cytokines may play a role in the development of disease (155, 156). However, while the production of IL-17 played an important role in the development of Lyme arthritis in the vaccination and challenge model, these results may not resemble what occurs during a more routinely used model of experimental Lyme disease. In the present study, we wanted to determine whether there was any role for IL-17 in the development of arthritis or carditis in experimental Lyme borreliosis. We found that an absence of IL-17 signaling resulted in no impairment in the development of the immune response to experimental Lyme disease.

To assess the contribution of IL-17 to disease pathogenesis in the experimental Lyme borreliosis infection model, we generated IL-17RA-deficient mice on the susceptible C3H/HeJ genetic background. Both WT and IL-17RA-deficient mice were infected with *B. burgdorferi*, and disease development as well as the immune response was

measured. We observed no significant differences in ankle swelling at any time point throughout the infection time-course. IL-17RA-deficient mice followed a normal swelling curve that began as early as day 7, peaked around day 21 and resolved shortly after. Disease severity was assessed in both rear ankle joint and heart tissue using H&E stained sections. IL-17RA-deficient mice showed the same level of tissue damage and cellular infiltrate as WT controls. IL-17RA signaling is critical for CXC chemokine generation, and therefore, neutrophil recruitment. In an infectious model of acute lung injury, an absence of IL-17RA signaling resulted in less lung destruction due to less reactive oxygen intermediates (146). Similar results have been seen in *Toxoplasma gondii* (157), and *Klebsiella pneumonia* (147) infections. Less inflammation is usually associated with significantly reduced neutrophil recruitment and higher bacterial loads (19). Because neutrophils are critical mediators in the development of Lyme arthritis (76), we set out to assess neutrophil recruitment in the *B. burgdorferi*-infected IL-17RA-deficient mice. Using cell specific markers for flow cytometry, we were able to determine numbers of neutrophils, macrophages, B cells and T cells. IL-17RA-deficient mice had very similar numbers of all cell types analyzed at both days 21 and 42 post-infection compared to WT controls. From this data, we conclude that IL-17RA signaling is not required for cellular recruitment into the joint after *B. burgdorferi* infection.

Although cellular recruitment into the infected tissues was identical, we wanted to ensure that appropriate *B. burgdorferi*-specific antibodies could be generated and bacterial clearance was not impaired by the absence of IL-17 signaling. IL-17 has

been shown to play a role in antibody production, germinal center formation and antibody class-switching in autoimmune disease (158), so a defect in IL-17 signaling could indirectly impact spirochete clearance by a failure to make appropriate antibodies. It is thought that *B. burgdorferi*-specific antibodies are primarily responsible for clearance of bacteria from the tissue (152). Upon infection, *B. burgdorferi* disseminate quickly upon entry into the host and, even at resolution, can be found residing in the ear tissue of infected mice (11). Using qRT-PCR, we analyzed bacterial loads from ear tissue of WT and IL-17RA-deficient mice. No defect was found in bacterial clearance, indicating that lack of IL-17 signaling does not impair the immune response's ability to eliminate spirochetes. Additionally, serum collected at day 24 post-infection revealed no defect in production of *B. burgdorferi* specific IgM or IgG antibodies in the IL-17RA-deficient mice.

It has been demonstrated that IL-17 is elevated in the serum of *B. burgdorferi*-infected patients (137). We have previously reported that IL-17 can be detected in the serum of *B. burgdorferi*-infected mice (153), but it has never been successfully measured form infected tissue. We measured IL-17A levels from serum and infected ankle joint and heart tissue from WT and IL-17RA-deficient mice. Unsurprisingly, IL-17 was readily detected in serum. IL-17RA-deficient mice have slightly elevated levels within serum, most likely due to an inability to signal through the appropriate receptor. IL-17 levels were very low in heart tissue and undetectable in joint tissue, mirroring previous reports (148). Taken together, we found no significant effects on the host response to *B. burgdorferi* infection in IL-17RA-deficient mice. We

conclude there is no role for IL-17 in the development of disease or host response in infectious experimental Lyme borreliosis.

CHAPTER VIII

DISCUSSION

The causative agent of Lyme disease, *Borrelia burgdorferi*, was discovered in 1981 by Willy Burgdorfer, Alan Barbour and Jorge Benach (1). Since then, the majority of our understanding of Lyme disease has been derived from a murine model of experimental Lyme borreliosis (11). In 1990, it was readily apparent that an unknown genetic component determined susceptibility to disease (91). Although all strains of mice can be infected with *B. burgdorferi*, only a select few develop arthritis and carditis (91). C3H/He and SWR mouse strains are susceptible to disease pathogenesis whereas the C57BL/6, BALB/c, and SJL are resistant (91). Using histopathology, it was determined that a large number of polymorphonuclear cells infiltrated joint tissue whereas mononuclear cells predominately entered the connective tissue near the base of the heart following *B. burgdorferi* infection of susceptible mice (91).

My graduate studies began with the goal of creating a new, more efficient way to study the cellular inflammatory response within the joint and heart tissue of *B. burgdorferi*-infected mice. Flow cytometry is a rapidly growing tool within the scientific field and can be used to analyze everything from cell phenotype, cell death, and intracellular protein production to protein-protein interactions and gene expression (159-161). Flow cytometry functions using three main systems: fluidics, optics, and electronics. The fluidics system draws up the cells and focuses them for excitation in a single cell-wide laminar flow column. This fluid column passes

through laser light which causes emission of photons at known wavelengths, which correlate to specific fluorophores. All wavelengths are collected by optical detectors and the computer digitizes these signals for analysis. This allows for scientists to label a cell or protein with a specific fluorophore in order to determine presence, absence, and intensity of the marker of interest (162, 163).

Within the murine model of Lyme borreliosis, analyzing cells and their proteins from joint tissue using flow cytometry proved to be difficult. Avoiding blood and bone marrow contamination was critical so excess muscle tissue was gently removed from joints. Additionally, joint tissue requires a long processing time which causes cell death, resulting in free DNA. Neutrophils, specifically, do not tolerate free DNA and will die before analysis can occur (164, 165) giving the appearance that neutrophils are not present within the tissue. By adding DNase into the processing assay, we were able to eliminate this problem and successfully assess cellular infiltrate into inflamed ankle joints.

Following infection with *B. burgdorferi*, C3H mice developed swelling of the tibiotarsal joints and had elevated numbers of all hematopoietic cells including neutrophils, macrophages, and B and T lymphocytes. We were able to effectively characterize and enumerate cellular infiltrate into the joints and hearts of *B. burgdorferi*-infected mice. Our data recapitulated that seen in early immunohistochemical analyses of experimental Lyme disease (10, 91). Neutrophils were the predominant infiltrating cell type during arthritis, with as many as $1x10^6$

cells at the peak of inflammation. Signaling of the chemokine KC, through its receptor CXCR2 mediates neutrophil migration (76). In the absence of KC, neutrophil migration was defective and arthritis development failed to occur (76), demonstrating the importance of neutrophil recruitment to disease development. We determined that within the infected hearts, macrophages were the most heavily recruited cell type, accounting for 1/3 of the population of hematopoietic cells. Macrophages can directly mediate inflammation in the heart, as suggested by the development of experimental Lyme carditis in the absence of both B and T lymphocytes and MHC II determinants (7, 20, 21). Macrophage recruitment into the heart tissue was mediated by CCR2; in the absence of CCR2, macrophage infiltration was arrested (22). Characterizing the cellular infiltrate of the joints and hearts of *B. burgdorferi*-infected mice using flow cytometry is a novel technique and will provide an additional method for understanding the natural inflammatory response during experimental Lyme disease. Newer flow cytometric techniques are being developed rapidly (166), and the ability to harvest joint cells for flow cytometric analysis will allow for continued progress and understanding. The majority of work outlined in this dissertation stemmed from the development of this technique and has allowed us to answer important questions.

Macrophage heterogeneity has been known to exist for quite some time and is evident by the differential expression of surface markers (167). Macrophage phenotype can be generalized into two major subsets: pro-inflammatory M1 and anti-inflammatory M2 macrophages (168). Characterization using cell surface markers has been

predominantly studied during polarization under *in vitro* conditions (55). Addition of IFN-γ and LPS, or IL-4 with or without IL-13, to BMDM induced an M1 and M2 phenotype, respectively (169, 170). M1 macrophages are commonly identified by expression of NOS2, Marco, and IL-12b, whereas M2 macrophages express CD206 and CD163 (57, 171). It has been established that macrophage polarization is essential in efficient clearance of a variety of bacteria (61, 94, 95). Additionally, it has been suggested that "M1-like" macrophages play an important role in both experimental models of arthritis and human rheumatoid arthritis (172, 173). Since macrophage polarization has been demonstrated to be important in both autoimmune arthritis and bacterial infection, we questioned whether macrophage polarization played an active role in development and resolution of experimental Lyme disease.

We found that BMDMs stimulated with *B. burgdorferi* underwent a drastic shift to the NOS2-producing M1 macrophage phenotype. This *in vitro* data suggested that M1 macrophages early on may help drive disease pathogenesis in joint and heart tissue. Upon spirochete clearance, macrophage plasticity could allow for a reprogramming to that of an anti-inflammatory M2-like cell promoting the spontaneous resolution of disease seen in our mice. In reality, we found that M2-like macrophages dominated the macrophage response within the joint, outnumbering M1-like macrophages by 10-fold. This dramatic skewing towards an M2-like phenotype may explain why depletion of iNOS during experimental Lyme arthritis resulted in no defect in disease development (103, 104). Throughout the infection time-course, we identified a small number of macrophages that expressed both M1

(NOS2) and M2 (CD206) specific markers. These cells dramatically increased near the time of disease resolution. We hypothesized that these cells were resolution phase macrophages, as described by others (71). Resolution phase macrophages are neither classically nor alternatively activated, share both M1 and M2 specific markers, and have been shown to induce resolution in a peritonitis model (71). We are the first to describe these cells in a model of experimental Lyme arthritis (174), but future studies need to be undertaken to address their importance in resolution.

As presented in Chapter 3, macrophages were the primary infiltrating cell type into the infected heart during experimental Lyme carditis, and they are known to drive the majority of inflammation seen (22). We found that at the peak of inflammation in the hearts, M1-like macrophages predominated and were replaced by M2-like macrophages at the time of resolution. This indicated that macrophage polarization may play a unique role in disease development and resolution within the heart. Although likely, it is currently unknown whether the M1-like macrophages seen early on in infection are switching to M2-like macrophages or if M2-like macrophages are recruited to the site of infection. Future studies will address this question. Overall, this study stresses the potential setbacks of drawing conclusions solely based on *in vitro* data. Macrophage phenotype in disease is manipulated by a variety of complex signaling pathways that cannot be replicated in a dish, and care should be taken when reporting their role in disease. Using flow cytometry, we have characterized macrophage phenotype in *B. burgdorferi*-infected joint and heart tissue.

During the analysis of cellular infiltrate described in Chapter 3, we found that macrophages were not the only unique cell type present during disease. We found a surprisingly large number of $B220^+$ cells within the joints, with numbers peaking around 400,000. Initially, we dismissed these solely as classical B cells, for B cells play an important role in antibody-mediated clearance of *B. burgdorferi* (16). However, further analysis revealed a small subset of these cells also expressed monocyte/macrophage specific markers including CD11b and F4/80, indicating lineage promiscuity. Similar cells have been described from long-term cultures of $CD5^+$ B cell lymphomas and their presence was indicative of a poor prognosis (112). It was later found that upon stimulation with M-CSF and GM-CSF *in vitro*, normal B cells could be induced to express both B cell and myeloid cell surface markers, and were termed a Biphenotypic B/Macrophage cell (108, 109, 175). However, the presence of these cells *in vivo* during a normal immune response had not been described.

Following infection with *B. burgdorferi*, a small number of Biphenotypic B/Macrophage cells expressing B220, IgM, CD11b, and F4/80 were identified in both joint and heart tissue. Their numbers dramatically increased within the joint as disease resolution occurred, suggesting that they may possess an anti-inflammatory role. The numbers of Biphenotypic B/Macrophage cells within infected heart tissue were significantly lower than those found in joint tissue, and no increase was seen at disease resolution. This is the first report of Biphenotypic B/Macrophages during an infectious disease, and the exact role of these cells is still unknown. To understand

the biology of these cells better, we analyzed surface marker expression over time in culture. We found that purified $CD19^{+}B220^{+}IgM^{+}F4/80^{-}CD11b^{-}$ B cells cultured in the presence of M-CSF and GM-CSF began to express F4/80 and CD11b as early as day 7. Expression of CD19 was completely abrogated by day 21 in culture, whereas CD11b expression was dramatically increased. B220 and IgM expression were maintained throughout the culture. Since current B cell isolation kits yield B cells of 97% purity, it was important to ensure that the cells being analyzed were not an outgrowth of contaminating macrophages. To prove this, we analyzed the cells for heavy chain gene rearrangements, indicative of B cell origin (176). We found that Biphenotypic B/Macrophage cells grown in culture did undergo gene rearrangement identical to purified B cells, demonstrating their lymphocyte lineage.

Our lab has successfully identified Biphenotypic B/Macrophage cells in both experimental Lyme disease and in *Francisella tularensis* infection. Some preliminary experiments have been completed, but many questions remain. For example, Biphenotypic B/Macrophage cells possess shared phenotypic characteristics of both B cells and macrophages, so we are interested in determining whether these cells possess both the phagocytic ability of a macrophage and the antibody-secreting ability of a B cell. Preliminary experiments suggest that Biphenotypic B/Macrophage cells can phagocytose both GFP-labeled *B. burgdorferi* and opsonized murine red blood cells, but do so poorly. Phagocytosis efficiency resembles that of a B cell, measured previously in Chapter 3. Additionally, we would like to investigate what transcriptionally occurs to induce the hybrid state seen in these unique cells. It has

been demonstrated that forcing transcription of CCAAT Enhancer Binding Protein alpha (CEBP-α) in pre-B cells caused the de-repression of myeloid target genes, transforming these cells to macrophages (110, 111). We have yet to measure CEBP-α expression over time from transitioning mature B cells, but we hypothesize that CEBP-α will be up-regulated following addition of M-CSF. It has been reported that signaling through the M-CSF receptor indirectly stimulates CEBP-α phosphorylation, preferentially generating monocytic myeloid cells (117). Currently, no one has successfully described the signaling pathway that forces fully differentiated B cells to alter their phenotype to that of a Biphenotypic B/Macrophage cell. It is also unknown whether Biphenotypic B/Macrophage cells are recruited to the tissue following infection or whether resident B cells are induced to become Biphenotypic B/Macrophage cells at the site of infection. Our preliminary data suggested that both are likely to occur. CFSE-labeled peritoneal cells adoptively transferred to the peritoneum of *B. burgdorferi*-infected mice were identified as Biphenotypic B/Macrophage cells in the infected joint tissue 21 days later, indicating active recruitment to the inflamed joint. Additionally, we found levels of M-CSF were significantly elevated within inflamed joint tissue 24 days after infection. It is likely that a small population of B cells within the joint would undergo phenotypic changes in the presence of elevated M-CSF levels. It would be of interest to identify what pre-disposes some B cells to transition and others to resist. In culture, only about 10% of B cells were responsive to M-CSF treatment and less than 1% convert under *in vivo* conditions. New research is finding that the immunological roles of B cells are much more complex than plasma cell differentiation and antibody production

(177). A growing understanding of B cell immunology may help elucidate what predisposes some B cells to undergo lineage promiscuity and others to retain a pure lymphoid identity (177). Overall, our findings indicate that Biphenotypic B/Macrophage cells exist during experimental Lyme disease, but more extensive research must be done in order fully appreciate the role of these cells during the inflammatory response.

The inflammatory response to *B. burgdorferi* has been much studied and is initiated primarily by signaling through both Toll-like receptors (TLR) and Nod-like receptors (NLR) (178). TLR-2 is important in the recognition of Outer surface protein (Osp) A of *B. burgdorferi*, and in conjunction with TLR-8, is responsible for phagocytosis of the spirochete (48). Once internalized, bacterial components have been shown to signal through TLR-7, 8 and 9, as well NOD-2, resulting in Type I IFN production which helps initiate Lyme arthritis development (179, 180). Since recognition of the bacteria is critical in generating an appropriate immune response, it was hypothesized that TLR-2-deficient mice would have less severe inflammation and higher bacterial loads following infection with *B. burgdorferi*. We and others (45, 47, 78) have shown that TLR-$2^{-/-}$ mice have significantly worse ankle swelling and a larger recruitment of both innate immune cells and T cells into inflamed joint tissue (78). Additionally, these mice have higher bacterial loads in tissues despite an efficient *B. burgdorferi*-specific antibody response (47).

Our goal was to more fully understand the modified immune response in the absence of TLR-2 signaling. In all studies analyzing the response of TLR-2-deficient mice to *B. burgdorferi* infection, carditis severity was never assessed. Additionally, the phenotype and role of the T cells within the joint was unknown. We found a five-fold and four-fold increase in T cell infiltration within the joints and hearts, respectively, in *B. burgdorferi* infected TLR-2-deficient mice. This was surprising because it is normally T-independent responses that are responsible for protective immunity and disease resolution during experimental Lyme arthritis (35). Upon further investigation, we determined that the joints had significantly elevated numbers of $CD8^+$ T cells whereas the hearts had more $CD4^+$ T cells compared to WT mice. Upon depletion of either $CD4^+$ or $CD8^+$ T cells, both neutrophil and macrophage recruitment was greatly impaired. This resulted in significantly reduced ankle swelling and less severe inflammation in both joint and heart tissue. These results indicated that TLR-2 independent signaling relies on an early T cell response to either directly or indirectly recruit innate immune cells. The mechanism by which this happens is still unknown. Surprisingly, the reduced number of innate immune cells recruited to the joints did not impair bacterial clearance, but rather aided in it. As shown previously (47), TLR-2-deficient mice have increased bacterial burdens despite a robust neutrophil response. After T cell depletion, the recruitment of innate immune cells is returned to the levels of WT mice, and bacteria can be efficiently cleared. The overwhelming inflammatory response in the TLR-2-deficient mice actually hinders the clearance of bacteria, and if this response is dampened, the cells can function properly. There have been reports suggesting that the innate immune

response in TLR-2-deficient mice is defective (47, 49) . BMDM from TLR-2-deficient mice stimulated with OspA displayed a defect in nitric oxide, IL-6, and TNF-α production (45). We found that BMDM from TLR-2-deficient mice do not polarize to the M1 (IFN-γ & LPS) or M2 (IL-4) phenotype as efficiently as WT BMDM. This may explain the reduced capacity for cytokine production from OspA-stimulated TLR-2-deficient macrophages (45). To our knowledge, neutrophil phagocytic and bactericidal response had not been tested in the TLR-2-deficient mice. Because neutrophil infiltration into the infected joint tissue was so greatly increased in the TLR-2-deficient mice, but unable to clear spirochetes efficiently, we hypothesized that they would display a reduced phagocytic response. To our surprise, TLR-2-deficient neutrophils readily phagocytosed *B. burgdorferi* in culture. Our results suggest that it is unlikely that an impaired innate immune response hinders bacterial clearance in the TLR-2-deficient mice. It appears that an overly exuberant innate immune cell response, and not a defect in innate immune cell function or antibody production, results in poor bacterial clearance. We have proven that while a robust immune response is generated in response to *B. burgdorferi* in the absence of TLR-2, it is somehow ineffective. Modification of the T cell response allows for a subdued innate immune response and more appropriate bacterial clearance. It will be of interest to determine whether MyD88-deficient mice display a similar phenotype and cellular recruitment in response to *B. burgdorferi* infection, as it is an adaptor molecule of TLR-2 (181).

In the presence of TLR-2, it has been demonstrated that *B. burgdorferi* activates caspase-1 (182), and through this activation cells produced increased levels of IFN-γ and IL-17 (40). T cells isolated from the synovium of Lyme disease patients stimulated with *Borrelia* lipoproteins produced significant levels of IL-17 (139). In a *Borrelia* vaccination and challenge model of Lyme arthritis, it was found that IL-17 was directly involved in the development of disease. Vaccinated mice given neutralizing IL-17 antibodies and challenged with *B. burgdorferi* isolate 297 failed to develop arthritis (156). Our lab sought to determine whether IL-17 signaling played a role in disease development using the more traditional model of experimental Lyme disease.

Following infection with *B. burgdorferi*, we found that IL-17RA-deficient mice displayed no defect in either arthritis or carditis development. Using flow cytometry, we found no difference in innate or adaptive immune cell recruitment. Although IL-17 is known to play a role in phagocytosis (183), we found no defect in the ability of IL-17RA neutrophils to uptake GFP-labeled *B. burgdorferi*. A previous report from our lab found that COX-1-deficient mice made a poor *B. burgdorferi*-specific IgG response as a result of poor germinal center formation (153). Addition of IL-17 could correct this phenotype, enabling antibody-mediated clearance of the spirochetes (153). Surprisingly, we found that in the absence of IL-17 signaling, mice made an efficient bacterial-specific IgM and IgG response indicating IL-17RA-deficient mice did not display a defect in germinal center formation. Because of this and an efficient innate immune response, IL-17RA-deficient mice efficiently cleared *B. burgdorferi*

from tissue. We found no role for IL-17 in the development of experimental Lyme disease. This does not necessarily indicate that IL-17 has no role in human Lyme disease, but we found that a murine model is not the ideal system in which to assess this.

The studies contained in this thesis contribute significantly to our understanding of the immune response to experimental Lyme borreliosis. Additionally, we provide an innovative technique in which to assess the immune response within inflamed joints. This method will not only be useful to the study of Lyme arthritis, but also other models of infectious and autoimmune arthritis. Using this method, we have discovered the presence of novel cell types including resolution phase macrophages and Biphenotypic B/Macrophage cells. It appears these cells may play an important role in resolving inflammation, although future work will be needed to address the possibility of using these cells therapeutically. We have also demonstrated a detrimental role of T cells in TLR-2 independent signaling of *B. burgdorferi*. All studies presented herein provide a foundation on which future studies will be built from in the hopes of providing better treatment for Lyme Disease patients in the future.

REFERENCES

1. **Haake DA.** 2010. Borrelia Molecular Biology, Host Interaction and Pathogenesis. Caister Academic Press, Norfolk, UK.
2. **CDC.** 2014. Lyme Disease, *on* Centers for Disease Control and Prevention. http://www.cdc.gov/lyme/.
3. **Dandache P, Nadelman RB.** 2008. Erythema Migrans. Infect Dis Clin N Am **22:**235-260.
4. **Wormser GP, Dattwyler RJ, Shapiro ED, Halperin JJ, Steere AC, Klempner MS, Krause PJ, Bakken JS, Strle F, Stanek G, Bockenstedt L, Fish D, Dumler JS, Nadelman RB.** 2006. The clinical assessment, treatment, and prevention of Lyme disease, human granulocytic anaplasmosis, and babesiosis: clinical practice guidelines by the infectious diseases society of America. Clin Infect Dis **43:**1089-1134.
5. **Shih C-M, Pollack RJ, Telford SR, Spielman A.** 1992. Delayed dissemination of Lyme disease spirochetes from the site of deposition in the skin of mice. J Infect Dis **166:**827-831.
6. **de Koning J, Hoogkamp-Korstanje JAA, van der Linde MR, Crijns HJGM.** 1989. Demonstration of spirochetes in cardiac biopsies of patients with Lyme disease. J Infect Dis **160:**150-153.
7. **Armstrong AL, Barthold SW, Persing DH, Beck DS.** 1992. Carditis in Lyme disease susceptible and resistant strains of laboratory mice infected with *Borrelia burgdorferi*. Am J Trop Med Hyg **47:**249-258.
8. **Borgermans L, Goderis G, Vandevoorde J, Devroey D.** 2014. Relevance of chronic Lyme disease to family medicine as a complex multidimensional chronic disease construct: a systematic review. Int J Family Med **2014:**138016.
9. **Radolf JD, Caimano MJ, Stevenson B, Hu LT.** 2012. Of ticks, mice and men: understanding the dual-host lifestyle of Lyme disease spirochaetes. Nat Rev Micro **10:**87-99.
10. **Barthold SW, Persing DH, Armstrong AL, Peeples RA.** 1991. Kinetics of *Borrelia burgdorferi* dissemination and evolution of disease after intradermal inoculation of mice. Am J Pathol **139:**263-273.
11. **Barthold SW.** 1991. Infectivity of *Borrelia burgdorferi* relative to route of inoculation and genotype in laboratory mice. J Infect Dis **163:**419-420.
12. **Brown CR, Reiner SL.** 1998. Clearance of *Borrelia burgdorferi* may not be required for resistance to experimental Lyme arthritis. Infect Immun **66:**2065-2071.
13. **Motameni A-RT, Bates TC, Juncadella IJ, Petty C, Hedrick MN, Anguita J.** 2005. Distinct bacterial dissemination and disease outcome in mice subcutaneously infected with Borrelia burgdorferi in the midline of the back and the footpad. FEMS **45:**279-284.
14. **Fikrig E, Barthold S, Kantor F, Flavell R.** 1990. Protection of mice against the Lyme disease agent by immunizing with recombinant OspA. Science **250:**553-556.
15. **Fikrig E, Barthold SW, Chen M, Chang CH, Flavell RA.** 1997. Protective antibodies develop, and murine Lyme arthritis regresses, in the absence of MHC class II and CD4+ T cells. J Immunol **159:**5682-5686.
16. **Connolly SE, Benach JL.** 2005. The versatile roles of antibodies in *Borrelia* infections. Nat Rev Micro **3:**411-420.
17. **Barthold SW, de Souza MS, Janotka JL, Smith AL, Persing DH.** 1993. Chronic Lyme borreliosis in the laboratory mouse. Am J Pathol **143:**959-971.

18. **Brown CR, Blaho VA, Loiacono CM.** 2003. Susceptibility to experimental Lyme arthritis correlates with KC and Monocyte Chemoattractant Protein-1 production in joints and requires neutrophil recruitment via CXCR2. J Immunol **171:**893-901.
19. **Xu Q, Seemanapalli SV, Reif KE, Brown CR, Liang FT.** 2007. Increasing the recruitment of neutrophils to the site of infection dramatically attenuates *Borrelia burgdorferi* infectivity. J Immunol **178:**5109-5115.
20. **Zimmer G, Schaible U, Kramer M, Mall G, Museteanu C, Simon M.** 1990. Lyme carditis in immunodeficient mice during experimental infection of *Borrelia burgdorferi*. Virchows Archiv A **417:**129-135.
21. **Ruderman EM, Kerr JS, Telford SR, Spielman A, Glimcher LH, Gravallese EM.** 1995. Early murine Lyme carditis has a macrophage predominance and is independent of major histocompatibility complex class Ii-Cd4+ T cell interactions. J Infect Dis **171:**362-370.
22. **Montgomery RR, Booth CJ, Wang X, Blaho VA, Malawista SE, Brown CR.** 2007. Recruitment of macrophages and polymorphonuclear leukocytes in Lyme carditis. Infect Immun **75:**613-620.
23. **Yssel H, Nakamoto T, Schneider P, Freltas V, Collins C, Webb D, Mensi N, Soderberg C, Peltz G.** 1990. Analysis of T lymphocytes cloned from the synovial fluid and blood of a patient with lyme arthritis. Int Immunol **2:**1081-1089.
24. **Yoshinari NH, Reinhardt BN, Steere AC.** 1991. T cell responses to polypeptide fractions of *Borrelia burgdorferi* in patients with lyme arthritis. Arthr Rheum **34:**707-713.
25. **Forsberg P, Ernerudh J, Ekerfelt C, Roberg M, Vrethem M, Bergström S.** 1995. The outer surface proteins of Lyme disease borrelia spirochetes stimulate T cells to secrete interferon-gamma (IFN-gamma): diagnostic and pathogenic implications. Clin Exp Immunol **101:**453-460.
26. **Lim LC, England DM, DuChateau BK, Glowacki NJ, Schell RF.** 1995. *Borrelia burgdorferi*-specific T lymphocytes induce severe destructive Lyme arthritis. Infect Immun **63:**1400-1408.
27. **Schaible UE, Kramer MD, Justus CW, Museteanu C, Simon MM.** 1989. Demonstration of antigen-specific T cells and histopathological alterations in mice experimentally inoculated with *Borrelia burgdorferi*. Infect Immun **57:**41-47.
28. **McKisic MD, Redmond WL, Barthold SW.** 2000. Cutting Edge: T cell-mediated pathology in murine Lyme borreliosis. J Immunol **164:**6096-6099.
29. **Kang I, Barthold SW, Persing DH, Bockenstedt LK.** 1997. T-helper-cell cytokines in the early evolution of murine Lyme arthritis. Infect Immun **65:**3107-3111.
30. **Anguita J, Rincón M, Samanta S, Barthold SW, Flavell RA, Fikrig E.** 1998. *Borrelia burgdorferi*-infected, Interleukin-6-deficient mice have decreased Th2 responses and increased Lyme arthritis. J Infect Dis **178:**1512-1515.
31. **Gross DM, Steere AC, Huber BT.** 1998. T helper 1 response is dominant and localized to the synovial fluid in patients with Lyme arthritis. J Immunol **160:**1022-1028.
32. **Bockenstedt LK, Kang I, Chang C, Persing D, Hayday A, Barthold SW.** 2001. CD4+ T helper 1 cells facilitate regression of murine Lyme carditis. Infect Immun **69:**5264-5269.
33. **Brown CR, Blaho VA, Fritsche KL, Loiacono CM.** 2006. Stat1 Deficiency Exacerbates Carditis but Not Arthritis During Experimental Lyme Borreliosis. J Interferon Cytokine Res **26:**390-399.
34. **Brown CR, Reiner SL.** 1999. Experimental Lyme arthritis in the absence of Interleukin-4 or gamma interferon. Infect Immun **67:**3329-3333.

35. **McKisic MD, Barthold SW.** 2000. T-cell-independent responses to *Borrelia burgdorferi* are critical for protective immunity and resolution of Lyme disease. Infect Immun **68:**5190-5197.
36. **Štěrba J, Vancová M, Rudenko N, Golovchenko M, Tremblay T-L, Kelly JF, MacKenzie CR, Logan SM, Grubhoffer L.** 2008. Flagellin and outer surface proteins from *Borrelia burgdorferi a*re not glycosylated. J Bacteriol **190:**2619-2623.
37. **Habicht GS, Beck G, Benach JL, Coleman JL.** 1986. *Borrelia burgdorferi* lipopolysaccharide and its role in the pathogenesis of lyme disease. Zentralblatt für Bakteriologie, Mikrobiologie und Hygiene Series A: Medical Microbiology, Infectious Diseases, Virology, Parasitology **263:**137-141.
38. **Kenedy MR, Lenhart TR, Akins DR.** 2012. The role of *Borrelia burgdorferi* outer surface proteins. FEMS **66:**1-19.
39. **Oosting M, Berende A, Sturm P, ter Hofstede HJM, de Jong DJ, Kanneganti T-D, van der Meer JWM, Kullberg B-J, Netea MG, Joosten LAB.** 2010. Recognition of *Borrelia burgdorferi* by NOD2 Is central for the induction of an inflammatory reaction. J Infect Dis **201:**1849-1858.
40. **Oosting M, van de Veerdonk FL, Kanneganti T-D, Sturm P, Verschueren I, Berende A, van der Meer JWM, Kullberg B-J, Netea MG, Joosten LAB.** 2011. *Borrelia* species induce inflammasome activation and IL-17 production through a caspase-1-dependent mechanism. Eur J Immunol **41:**172-181.
41. **Schwan TG, Piesman J, Golde WT, Dolan MC, Rosa PA.** 1995. Induction of an outer surface protein on *Borrelia burgdorferi* during tick feeding. PNAS **92:**2909-2913.
42. **Li X, Neelakanta G, Liu X, Beck DS, Kantor FS, Fish D, Anderson JF, Fikrig E.** 2007. Role of outer surface protein D in the *Borrelia burgdorferi* life cycle. Infect Immun **75:**4237-4244.
43. **Schwan TG, Piesman J.** 2000. Temporal changes in outer surface proteins A and C of the Lyme disease-associated spirochete, *Borrelia burgdorferi*, during the chain of infection in ticks and mice. J Clin Microbiol **38:**382-388.
44. **Hirschfeld M, Kirschning CJ, Schwandner R, Wesche H, Weis JH, Wooten RM, Weis JJ.** 1999. Cutting Edge: Inflammatory signaling by *Borrelia burgdorferi* lipoproteins is mediated by Toll-Like Receptor 2. J Immunol **163:**2382-2386.
45. **Wooten RM, Ma Y, Yoder RA, Brown JP, Weis JH, Zachary JF, Kirschning CJ, Weis JJ.** 2002. Toll-Like Receptor 2 is required for innate, but not acquired, host defense to *Borrelia burgdorferi*. J Immunol **168:**348-355.
46. **Oosting M, ter Hofstede H, Sturm P, Adema GJ, Kullberg B-J, van der Meer JWM, Netea MG, Joosten LAB.** 2011. TLR1/TLR2 heterodimers play an important role in the recognition of *Borrelia* spirochetes. PLoS ONE **6:**e25998.
47. **Wang G, Ma Y, Buyuk A, McClain S, Weis JJ, Schwartz I.** 2004. Impaired host defense to infection and Toll-like receptor 2-independent killing of *Borrelia burgdorferi* clinical isolates in TLR2-deficient C3H/HeJ mice, vol 231.
48. **Cervantes JL, Dunham-Ems SM, La Vake CJ, Petzke MM, Sahay B, Sellati TJ, Radolf JD, Salazar JC.** 2011. Phagosomal signaling by *Borrelia burgdorferi* in human monocytes involves Toll-like receptor (TLR) 2 and TLR8 cooperativity and TLR8-mediated induction of IFN-β. PNAS **108:**3683-3688.
49. **Hajishengallis G, Wang M, Bagby GJ, Nelson S.** 2008. Importance of TLR2 in early innate immune response to acute pulmonary infection with Porphyromonas gingivalis in mice. J Immunol **181:**4141-4149.

50. **Benoit M, Desnues B, Mege J-L.** 2008. Macrophage polarization in bacterial infections. J Immunol **181:**3733-3739.
51. **Erwig L-P, Kluth DC, Walsh GM, Rees AJ.** 1998. Initial cytokine exposure determines function of macrophages and renders them unresponsive to other cytokines. J Immunol **161:**1983-1988.
52. **Wallet MA, Wallet SM, Guiulfo G, Sleasman JW, Goodenow MM.** 2010. IFNγ primes macrophages for inflammatory activation by high molecular weight hyaluronan. Cell Immunol **262:**84-88.
53. **Laskin DL.** 2009. Macrophages and inflammatory mediators in chemical toxicity: a battle of forces. Chem Res Toxicol **22:**1376-1385.
54. **Murray PJ, Wynn TA.** 2011. Protective and pathogenic functions of macrophage subsets. Nat Rev Immunol **11:**723-737.
55. **Mantovani A, Sica A, Sozzani S, Allavena P, Vecchi A, Locati M.** 2004. The chemokine system in diverse forms of macrophage activation and polarization. Trends in Immunology **25:**677-686.
56. **Misson P, van den Brûle S, Barbarin V, Lison D, Huaux F.** 2004. Markers of macrophage differentiation in experimental silicosis. J Leuk Biol **76:**926-932.
57. **Lolmede K, Campana L, Vezzoli M, Bosurgi L, Tonlorenzi R, Clementi E, Bianchi ME, Cossu G, Manfredi AA, Brunelli S, Rovere-Querini P.** 2009. Inflammatory and alternatively activated human macrophages attract vessel-associated stem cells, relying on separate HMGB1- and MMP-9-dependent pathways. J Leuk Biol **85:**779-787.
58. **Krausgruber T, Blazek K, Smallie T, Alzabin S, Lockstone H, Sahgal N, Hussell T, Feldmann M, Udalova IA.** 2011. IRF5 promotes inflammatory macrophage polarization and TH1-TH17 responses. Nat Immunol **12:**231-238.
59. **Biswas SK, Gangi L, Paul S, Schioppa T, Saccani A, Sironi M, Bottazzi B, Doni A, Vincenzo B, Pasqualini F, Vago L, Nebuloni M, Mantovani A, Sica A.** 2006. A distinct and unique transcriptional program expressed by tumor-associated macrophages (defective NF-κB and enhanced IRF-3/STAT1 activation), vol 107.
60. **Satoh N, Shimatsu A, Himeno A, Sasaki Y, Yamakage H, Yamada K, Suganami T, Ogawa Y.** 2010. Unbalanced M1/M2 phenotype of peripheral blood monocytes in obese diabetic patients: effect of pioglitazone. Diabetes Care **33:**e7.
61. **Pfeffer K, Matsuyama T, Kündig TM, Wakeham A, Kishihara K, Shahinian A, Wiegmann K, Ohashi PS, Krönke M, Mak TW.** 1993. Mice deficient for the 55 kd tumor necrosis factor receptor are resistant to endotoxic shock, yet succumb to *L. monocytogenes* infection. Cell **73:**457-467.
62. **Shaughnessy LM, Swanson JA.** 2007. The role of the activated macrophage in clearing *Listeria monocytogenes* infection. Front Biosci **12:**2683-2692.
63. **Igietseme JU, Perry LL, Ananaba GA, Uriri IM, Ojior OO, Kumar SN, Caldwell HD.** 1998. Chlamydial infection in inducible nitric oxide synthase knockout mice. Infect Immun **66:**1282-1286.
64. **Rottenberg MnE, Gigliotti-Rothfuchs A, Wigzell H.** 2002. The role of IFN-γ in the outcome of chlamydial infection. Curr Opin Immunol **14:**444-451.
65. **Laskin DL, Sunil VR, Gardner CR, Laskin JD.** 2011. Macrophages and tissue injury: agents of defense or destruction? Annu Rev Pharmacol Toxicol **51:**267-288.
66. **Davis MJ, Tsang TM, Qiu Y, Dayrit JK, Freij JB, Huffnagle GB, Olszewski MA.** 2013. Macrophage M1/M2 polarization dynamically adapts to changes in cytokine microenvironments in Cryptococcus neoformans infection. mBio **4**.

67. **Takeda Y, Costa S, Delamarre E, Roncal C, Leite de Oliveira R, Squadrito ML, Finisguerra V, Deschoemaeker S, Bruyere F, Wenes M, Hamm A, Serneels J, Magat J, Bhattacharyya T, Anisimov A, Jordan BF, Alitalo K, Maxwell P, Gallez B, Zhuang ZW, Saito Y, Simons M, De Palma M, Mazzone M.** 2011. Macrophage skewing by Phd2 haplodeficiency prevents ischaemia by inducing arteriogenesis. Nature **479:**122-126.
68. **Sindrilaru A, Peters T, Wieschalka S, Baican C, Baican A, Peter H, Hainzl A, Schatz S, Qi Y, Schlecht A, Weiss JM, Wlaschek M, Sunderkötter C, Scharffetter-Kochanek K.** 2011. An unrestrained proinflammatory M1 macrophage population induced by iron impairs wound healing in humans and mice. J Clin Invest **121:**985-997.
69. **Kobayashi M, Jeschke MG, Shigematsu K, Asai A, Yoshida S, Herndon DN, Suzuki F.** 2010. M2b monocytes predominated in peripheral blood of severely burned patients. J Immunol **185:**7174-7179.
70. **Davies LC, Taylor PR.** 2015. Tissue-resident macrophages: then and now. Immunology **144:**541-548.
71. **Bystrom J, Evans I, Newson J, Stables M, Toor I, van Rooijen N, Crawford M, Colville-Nash P, Farrow S, Gilroy DW.** 2008. Resolution-phase macrophages possess a unique inflammatory phenotype that is controlled by cAMP, vol 112.
72. **Stables MJ, Shah S, Camon EB, Lovering RC, Newson J, Bystrom J, Farrow S, Gilroy DW.** 2011. Transcriptomic analyses of murine resolution-phase macrophages, vol 118.
73. **Benach JL, Habicht GS, Gocinski BL, Coleman JL.** 1984. Phagocytic cell responses to in vivo and in vitro exposure to the Lyme disease spirochete. Yale J Biol Med **57:**599-605.
74. **Barthold SW.** 1996. Serum-mediated resolution of Lyme arthritis in mice. Lab Invest **74:**57-67.
75. **Wooten RM, Weis JJ.** 2001. Host–pathogen interactions promoting inflammatory Lyme arthritis: use of mouse models for dissection of disease processes. Curr Opin Microbiol **4:**274-279.
76. **Ritzman AM, Hughes-Hanks JM, Blaho VA, Wax LE, Mitchell WJ, Brown CR.** 2010. The chemokine receptor CXCR2 ligand KC (CXCL1) mediates neutrophil recruitment and is critical for development of experimental Lyme arthritis and carditis. Infect Immun **78:**4593-4600.
77. **Lochhead RB, Sonderegger FL, Ma Y, Brewster JE, Cornwall D, Maylor-Hagen H, Miller JC, Zachary JF, Weis JH, Weis JJ.** 2012. Endothelial cells and fibroblasts amplify the arthritogenic Type I IFN response in murine Lyme Disease and are major sources of chemokines in *B. burgdorferi*-infected joint tissue. J Immunol **189:**2488-2501.
78. **Wang X, Ma Y, Yoder A, Crandall H, Zachary JF, Fujinami RS, Weis JH, Weis JJ.** 2008. T cell infiltration is associated with increased Lyme arthritis in TLR2$^{-/-}$ mice, vol 52.
79. **Weis JJ, McCracken BA, Ma Y, Fairbairn D, Roper RJ, Morrison TB, Weis JH, Zachary JF, Doerge RW, Teuscher C.** 1999. Identification of quantitative trait loci governing arthritis severity and humoral responses in the murine model of Lyme disease. J Immunol **162:**948-956.
80. **Maruyama K, Fukasaka M, Vandenbon A, Saitoh T, Kawasaki T, Kondo T, Yokoyama Kazunari K, Kidoya H, Takakura N, Standley D, Takeuchi O, Akira S.** 2012. The Transcription Factor Jdp2 Controls Bone Homeostasis and Antibacterial Immunity by Regulating Osteoclast and Neutrophil Differentiation. Immunity **37:**1024-1036.
81. **Blaho VA, Zhang Y, Hughes-Hanks JM, Brown CR.** 2011. 5-Lipoxygenase–deficient mice infected with *Borrelia burgdorferi* develop persistent arthritis. J Immunol **186:**3076-3084.

82. **Parra D, Rieger AM, Li J, Zhang Y-A, Randall LM, Hunter CA, Barreda DR, Sunyer JO.** 2012. Pivotal Advance: peritoneal cavity B-1 B cells have phagocytic and microbicidal capacities and present phagocytosed antigen to CD4(+) T cells. J Leuk Biol **91:**525-536.
83. **Nakashima M, Kinoshita M, Nakashima H, Habu Y, Miyazaki H, Shono S, Hiroi S, Shinomiya N, Nakanishi K, Seki S.** 2012. Pivotal Advance: characterization of mouse liver phagocytic B cells in innate immunity. J Leuk Biol **91:**537-546.
84. **Montgomery RR, Lusitani D, de Boisfleury Chevance A, Malawista SE.** 2002. Human phagocytic cells in the early innate immune response to *Borrelia burgdorferi*. J Infect Dis **185:**1773-1779.
85. **Schaible UE, Gay S, Museteanu C, Kramer MD, Zimmer G, Eichmann K, Museteanu U, Simon MM.** 1990. Lyme borreliosis in the severe combined immunodeficiency (scid) mouse manifests predominantly in the joints, heart, and liver. Am J Pathol **137:**811-820.
86. **Gordon S.** 2007. Macrophage heterogeneity and tissue lipids. J of Clin Invest **117:**89-93.
87. **Montgomery RR, Malawista SE.** 1996. Entry of *Borrelia burgdorferi* into macrophages is end-on and leads to degradation in lysosomes. Infect immun **64:**2867-2872.
88. **Chung Y, Zhang N, Wooten RM.** 2013. *Borrelia burgdorferi* elicited-IL-10 suppresses the production of inflammatory mediators, phagocytosis, and expression of co-stimulatory receptors by murine macrophages and/or dendritic cells. PLoS ONE **8:**e84980.
89. **Hawley K, Navasa N, Olson CM, Bates TC, Garg R, Hedrick MN, Conze D, Rincón M, Anguita J.** 2012. Macrophage p38 mitogen-activated protein kinase activity regulates invariant natural killer T-cell responses during *Borrelia burgdorferi* infection. J Infect Dis **206:**283-291.
90. **Gautam A, Dixit S, Embers M, Gautam R, Philipp MT, Singh SR, Morici L, Dennis VA.** 2012. Different patterns of expression and of IL-10 modulation of inflammatory mediators from macrophages of Lyme disease-resistant and -susceptible mice. PLoS ONE **7:**e43860.
91. **Barthold SW, Beck DS, Hansen GM, Terwilliger GA, Moody KD.** 1990. Lyme borreliosis in selected strains and ages of laboratory mice. J Infect Dis **162:**133-138.
92. **Shi C, Pamer EG.** 2011. Monocyte recruitment during infection and inflammation. Nat Rev Immunol **11:**762-774.
93. **Wynn TA, Chawla A, Pollard JW.** 2013. Macrophage biology in development, homeostasis and disease. Nature **496:**445-455.
94. **Chacón-Salinas R, Serafín-López J, Ramos-Payán R, Méndez-Aragón P, Hernández-Pando R, Van Soolingen D, Flores-Romo L, Estrada-Parra S, Estrada-García I.** 2005. Differential pattern of cytokine expression by macrophages infected in vitro with different *Mycobacterium tuberculosis* genotypes. Clin Exp Immunol **140:**443-449.
95. **Kyrova K, Stepanova H, Rychlik I, Faldyna M, Volf J.** 2012. SPI-1 encoded genes of *Salmonella Typhimurium* influence differential polarization of porcine alveolar macrophages in vitro. BMC Vet Res **8:**115-115.
96. **Liu YC ZX, Chai YF, Yao YM.** 2014. Macrophage polarization in inflammatory diseases. Int J Biol Sci **10:**520-529.
97. **Fernandes DM, Baldwin CL.** 1995. Interleukin-10 downregulates protective immunity to Brucella abortus. Infect Immun **63:**1130-1133.
98. **Tomioka H, Tatano Y, Maw WW, Sano C, Kanehiro Y, Shimizu T.** 2012. Characteristics of suppressor macrophages induced by Mycobacterial and Protozoal infections in relation to alternatively activated M2 macrophages. Clin Dev Immunol **2012:**19.
99. **Cao L, He C.** 2013. Polarization of macrophages and microglia in inflammatory demyelination. Neuroscience Bulletin **29:**189-198.

100. **Lumeng CN, Bodzin JL, Saltiel AR.** 2007. Obesity induces a phenotypic switch in adipose tissue macrophage polarization. J Clin Invest **117:**175-184.
101. **Aron-Wisnewsky J, Tordjman J, Poitou C, Darakhshan F, Hugol D, Basdevant A, Aissat A, Guerre-Millo M, Clément K.** 2009. Human adipose tissue macrophages: M1 and M2 cell surface markers in subcutaneous and omental depots and after weight Loss. J Clin Endocrinol Metab **94:**4619-4623.
102. **Mikita J, Dubourdieu-Cassagno N, Deloire MS, Vekris A, Biran M, Raffard G, Brochet B, Canron M-H, Franconi J-M, Boiziau C, Petry KG.** 2011. Altered M1/M2 activation patterns of monocytes in severe relapsing experimental rat model of multiple sclerosis. Amelioration of clinical status by M2 activated monocyte administration. Mult Scler J **17:**2-15.
103. **Brown CR, Reiner SL.** 1999. Development of Lyme arthritis in mice deficient in inducible nitric oxide synthase. J Infect Dis **179:**1573-1576.
104. **Seiler KP, Vavrin Z, Eichwald E, Hibbs JB, Weis JJ.** 1995. Nitric oxide production during murine Lyme disease: lack of involvement in host resistance or pathology. Infect Immun **63:**3886-3895.
105. **Peters-Golden M, Henderson WR.** 2007. Leukotrienes. New Engl J Med **357:**1841-1854.
106. **Rådmark O, Samuelsson B.** 2010. Regulation of the activity of 5-lipoxygenase, a key enzyme in leukotriene biosynthesis. Biochem Biophys Res Commun **396:**105-110.
107. **Akashi K.** 2005. Lineage promiscuity and plasticity in hematopoietic development. Ann NY Acad Sci **1044:**125-131.
108. **Borrello MA, Phipps RP.** 1999. Fibroblast-secreted macrophage colony-stimulating factor is responsible for generation of Biphenotypic B/Macrophage cells from a subset of mouse B lymphocytes. J Immunol **163:**3605-3611.
109. **Borrello MA, Phipps RP.** 1995. Fibroblasts support outgrowth of splenocytes simultaneously expressing B lymphocyte and macrophage characteristics. J Immunol **155:**4155-4161.
110. **Di Tullio A, Manh TPV, Schubert A, Castellano G, Månsson R, Graf T.** 2011. CCAAT/enhancer binding protein α (C/EBPα)-induced transdifferentiation of pre-B cells into macrophages involves no overt retrodifferentiation. PNAS **108:**17016-17021.
111. **Kallin Eric M, Rodríguez-Ubreva J, Christensen J, Cimmino L, Aifantis I, Helin K, Ballestar E, Graf T.** 2012. Tet2 facilitates the derepression of myeloid target genes during CEBPα-induced transdifferentiation of pre-B cells. Mol Cell **48:**266-276.
112. **Dawe CJ, Potter, M.** 1957. Morphologic and biologic progression of a lymphoid neoplasm of the mouse *in vivo* and *in vitro*. Am J Pathol **33:**603.
113. **Borrello MA, Phipps RP.** 1996. The B/macrophage cell: an elusive link between CD5+ B lymphocytes and macrophages. Immunol Today **17:**471-475.
114. **Popi AF, Motta FLT, Mortara RA, Schenkman S, Lopes JD, Mariano M.** 2009. Co-ordinated expression of lymphoid and myeloid specific transcription factors during B-1b cell differentiation into mononuclear phagocytes in vitro. Immunology **126:**114-122.
115. **Almeida SR, Aroeira LS, Frymuller E, Dias MÂA, Bogsan CSB, Lopes JD, Mariano M.** 2001. Mouse B-1 cell-derived mononuclear phagocyte, a novel cellular component of acute non-specific inflammatory exudate. Int Immunol **13:**1193-1201.
116. **Boyd AW, Schrader JW.** 1982. Derivation of macrophage-like lines from the pre-B lymphoma ABLS 8.1 using 5-azacytidine. Nature **297:**691-693.
117. **Jack GD, Zhang L, Friedman AD.** 2009. M-CSF elevates c-Fos and phospho-C/EBPα(S21) via ERK whereas G-CSF stimulates SHP2 phosphorylation in marrow progenitors to contribute to myeloid lineage specification, vol 114.

118. **Stevenson B, Schwan TG, Rosa PA.** 1995. Temperature-related differential expression of antigens in the Lyme disease spirochete, *Borrelia burgdorferi*. Infect Immun **63:**4535-4539.
119. **Alexopoulou L, Thomas V, Schnare M, Lobet Y, Anguita J, Schoen RT, Medzhitov R, Fikrig E, Flavell RA.** 2002. Hyporesponsiveness to vaccination with *Borrelia burgdorferi* OspA in humans and in TLR1- and TLR2-deficient mice. Nat Med **8:**878-884.
120. **Drennan MB, Nicolle D, Quesniaux VJF, Jacobs M, Allie N, Mpagi J, Frémond C, Wagner H, Kirschning C, Ryffel B.** 2004. Toll-Like Receptor 2-deficient mice succumb to *Mycobacterium tuberculosis* infection. Am J pathol **164:**49-57.
121. **Loures F, Pina, A, Felonato, M, Calich, VLG.** 2009. TLR2 ss a negative regulator of Th17 cells and tissue pathology in a pulmonary model of fungal infection. J Immunol **183:**1279-1290.
122. **Echchannaoui H, Frei K, Schnell C, Leib SL, Zimmerli W, Landmann R.** 2002. Toll-Like Receptor 2–deficient mice are highly susceptible to *Streptococcus pneumoniae* meningitis because of reduced bacterial clearing and enhanced inflammation. J Infect Dis **186:**798-806.
123. **Turner J-E, Paust H-J, Steinmetz OM, Peters A, Riedel J-H, Erhardt A, Wegscheid C, Velden J, Fehr S, Mittrücker H-W, Tiegs G, Stahl RAK, Panzer U.** 2010. CCR6 recruits regulatory T Cells and Th17 Cells to the kidney in glomerulonephritis. J Am Soc Nephrol **21:**974-985.
124. **Godfrey DI, Hammond KJL, Poulton LD, Smyth MJ, Baxter AG.** 2000. NKT cells: facts, functions and fallacies. Immunology Today **21:**573-583.
125. **Zhu J, Paul WE.** 2008. CD4 T cells: fates, functions, and faults. Blood **112:**1557-1569.
126. **Haslett C, Guthrie LA, Kopaniak MM, Johnston RB, Henson PM.** 1985. Modulation of multiple neutrophil functions by preparative methods or trace concentrations of bacterial lipopolysaccharide. Am J Pathol **119:**101-110.
127. **Blaho VA, Buczynski MW, Brown CR, Dennis EA.** 2009. Lipidomic analysis of dynamic eicosanoid responses during the induction and resolution of Lyme arthritis. J Biol Chem **284:**21599-21612.
128. **Müller M, Carter S, Hofer MJ, Campbell IL.** 2010. Review: The chemokine receptor CXCR3 and its ligands CXCL9, CXCL10 and CXCL11 in neuroimmunity – a tale of conflict and conundrum. Neuropath Appl Neurobiol **36:**368-387.
129. **Schwan T.** 2003. Temporal regulation of outer surface proteins of the Lyme-disease spirochaete *Borrelia burgdorferi*. Biochem Soc Trans **21:**108-112.
130. **Godfrey DI, Berzins SP.** 2006. NKT cells join the war on Lyme disease. Nat Immunol **7:**904-906.
131. **Keane-Myers A, Nickell SP.** 1995. Role of IL-4 and IFN-gamma in modulation of immunity to *Borrelia burgdorferi* in mice. J Immunol **155:**2020-2028.
132. **Matyniak J, Reiner, SL.** 1995. T helper phenotype and genetic susceptibility in experimental Lyme disease. J Exp Med **181:**1251-1254.
133. **Yin Z, Braun, J, Neure, L, Wu, P, Eggens, U, Krause, A, Kamradt, T, Sieper, J.** 1997. T cell cytokine pattern in the joints of patients with Lyme arthritis and its regulation by cytokines and anticytokines. Arthr Rheum **40:**69-79.
134. **Nichols JR, Aldrich AL, Mariani MM, Vidlak D, Esen N, Kielian T.** 2009. Toll-like receptor 2 (TLR2) deficiency leads to increased Th17 infiltrates in experimental brain abscesses. J Immunol **182:**7119-7130.
135. **Medzhitov R, Horng T.** 2009. Transcriptional control of the inflammatory response. Nat Rev Immunol **9:**692-703.

136. **Gasperini S, Marchi M, Calzetti F, Laudanna C, Vicentini L, Olsen H, Murphy M, Liao F, Farber J, Cassatella MA.** 1999. Gene expression and production of the monokine induced by IFN-γ (MIG), IFN-Inducible T cell α chemoattractant (I-TAC), and IFN-γ-Inducible Protein-10 (IP-10) chemokines by human neutrophils. J Immunol **162:**4928-4937.
137. **Infante-Duarte C, Horton HF, Byrne MC, Kamradt T.** 2000. Microbial lipopeptides induce the production of IL-17 in Th cells. J Immunol **165:**6107-6115.
138. **Nardelli DT, Burchill MA, England DM, Torrealba J, Callister SM, Schell RF.** 2004. Association of CD4(+) CD25(+) T cells with prevention of severe destructive arthritis in *Borrelia burgdorferi*-vaccinated and challenged Gamma Interferon-deficient mice treated with Anti-Interleukin-17 antibody. Clin Diag Lab Immun **11:**1075-1084.
139. **Codolo G, Amedei A, Steere AC, Papinutto E, Cappon A, Polenghi A, Benagiano M, Paccani SR, Sambri V, Del Prete G, Baldari CT, Zanotti G, Montecucco C, D'Elios MM, de Bernard M.** 2008. *Borrelia burgdorferi* NapA–driven Th17 cell inflammation in lyme arthritis. Arthr Rheum **58:**3609-3617.
140. **Leipe J, Grunke M, Dechant C, Reindl C, Kerzendorf U, Schulze-Koops H, Skapenko A.** 2010. Th17 cells in autoimmune arthritis. Annal Rheum Dis **69:**A69-A70.
141. **Millward JM, Løbner M, Wheeler RD, Owens T.** 2010. Inflammation in the central nervous system and Th17 responses are inhibited by IFN-γ–induced IL-18 binding protein. J Immunol **185:**2458-2466.
142. **Mus A-M, Corneth O, Asmawidjaja P, Lubberts E.** 2011. Lack of IL-17RA signalling prevents autoimmune inflammation of the joint and give rise to a Th2-like phenotype in collagen-induced arthritis. Annal Rheum Dis **70:**A50-A51.
143. **Jin W, Dong C.** 2013. IL-17 cytokines in immunity and inflammation. Emerg Microbes Infect **2:**e60.
144. **Cua DJ, Tato CM.** 2010. Innate IL-17-producing cells: the sentinels of the immune system. Nat Rev Immunol **10:**479-489.
145. **Zepp J, Wu L, Li X.** 2011. IL-17 receptor signaling and T helper 17-mediated autoimmune demyelinating disease. Trends Immunol **32:**232-239.
146. **Crowe CR, Chen K, Pociask DA, Alcorn JF, Krivich C, Enelow RI, Ross TM, Witztum JL, Kolls JK.** 2009. Critical role of IL-17RA in immunopathology of influenza infection. J Immunol **183:**5301-5310.
147. **Ye P, Garvey PB, Zhang P, Nelson S, Bagby G, Summer WR, Schwarzenberger P, Shellito JE, Kolls JK.** 2001. Interleukin-17 and lung host defense against *Klebsiella pneumoniae* infection. Am J Respir Cell Mol Biol **25:**335-340.
148. **Nardelli DT, Luedtke JO, Munson EL, Warner TF, Callister SM, Schell RF.** 2010. Significant differences between the Borrelia-infection and *Borrelia*-vaccination and -infection models of Lyme arthritis in C3H/HeN mice. FEMS **60:**78-89.
149. **von Vietinghoff S, Ley K.** 2009. Interleukin 17A controls Interleukin 17F production and maintains blood neutrophil counts in mice. J Immunol **183:**865-873.
150. **Brown CR, Blaho VA, Loiacono CM.** 2004. Treatment of mice with the neutrophil-depleting antibody RB6-8C5 results in early development of experimental Lyme arthritis via the recruitment of Gr-1(−) polymorphonuclear leukocyte-like cells. Infect Immun **72:**4956-4965.
151. **Laan M, Cui Z-H, Hoshino H, Lötvall J, Sjöstrand M, Gruenert DC, Skoogh B-E, Lindén A.** 1999. Neutrophil recruitment by human IL-17 via C-X-C chemokine release in the airways. J Immunol **162:**2347-2352.

152. **Barthold SW, Hodzic E, Tunev S, Feng S.** 2006. Antibody-mediated disease remission in the mouse model of Lyme borreliosis. Infect Immun **74:**4817-4825.
153. **Blaho VA, Buczynski MW, Dennis EA, Brown CR.** 2009. Cyclooxygenase-1 orchestrates germinal center formation and antibody class-switch via regulation of IL-17. J Immunol **183:**5644-5653.
154. **Hsu S-C, Wang L-T, Yao C-L, Lai H-Y, Chan K-Y, Liu B-S, Chong P, Lee OK-S, Chen H-W.** 2013. Mesenchymal stem cells promote neutrophil activation by inducing IL-17 production in CD4+ CD45RO+ T cells. Immunobiology **218:**90-95.
155. **Burchill MA, Nardelli DT, England DM, DeCoster DJ, Christopherson JA, Callister SM, Schell RF.** 2003. Inhibition of Interleukin-17 prevents the development of arthritis in vaccinated mice challenged with *Borrelia burgdorferi*. Infect Immun **71:**3437-3442.
156. **Nardelli DT, Kevin Luk KH, Kotloski NJ, Warner TF, Torrealba JR, Callister SM, Schell RF.** 2008. Role of IL-17, transforming growth factor-β, and IL-6 in the development of arthritis and production of anti-outer surface protein A borreliacidal antibodies in *Borrelia*-vaccinated and -challenged mice, vol 53.
157. **Guiton R, Vasseur V, Charron S, Torres Arias M, Van Langendonck N, Buzoni-Gatel D, Ryffel B, Dimier-Poisson I.** 2010. Interleukin 17 receptor signaling is deleterious during *Toxoplasma gondii* infection in susceptible BL6 mice. J Infect Dis **202:**427-435.
158. **Hsu H-C, Yang P, Wang J, Wu Q, Myers R, Chen J, Yi J, Guentert T, Tousson A, Stanus AL, Le T-vL, Lorenz RG, Xu H, Kolls JK, Carter RH, Chaplin DD, Williams RW, Mountz JD.** 2008. Interleukin 17-producing T helper cells and interleukin 17 orchestrate autoreactive germinal center development in autoimmune BXD2 mice. Nat Immunol **9:**166-175.
159. **Mittag A, Tarnok A.** 2011. Chapter 1 - Recent Advances in Cytometry Applications: Preclinical, Clinical, and Cell Biology, p 1-20. *In* Zbigniew Darzynkiewicz EHAOWT, Donald W (ed), Methods in Cell Biology, vol Volume 103. Academic Press.
160. **Jaye DL, Bray RA, Gebel HM, Harris WAC, Waller EK.** 2012. Translational applications of flow cytometry in clinical practice. J Immunol **188:**4715-4719.
161. **Blazer LL, Roman DL, Muxlow MR, Neubig RR.** 2010. Use of flow cytometric methods to quantify protein-protein interactions. Curr Protoc Cytom **CHAPTER:**Unit-13.1115.
162. **Herzenberg LA, Parks D, Sahaf B, Perez O, Roederer M, Herzenberg LA.** 2002. The history and future of the fluorescence activated cell sorter and flow cytometry: a view from Stanford. Clin Chem **48:**1819-1827.
163. **Herzenberg L, Sweet, RG, Herzenberg, LA.** 1976. Fluorescence-activated cell sorting. Sci Am **234:**108-117.
164. **Rydell-Törmänen K, Uller L, Erjefält JS.** 2006. Direct evidence of secondary necrosis of neutrophils during intense lung inflammation. Eur Respir J **28:**268-274.
165. **Iba T, Hashiguchi N, Nagaoka I, Tabe Y, Murai M.** 2013. Neutrophil cell death in response to infection and its relation to coagulation. J Intensive Care **1:**13.
166. **Porichis F, Hart MG, Griesbeck M, Everett HL, Hassan M, Baxter AE, Lindqvist M, Miller SM, Soghoian DZ, Kavanagh DG, Reynolds S, Norris B, Mordecai SK, Nguyen Q, Lai C, Kaufmann DE.** 2014. High-throughput detection of miRNAs and gene-specific mRNA at the single-cell level by flow cytometry. Nat Commun **5**.
167. **Gordon S, Taylor PR.** 2005. Monocyte and macrophage heterogeneity. Nat Rev Immunol **5:**953-964.
168. **Chawla A, Nguyen KD, Goh YPS.** 2011. Macrophage-mediated inflammation in metabolic disease. Nat Rev Immunol **11:**738-749.
169. **Gordon S.** 2003. Alternative activation of macrophages. Nat Rev Immunol **3:**23-35.

170. **Menzies FM, Henriquez FL, Alexander J, Roberts CW.** 2010. Sequential expression of macrophage anti-microbial/inflammatory and wound healing markers following innate, alternative and classical activation. Clin Exp Immunol **160:**369-379.
171. **Yoichiro K, Haruki I, Yoshitaka M, Masanobu M, Masashi S, Tomotaka K, Tomotaka H.** 2014. M2 macrophage marker CD163, CD204 and CD206 expression on alveolar macrophages in the lung of patients with chronic obstructive pulmonary, p A2989-A2989, B44 COPD: GENETICS doi:doi:10.1164/ajrccm-conference.2014.189.1_MeetingAbstracts.A2989

10.1164/ajrccm-conference.2014.189.1_MeetingAbstracts.A2989. American Thoracic Society.
172. **Hofkens W, Storm G, van den Berg W, van Lent P.** 2011. Inhibition of M1 macrophage activation in favour of M2 differentiation by liposomal targeting of glucocorticoids to the synovial lining during experimental arthritis. Annal Rheum Dis **70:**A40.
173. **Kennedy A, Fearon U, Veale DJ, Godson C.** 2011. Macrophages in synovial inflammation. Front Immun **2:**52.
174. **Lasky CE, Olson RM, Brown CR.** 2015. Macrophage polarization during murine Lyme borreliosis. Infect Immun doi:10.1128/iai.00369-15.
175. **Borrello MA, Palis J, Phipps RR.** 2001. The relationship of CD5+ B lymphocytes to macrophages: insights from normal biphenotypic B/Macrophage cells. Int Rev Immunol **20:**137-155.
176. **Gleifiner B, Maurer J, Thiel E.** 2000. Detection of immunoglobulin heavy chain genes rearrangements in B-cell leukemias, lymphomas, multiple myelomas, monoclonal and polyclonal gammopathies. Leukemia & Lymphoma **39:**151-155.
177. **Garraud O, Borhis G, Badr G, Degrelle S, Pozzetto B, Cognasse F, Richard Y.** 2012. Revisiting the B-cell compartment in mouse and humans: more than one B-cell subset exists in the marginal zone and beyond. BMC Immunology **13:**63.
178. **Oosting M, Buffen K, van der Meer JWM, Netea MG, Joosten LAB.** 2014. Innate immunity networks during infection with *Borrelia burgdorferi*. Crit Rev Microbiol doi:10.3109/1040841X.2014.929563**:**1-12.
179. **Miller JC, Ma Y, Bian J, Sheehan KCF, Zachary JF, Weis JH, Schreiber RD, Weis JJ.** 2008. A critical role for Type I IFN in arthritis development following *Borrelia burgdorferi* infection of mice. J Immunol **181:**8492-8503.
180. **Miller JC, Maylor-Hagen H, Ma Y, Weis JH, Weis JJ.** 2010. The Lyme disease spirochete *Borrelia burgdorferi* utilizes multiple ligands, including RNA, for Interferon Regulatory Factor 3-dependent induction of Type I Interferon-responsive genes. Infect Immun **78:**3144-3153.
181. **Castoldi A, Braga TT, Correa-Costa M, Aguiar CF, Bassi ÊJ, Correa-Silva R, Elias RM, Salvador F, Moraes-Vieira PM, Cenedeze MA, Reis MA, Hiyane MI, Pacheco-Silva Á, Gonçalves GM, Câmara NOS.** 2012. TLR2, TLR4 and the MYD88 signaling pathway are crucial for neutrophil migration in acute kidney injury induced by sepsis. PLoS ONE **7:**e37584.
182. **Oosting M, Buffen K, Malireddi SRK, Sturm P, Verschueren I, Koenders MI, van de Veerdonk FL, van der Meer JWM, Netea MG, Kanneganti T-D, Joosten LAB.** 2012. Murine *Borrelia* arthritis is highly dependent on ASC and caspase-1, but independent of NLRP3. Arthritis Res Ther **14:**R247-R247.
183. **Zizzo G, Cohen PL.** 2013. IL-17 stimulates differentiation of human anti-inflammatory macrophages and phagocytosis of apoptotic neutrophils in response to IL-10 and glucocorticoids. J Immunol **190:**5237-5246.

VITA

Carrie Lasky was born to Richard and Debbie Lasky on October 29th, 1987 in Cape Girardeau, MO. She is the older sister of Sarah Greene. Carrie graduated Cape Central Public High School in 2006 and did her undergraduate work at Southeast Missouri State University where she received her Bachelor's degree in Biomedical Science in 2010. She was accepted to the graduate school at the University of Missouri where she trained under the supervision of Dr. Charles R. Brown and received her PhD in Microbiology in 2015.